Analysis and Control of Limit Cycle Walking Based on Linearized Equation of Motion with State Jump

by

Xuan Xiao

submitted to
Japan Advanced Institute of Science and Technology
in partial fulfillment of the requirements
for the degree of
Doctor of Philosophy

Supervisor: Associate Professor Fumihiko Asano

School of Information Science
Japan Advanced Institute of Science and Technology

December, 2015

Abstract

Limit cycle walking which is proposed to measure and ensure stability by releasing the constraints of walkers, has a high energy efficiency because of zero or low feedback gains required for sustained local stability, and thus has more freedoms to increase versatility in optimizing walking state generation. To increase the ability of handle disturbance, however, limit cycle walking needs to bring high feed gains, which affects the energy efficiency. Considering all closed-loop control systems, the energy consumption by the feed-forward control system which can often significantly justify the extra cost, time and effort required to implement the technology is substantially lower than others. Therefore, if the mathematical model of limit cycle walking which is the requirement of the feed-forward control can be built, the feed-forward control can be proposed as the solution. In addition, the mathematical analysis of limit cycle walking can help to discover and generate the optimal walking states.

First, a general method is proposed to build the mathematical model of limit cycle walker driven by all the settling-time control systems. Through the analysis of discrete control systems, the general formula is proposed for all discrete control systems. Thus when the control input of the continuous control systems is discretized, the mathematical model of the continuous control systems can be built by the general formula of the discrete control systems. Based on the mathematical model, gait properties are analysed, critical and optimal walking states are discovered mathematically and target walking states are generated. All the results are verified by numerical simulations.

Second, feed-forward control is proposed based on the mathematical model of the combined rimless wheel (CRW). Thus, gait properties of state error are analysed and limit cycle walking at target constant walking speed is generated successfully. In addition, the ability of handle disturbance of the feed-forward control is tested by numerical simulations.

Finally, the limit-cycle-walking-based feed-forward control system is extended to the

underactuated rimless wheel with torso (URW), a two-DoF limit cycle walker. The optimal walking state, deadbeat mode, is analysed mathematically and generated by numerical simulations. In addition, a constant speed walking is generated on the uneven ground by the feed-forward control system.

keywords:Feed-forward control, Limit cycle walking, Optimal state analysis, Target walking states generation.

Contents

List of Figures

List of Tables

Chapter 1

Introduction

1.1 Limit Cycle Walking

For robotic walking, the artificial constraints can help to stabilize the complex dynamic walking motion, however, limit the optimizing gait generation. In previous research, the static stability which means that the vertical projection of the Center of Mass (CoM) is kept within the support polygon formed by the feet, was applied in bipedal walkers in early 70's. It ensured walking stability, but limited the speed of the walking motions that could be obtained [1]. Therefore, Zero Moment Point (ZMP) paradigm which constrains the stance foot to remain in the contact with the ground during each step, was developed in 1970 to reduce the restrictive of static walking, and thus greatly enhanced the flexibility of the robot [2–4]. Nevertheless, the robots are still cannot be compared with human walking in terms of efficiency, disturbance handling, and natural appearance [5–7]. Therefore, to release more constraints, limit cycle walking is proposed to measure and ensure stability as follows.

- Limit cycle walking is a nominally periodic sequence of steps that is stable as a whole but not locally stable at every instant in time [13].

Zero or low feedback gains required for sustained local stability makes energy efficiency the most important advantage of limit cycle walking. In addition, few restrictive helps

limit cycle walking to increase versatility in the ability to walk at different speeds [8, 9]. Hobbelen studied that walking speed could affect the walking stability in limit cycle walking. Therefore generating target steady walking states will be a progress on developing the optimal control [10–12]. Zero feedback gains or low feedback, however, also leads to a low ability of handle disturbances, which is the main disadvantage in limit cycle walking [13].

The rimless wheel (RW) is investigated as the most simplified model of passive dynamic walking. When the RW walks passively on a slope, it establishes a steady single-step cycle [14–18]. Based on the pioneering works of McGeer, the steady step period could be evaluated by the initial and terminal boundary conditions [14]. Considering that the steady walking speed can be calculated by the ratio between the step period and step length of the RW, therefore, a target steady walking speed can be generated by calculating the angle of the slope. Furthermore, Coleman found analytic approximations for the minimum required slope for stable rolling in three dimensions [19,20], which helped us to generate the lowest walking speed as a critical condition.

1.2 Closed-loop Control

A closed-loop control system is a control system which uses the concept of an open loop system as its forward path but has one or more feedback loops or paths between its output and input. In general, high feedback gains can help walkers to generate the complex dynamic walking motion and improve the ability of handle disturbance. The PID controller which calculates the error value as the difference between a measured process variable and a desired point is a common closed-loop controller architecture. Relying only on the measured process variable, not on knowledge of the underlying process, making a PID controller a broadly useful controller [21, 22]. Nevertheless, optimal control is not guaranteed in PID controllers. In addition, that processing high frequency measurement or noise can cause large amounts of change in the output is another problem of PID controllers.

Therefore, feed-forward controllers are considered as the solution [23, 24]. In a feed-

forward system, the control variable adjustment is based on knowledge about the process in the form of a mathematical model of the process or the process disturbances instead of error-based. The disturbances can be measured and accounted for by feed-forward control in advance, and thus the extra energy consumption can often significantly justified. Therefore, the feed-forward control system typically generates the optimal state.

1.3 Motivation and Research Goals

Even though the limit cycle walkers driven by open-loop control systems generated the target steady walking speed states, however, the gaits before the steady state can not be kept at a target walking speed. Different from generating a target angular position or a target angular velocity, a target walking speed for legged robot is based on an overall planning for a discrete time period and a space segment in one step. Therefore, accurately controlling the legged robot to keep a target walking speed is a complicated issue due to the irreversibility of time and space. Several approaches to accurately control the walking speed have been proposed. Kajita et. al. proposed a method by changing the foothold of a biped walker to modify the initial condition of the support phase to control the walking speed based on a PD feedback controller [25]. In addition, Juang et. al. proposed a learning scheme which trains the neuro-fuzzy controller to follow the designed trajectory as closely as possible for generating walking gaits at a certain speed [26]. The approach of feed-forward control system which is based on the mathematical model of the process, however, is still unclear.

Therefore, considering the advantage of limit cycle walking and feed-forward control, a combination of both can make the robot have high energy efficiency and high ability of handle disturbance, and obtain the optimal walking control based on the mathematical analysis [27]. In previous research, the mathematical analysis of passive limit cycle walking has been proposed and the critical and optimal walking states thus generated [19, 20]. When mathematical analysis is extended to the actuated limit cycle walker, target optimal walking states can be generated by the control systems which can be designed flexibly

and purposefully. In addition, analysing the gait properties based on the mathematical analysis instead of numerical simulations also make a progress on generating critical and optimal walking states. Different kinds of control systems, however, generate different simplification of the boundary conditions. The more complex the control system is, the more complex the boundary equations become. Therefore, developing a general method of mathematical analysis for all kinds of control systems and thus developing the feed-forward control based on it are the main topics in this thesis.

Four research goals should be achieved in this thesis.

- The discrete stepwise control systems should be developed, thus its the boundary equations are mathematically analysed, and target walking states of limit cycle walking can be generated. Finally, based on the analysis of some simple discrete stepwise control systems, a general formula for all discrete stepwise settling-time control systems should be derived.

- The mathematical model should be extended to continuous control systems. The control input of continuous piecewise control systems are discretized, and thus the continuous piecewise control systems are analysed by using the general formula of discrete stepwise control systems. The general formula for all continuous piecewise settling-time control systems should be proposed.

- The feed-forward control systems should be proposed based on the mathematical analysis of the actuated walker model. Different control input torques for each unstable gait are designed to generate the target walking speed states at the beginning of each step. In addition, the gait properties should be analysed mathematically and the ability of handle disturbance should be tested by numeral simulations.

- The mathematical analysis is extended to a more complex model, the underactuated limit cycle walker. Gait properties should be analysed and optimal walking states should be proposed. Thus target walking states are generated and the feed-forward control system is proposed for walking on uneven ground at target walking speed.

1.4 Outline of Thesis

This thesis is organized as follows. In Chapter 2, the model of CRW, control system, and Ridders' method are introduced as the background. In Chapter 3, the mathematical analysis of discrete stepwise control systems is developed. The formula of the steady step period and the target steady step period are derived, gait properties are analysed mathematically and the results are verified through numerical simulations. In Chapter 4, the method is extended to discrete stepwise control systems. The general formula of the boundary conditions in $(n+1)$-period stepwise control system are analysed mathematically and thus the general formula of steady step period are derived. In Chapter 5, the mathematical analysis is extended to the continuous piecewise control system by discretizing the control input. In Chapter 6, The feed-forward control systems are proposed and analysed based on the mathematical analysis of the actuated walker model. In Chapter 7, mathematical analysis is extended to a complex underactuated limit cycle walker for generating the optimal walking states. Chapter 8 contains conclusions and future works.

Chapter 2

Background

2.1 Actuated Combined Rimless Wheel

2.1.1 Modeling

Fig. 2.1 illustrates the model of a planar actuated CRW. It consists of two eight-legged rimless wheels (RWs) combined by a body frame. A motor attached on the frame supplies the joint torque, u, between the rear stance-leg and the body frame. The following statements are assumed in the thesis.

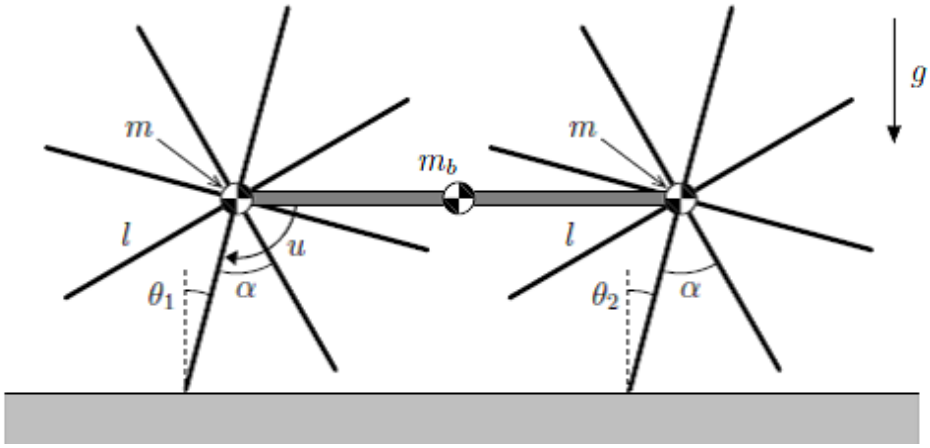

Figure 2.1: A planar actuated combined rimless wheel

- The fore and rear stance legs always contact with the ground without sliding.
- The inertia moments about the CoMs of all the frames can be neglected.
- The fore and rear RWs perfectly synchronize or rotate maintaining $\theta_1 \equiv \theta_2$.

2.1.2 Equations of Motion and Linearization

This model configures a four-bar linkage with the floor, and the joint torque, u, is thus equivalent to exerting the ankle-joint torque. The dynamics of the rear RW then becomes identical to that of an actuated RW with an ankle-joint torque, that is,

$$\ddot{\theta} = \omega^2 \sin\theta + \frac{u}{Ml^2}, \tag{2.1}$$

where $M := m_b + 2m$ [kg] is the total mass of the CRW, $\theta(= \theta_1 = \theta_2)$ is the stance-leg angle, and $\omega := \sqrt{g/l}$ [rad/s]. By linearizing this around $\theta = \dot{\theta} = 0$, the state-space realization of the RW dynamics becomes

$$\frac{\mathrm{d}}{\mathrm{d}t}\begin{bmatrix} \theta \\ \dot{\theta} \end{bmatrix} = \begin{bmatrix} 0 & 1 \\ \omega^2 & 0 \end{bmatrix}\begin{bmatrix} \theta \\ \dot{\theta} \end{bmatrix} + \begin{bmatrix} 0 \\ 1/Ml^2 \end{bmatrix} u. \tag{2.2}$$

In the following chapters, we denote Eq. (2.2) as $\dot{\boldsymbol{x}} = \boldsymbol{A}\boldsymbol{x} + \boldsymbol{B}u$.

In addition, to verify our linearization calculation, all the comparisons are made with the results of non-linearization simulation in the following chapters. There is an error due to the linearization.

2.1.3 Collision Equation

We define the state vector immediately before the (i)th impact as $\boldsymbol{x}_i^-$ and the state vector immediately after the (i)th impact as $\boldsymbol{x}_i^+$. In the collision phase we assume that the rear leg frame of each RW at impact (the previous stance leg) begins to leave the ground immediately after the landing of the fore leg frame (the next stance leg) according to the law of inelastic collision. Then the transition equation for the angular velocity becomes

$$\dot{\theta}_i^+ = \cos\alpha \dot{\theta}_i^-. \tag{2.3}$$

The transition equation for angular position is also determined as

$$\theta_i^+ = -\theta_i^- = -\frac{\alpha}{2}.$$

2.2 Settling-time Control System

The settling-time control systems are considered in this thesis. The motor forces the torque based on different control systems during the settling time, T_{set}, in each step. We define the moment immediately after impact as 0 [s] and the time parameter will be reset after every impact. Therefore, as the advantage of the settling-time, when and how the input ends in one step can be known, which can help to develop the mathematical model. During each settling time, we can design discrete or continuous control systems. The discrete control systems are named as "stepwise" and the continuous ones are named as "piecewise". In addition, the torque must supply enough kinetic energy to make the walkers overcome the potential barrier. In this thesis, we assume that the control is always completed by the next impact.

2.3 Ridders' Method

Considering that the feed-forward and feedback control system is based on the mathematical model, Ridders' method, a root-finding algorithm, is introduced in this thesis to calculate the numerical solution of optimal walking states [28]. Ridders' method is based on the false position method and the use of an exponential function to successively approximate a root of a function. In the following chapters, Ridders' method is denoted as $Ridder(f_{\text{R}}(x_{\text{R}}), x_1, x_2)$, where x_{R} is the root of the continuous function $f_{\text{R}}(x_{\text{R}}) = 0$ between x_1 and x_2 ($x_1 < x_{\text{R}} < x_2$). The method can be summarized by the formula as follows, where $x_3 = \dfrac{x_1 + x_2}{2}$.

$$x_4 = x_3 + (x_3 - x_1)\frac{\text{sign}(f_{\text{R}}(x_1) - f_{\text{R}}(x_2))f_{\text{R}}(x_3)}{\sqrt{f_{\text{R}}(x_3)^2 - f_{\text{R}}(x_1)f_{\text{R}}(x_2)}} \tag{2.4}$$

Chapter 3

Constant Control System

3.1 Equations of Motion of Constant Control System

First of all, the simplest control system, the constant (one-period) control torque, $u(t) = u_0 (t \geq 0)$, is considered where u_0 is the only parameter we can adjust. In this control system, the motor keeps a constant torque (current mode) which can supply enough kinetic energy to overcome the potential barrier at mid-stance. Similar with the passive walking on a slope, it can establish a steady rolling cycle on level ground.

The equation of motion thus becomes as follows.

$$\dot{\boldsymbol{x}} = \boldsymbol{A}\boldsymbol{x} + \boldsymbol{B}u_0 \tag{3.1}$$

3.2 Boundary Conditions of Constant Control System

As the solution of Eq. (3.1) [29], if we define the (i)th step period as T_i, the state vector immediately before the $(i+1)$th impact, $\boldsymbol{x}_{i+1}^-$, is written by the state vector immediately after the (i)th impact, $\boldsymbol{x}_i^+$, as

$$\boldsymbol{x}_{i+1}^- = \mathrm{e}^{\boldsymbol{A}T_i}\boldsymbol{x}_i^+ + \int_{0^+}^{T_i^-} \mathrm{e}^{\boldsymbol{A}(T_i - s)}\boldsymbol{B}u_0 \, \mathrm{d}s. \tag{3.2}$$

The state vector at t [s], $\boldsymbol{x}(t)$ can be written by the time t and the initial state vector $\boldsymbol{x}(0^+)$ as

$$\boldsymbol{x}(t) = \begin{bmatrix} \theta(t) \\ \dot{\theta}(t) \end{bmatrix} = \mathrm{e}^{\boldsymbol{A}t}\boldsymbol{x}(0^+) + \int_{0^+}^{t} \mathrm{e}^{\boldsymbol{A}(t-s)}\boldsymbol{B}u_0 \, \mathrm{d}s. \tag{3.3}$$

Therefore, the steady equation also becomes

$$\boldsymbol{x}_{\mathrm{eq}}^{-} = \mathrm{e}^{\boldsymbol{A}T^*}\boldsymbol{x}_{\mathrm{eq}}^{+} + \int_{0^+}^{T^*} \mathrm{e}^{\boldsymbol{A}(T^*-s)}\boldsymbol{B}u_0 \, \mathrm{d}s, \tag{3.4}$$

where the subscript "eq" means the steady state and T^* means the steady step period. The initial and terminal boundary conditions in a steady step are as follows.

$$\boldsymbol{x}_{\mathrm{eq}}^{+} = \boldsymbol{x}^*(0^+) = \begin{bmatrix} \theta^*(0^+) \\ \dot{\theta}^*(0^+) \end{bmatrix} = \begin{bmatrix} -\dfrac{\alpha}{2} \\ \dot{\theta}_{\mathrm{eq}}^{+} \end{bmatrix} \tag{3.5}$$

$$\boldsymbol{x}_{\mathrm{eq}}^{-} = \boldsymbol{x}^*((T^*)^-) = \begin{bmatrix} \theta^*((T^*)^-) \\ \dot{\theta}^*((T^*)^-) \end{bmatrix} = \begin{bmatrix} \dfrac{\alpha}{2} \\ \dot{\theta}_{\mathrm{eq}}^{-} \end{bmatrix} \tag{3.6}$$

According to the Eqs. (3.5), (3.6), and the transition equation, Eq. (2.3), in collision phase, we can derive the terminal boundary condition in the steady step as follows.

$$\boldsymbol{x}^*((T^*)^-) = \begin{bmatrix} \theta^*((T^*)^-) \\ \dot{\theta}^*((T^*)^-) \end{bmatrix} = \begin{bmatrix} \dfrac{\alpha}{2} \\ k\dot{\theta}_{\mathrm{eq}}^{+} \end{bmatrix} \tag{3.7}$$

Where $k = 1/\cos\alpha$ denotes the coefficient of transition equation.

As a result, the initial and terminal boundary conditions are detailed as

$$\frac{-2u_0 + A_1 + A_2}{2l^2M\omega^2} = \frac{\alpha}{2}, \tag{3.8}$$

$$\dot{\theta}_{\mathrm{eq}}^{+}\cosh(T^*\omega) + A_3\sinh(T^*\omega) = k\dot{\theta}_{\mathrm{eq}}^{+}, \tag{3.9}$$

where

$$\begin{aligned} A_1 &= \left(2u_0 - \alpha l^2 M\omega^2\right)\cosh(T^*\omega), \\ A_2 &= 2\dot{\theta}_{\mathrm{eq}}^{+} l^2 M\omega \sinh(T^*\omega), \ A_3 = \frac{u_0}{l^2 M\omega} - \frac{\alpha\omega}{2}. \end{aligned}$$

Finally, T^* and $\dot{\theta}^+_{\text{eq}}$ are the unknown parameters. After eliminating $\dot{\theta}^+_{\text{eq}}$ in Eqs. (3.8) and (3.9) to derive a single equation with T^*, the result after simplification becomes

$$\begin{aligned} u_0\left(-2k+2\cosh(T^*\omega)+2k\cosh(T^*\omega)-2\right) = \\ \alpha l^2 M\omega^2\left(k-\cosh(T^*\omega)+k\cosh(T^*\omega)-1\right). \end{aligned} \tag{3.10}$$

3.3 Formula of Steady Step Period of Constant Control Systems

When the control input, u_0, is known, we can calculate the steady step period, T^*, according to Eq. (3.10). When all the common factors of T^* are extracted, the Eq. (3.10) thus becomes

$$(2u_0+2ku_0-\lambda(1-k))\cosh(T^*\omega) = 2u_0+2ku_0+\lambda(1-k), \tag{3.11}$$

where $\lambda = \alpha l^2 M\omega^2$.

Since T^* is always a positive real number, we can solve the equation and choose correct the solution as follows.

$$T^* = \frac{1}{\omega}\text{arccosh}\left(\frac{2u_0+2ku_0-\lambda(1-k)}{2u_0+2ku_0+\lambda(1-k)}\right) \tag{3.12}$$

3.4 Target Walking Period Generation of Constant Control Systems

In addition, a target walking speed can also be generated based on the boundary equations. Considering the step length is constant in our model, the steady walking speed is determined by the steady walking period. Therefore, u_0 can be calculated for generating the target T^* in the Eq. (3.10).

After being extracted all the common factors of u_0, the Eq. (3.10) becomes

$$u_0(2k+2)(\cosh(T^*\omega)-1) = \lambda(k-1)(\cosh(T^*\omega)+1). \tag{3.13}$$

Table 3.1: Physical parameters of CRW

Parameters	Value	Unit
l	1.0	[m]
g	9.81	[m/s^2]
M	1.0	[kg]
α	$\frac{\pi}{4}$	[rad]

The solution is thus as follows.

$$u_0 = \frac{\lambda(k-1)(\cosh(T^*\omega)+1)}{(2k+2)(\cosh(T^*\omega)-1)} \tag{3.14}$$

3.5 Verification of Constant Control System by Simulations

To verify our results, we made the simulation of CRW and checked the steady step period in different simulations. The parameters were chosen as listed in Table 3.1.

First, we tested the calculation of T^* by Eq. (3.12) when u_0 was chose as 2, 3, 4 [N×m] for three simulations. The step period converged to a steady value step by step as shown in Fig. 3.1. The convergence values were recorded as the steady step period T^* in the simulation. Then we calculated the orbit of T^* when u_0 is from 2 to 4 [N×m] by Eq. (3.12). The red star points on the orbit of function in Fig. 3.2 were the calculation results. The comparison between two sets of values in Table 3.2 showed that the error was less than 0.4%.

Table 3.2: Verification results for T^* in constant control system

u_0 [N×m]	2	3	4
T^* in simulation [s]	0.417	0.324	0.275
T^* in function [s]	0.418	0.325	0.275

In addition, the control inputs u_0 for the target steady step periods of 0.4, 0.35, 0.3 [s] can also be calculated for these three cases. First, we calculated the value of u_0 by Eq. (3.14) for these three T^* values. The red star points on the orbit of function in Fig. 3.3 were the calculation results of control input. Second, we tested the three analytical solutions as the control input in the simulations and the step period converged to the steady value as shown in Fig. 3.4. Finally, we recorded the steady step periods in Table 3.3. The error is less than 0.4%.

In general, steady walking periods were calculated and the target walking speeds were generated well in the constant control systems.

Table 3.3: Verification results for target T^* in constant control system

Target T^* [s]	0.4	0.35	0.3
Analytical u_0 [N×m]	2.1413	2.6533	3.4445
T^* in simulation [s]	0.399	0.349	0.300

3.6 Critical Condition of Constant Control System

Since we have derived the formula of the steady step period, T^*, we can find more details of the gait property in the steady gait. According to Eq. (3.9), we can calculate the steady angular velocity immediately after impact, $\dot{\theta}^+_{\text{eq}}$, as

$$\dot{\theta}^+_{\text{eq}} = \frac{-A_3 \sinh(T^*\omega)}{\cosh(T^*\omega) - k}. \tag{3.15}$$

Therefore, time evolution of angular velocity in steady gait in Eq. (3.3) can also be calculated as below, where $\dot{\theta}^+_{\text{eq}}$ and T^* are in Eqs. (3.15) and (3.12).

$$\dot{\theta}(t) = \dot{\theta}^+_{\text{eq}} \cosh(t\omega) + A_3 \sinh(t\omega) \tag{3.16}$$

When $u_0 = 2.0$ [N·m], we can calculate the analytical solution of angular velocity in one steady step as Fig. 3.5 illustrates. It is almost the same with the step in the simulation.

Usually, when the input torque is large enough in the constant control system, there is no doubt the model can overcome the vertical position. As Fig. 3.5 illustrates, however, when the torque is low, the model has a deceleration and an acceleration. The boundary input torque for limit cycle walking can help to check whether the control system can supply enough kinetic energy or not. In addition, the boundary input torque will generate the lowest walking speed, and thus any target walking speed which is lower than the boundary speed is impossible to be generated. We can solve the boundary condition by our equations.

First, we need to find the lowest angular velocity in one steady step. According to Eq. (3.16), we could calculate its derivative function as follows.

$$\ddot{\theta}(t) = \omega\dot{\theta}^{+}_{\mathrm{eq}}\sinh(t\omega) + \omega A_3\cosh(t\omega) \tag{3.17}$$

If the torque is low, there will be an inflection in the derivative function and the point should be the lowest angular velocity in one steady step. We can find the point easily as below if there is one.

$$t_0 = \frac{1}{\omega}\mathrm{arctanh}\left(-\frac{A_3}{\dot{\theta}^{+}_{\mathrm{eq}}}\right) \tag{3.18}$$

We must control the input torque to make the lowest angular velocity high than 0, which means the critical condition is as follows.

$$\dot{\theta}(t_0) = 0 \tag{3.19}$$

So according to the Eqs. (3.12), (3.15), (3.16), (3.18) and the critical condition, the only unknown parameter, the input torque u_0, can be calculated by the computer. The final analytical result is $u_0 = 0.661$ [N×m]. Because of some error in the linearization, the critical input torque in the simulation is 0.6534 [N×m]. If the torque is lower than this value, the model will not finish one step and fall backward. Fig. 3.6 illustrates the time evolution of angular velocity when the input torque is 0.657 [N×m], in the simulation.

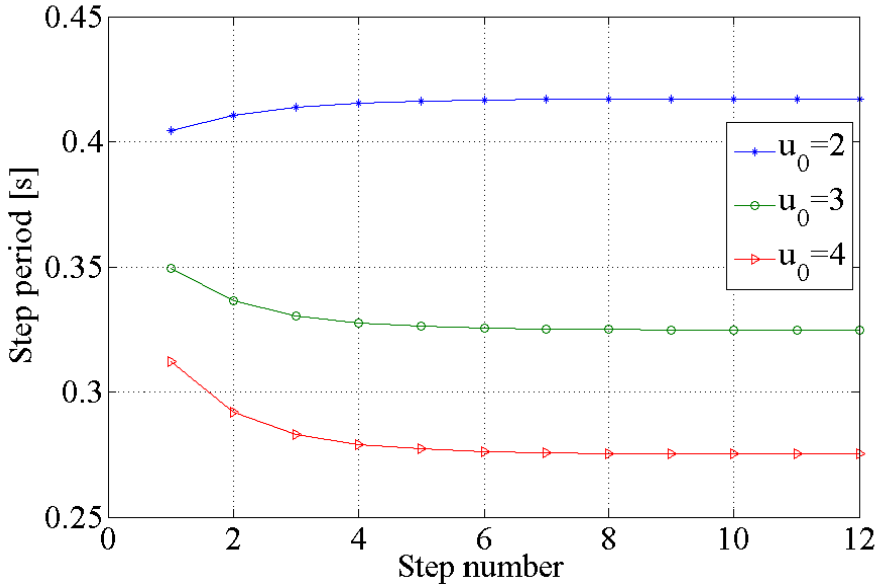

Figure 3.1: Evolutions of step periods in the simulations of constant control system

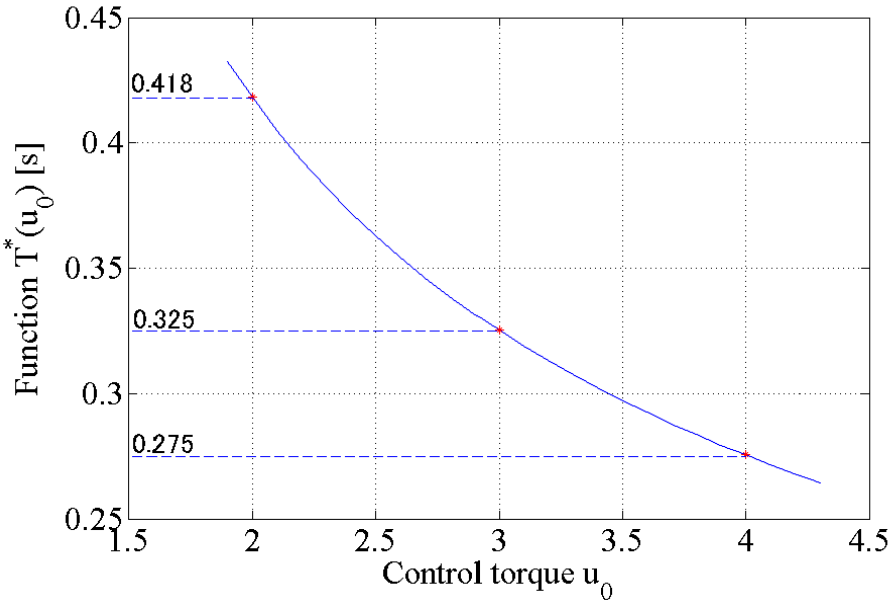

Figure 3.2: Analytical solution of T^* in constant control system

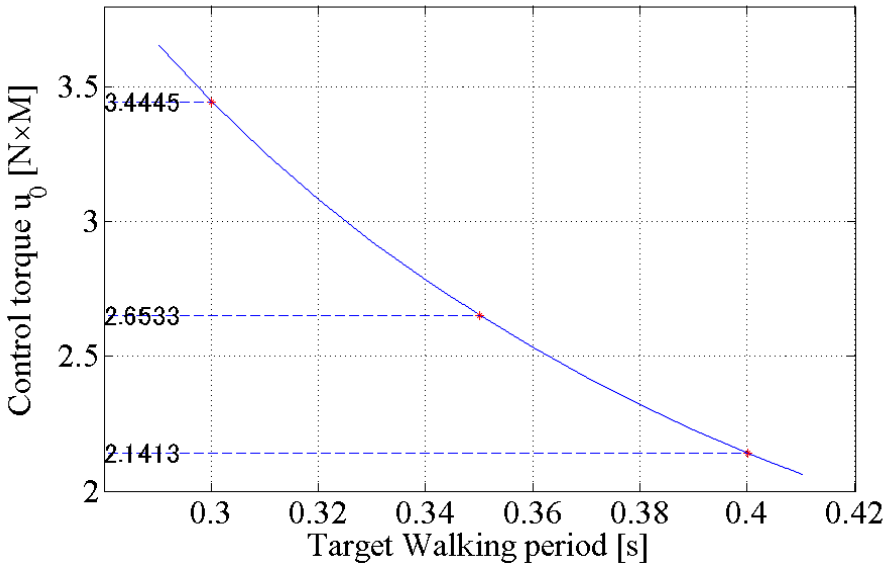

Figure 3.3: Analytical solution of u_0 to generate a target steady step period in constant control systems

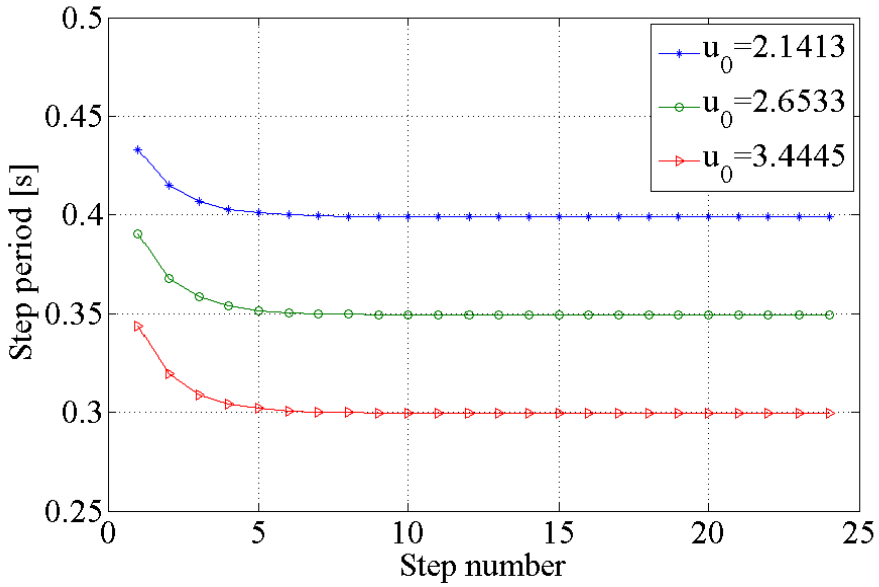

Figure 3.4: Evolutions of step periods for target step period in the simulations in constant control systems

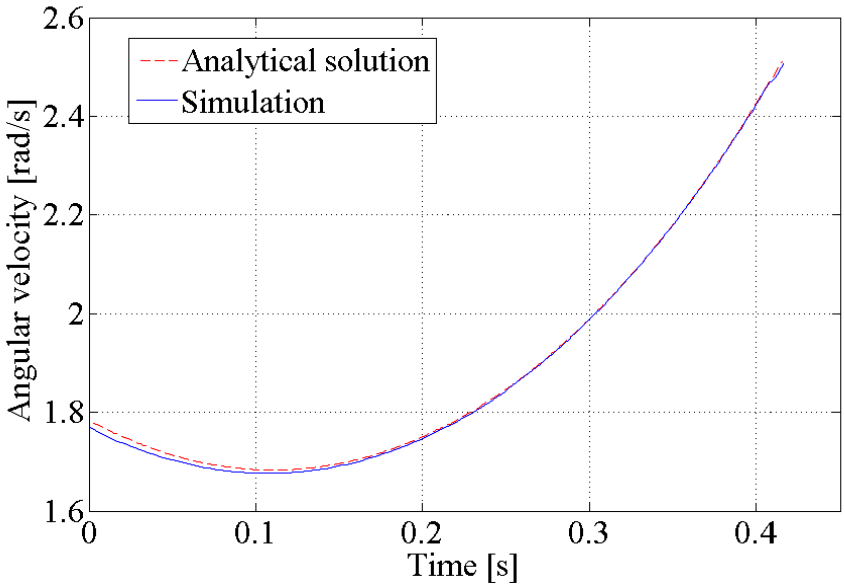

Figure 3.5: Evolutions of analytical solution and simulation of angular velocity in one steady step in the constant control system

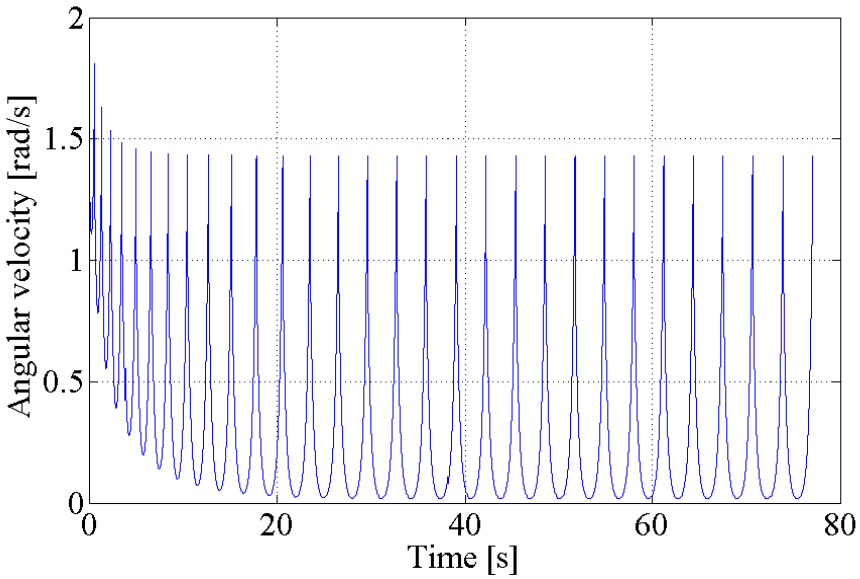

Figure 3.6: Evolution of angular velocity in the simulation under critical input in constant control system

Chapter 4

Discrete Stepwise Control System

4.1 Two-period Stepwise Control System

The constant control system is the simplest control system and we analysed the gait properties by the equation of boundary conditions in the chapter above. When we define the error between the steady walking state and a walking state before the steady ones as the state error, however, we cannot control the linear transfer function of state error in the constant control system [30]. Therefore, we need to consider some control systems with more periods to solve this problem. For example, the two-period stepwise control system as follows [30].

$$u(t) = \begin{cases} u_0 & (0 \leq t < T_{\text{set}}) \\ 0 & (t \geq T_{\text{set}}) \end{cases} \tag{4.1}$$

This control system can help us to analyse the state error step by step, and thus calculate the transfer function of a state error. The steady step period, T^*, is one of the most important parameters in the experiments. We hope the two-period stepwise control systems can also be analysed mathematically.

4.1.1 Boundary Conditions of Two-period Stepwise Control System

According to the control system in Eq. (4.1), when the time is longer than T_{set} in one step, the control torque is always 0. Therefore, the equation in the steady walking step is arranged as follows.

$$\begin{aligned} \boldsymbol{x}_{\text{eq}}^{-} &= \mathrm{e}^{\boldsymbol{A}T^*}\boldsymbol{x}_{\text{eq}}^{+} + \int_{0^+}^{T^*} \mathrm{e}^{\boldsymbol{A}(T^*-s)}\boldsymbol{B}u(s)\ \mathrm{d}s \\ &= \mathrm{e}^{\boldsymbol{A}T^*}\boldsymbol{x}_{\text{eq}}^{+} + \int_{0^+}^{T_{\text{set}}} \mathrm{e}^{\boldsymbol{A}(T^*-s)}\boldsymbol{B}u_0\ \mathrm{d}s \end{aligned}$$

Similarly, the boundary conditions are the same as Eqs. (3.5) and (3.6). Thus we eliminate the $\dot{\theta}_{\text{eq}}^{-}$ and the terminal boundary condition in the steady step. After the simplification of the initial and terminal boundary conditions according the properties of hyperbolic functions, we derive the single equation as follows.

$$\begin{aligned} 2u_0k(\cosh(T^*\omega)\cosh(T_{\text{set}}\omega) - \sinh(T^*\omega)\sinh(T_{\text{set}}\omega)) = \\ \lambda(1-k) + 2ku_0\cosh(T^*\omega) + \lambda\cosh(T^*\omega) \\ -\lambda k\cosh(T^*\omega) - 2u_0 + 2u_0\cosh(T_{\text{set}}\omega) \end{aligned} \tag{4.2}$$

4.1.2 Formula of Steady Step Period of Two-period Stepwise Control System

After the extraction of common factors, the result is thus as follows.

$$E_{1(2)}\cosh(T^*\omega) + E_{2(2)}\sinh(T^*\omega) = E_{3(2)} \tag{4.3}$$

Where $E_{1(2)}$ and $E_{2(2)}$ are coefficients of the hyperbolic cosine function and the hyperbolic sine function and $E_{3(2)}$ is the constant term. The number in the brackets is the number of the periods in the control system. Thus $E_{1(n)}$, $E_{2(n)}$ and $E_{3(n)}$ are used to express the boundary equation of n-period control system in the following chapters. The details of

$E_{1(2)}$, $E_{2(2)}$ and $E_{3(2)}$ are as follows.

$$\begin{aligned} E_{1(2)} &= 2u_0 k\cosh(T_{\text{set}}\omega) - 2ku_0 - \lambda + \lambda k \\ E_{2(2)} &= -2u_0 k\sinh(T_{\text{set}}\omega) \\ E_{3(2)} &= \lambda(1-k) - 2u_0 + 2\cosh(T_{\text{set}}\omega)u_0 \end{aligned}$$

Finally we can simplify the equation and derive the solution by computer. The positive solution is chosen as follows [31].

$$T^*(u_0, T_{\text{set}}) = \frac{1}{\omega}\ln\left(\frac{E_{3(2)} - \sqrt{-E_{1(2)}^2 + E_{2(2)}^2 + E_{3(2)}^2}}{E_{1(2)} + E_{2(2)}}\right) \tag{4.4}$$

In addition, if $-E_{1(2)}^2 + E_{2(2)}^2 + E_{3(2)}^2 < 0$, it can be caused by two reasons. The first one is that the motor cannot supply enough kinetic energy to make the CRW overcome the potential barrier. The second one is that the model cannot generate a one-step limit cycle walking [32]. This is an important topic and is left a future work.

4.1.3 Target Walking Period Generation of Two-period Stepwise Control System

Similar with the constant control system, we can still develop two-period stepwise control systems to generate a target walking speed. We can not only control the torque, u_0, but also the settling time, T_{set}, according to the boundary equation.

We extract all the common factors of u_0 in the Eq. (4.2) as below.

$$\begin{aligned} 2u_0 k\cosh(T^*\omega - T_{\text{set}}\omega) + 2u_0 \\ -2u_0\cosh(T_{\text{set}}\omega) - 2ku_0\cosh(T^*\omega) = \\ \lambda(1-k) + \lambda\cosh(T^*\omega) - \lambda k\cosh(T^*\omega) \end{aligned} \tag{4.5}$$

The equation is solved and the solution is as follows.

$$u_0 = \frac{\lambda(1-k) + \lambda\cosh(T^*\omega) - \lambda k\cosh(T^*\omega)}{2k\cosh(T_c\omega) + 2 - 2\cosh(T_{\text{set}}\omega) - 2k\cosh(T^*\omega)} \tag{4.6}$$

Where $T_c = T^* - T_{\text{set}}$.

4.1.4 Verification of Two-period Stepwise Control System by Simulations

Numerical simulations were developed to verify the calculation of the steady step period and the analysis solution of target walking speed generation.

First, the formula of T^* in Eq. (4.4) was tested under different input parameters, u_0, when T_{set} was constant. We plotted the orbit of function T^* when $T_{\text{set}} = 0.3$ [s] and u_0 is varied from 3 to 3.2 [N×m] in Fig. 4.1. The red star points on the orbit were the calculation results of three cases when u_0 were 3.0, 3.1, 3.2 [N×m]. Then, we conducted three numerical simulations with the same conditions of the analytical solutions in Fig. 4.2 and recorded the convergence values. Finally, Table 4.1 listed the steady step period obtained in the simulation and calculation. The error between two sets of value was less than 0.4%.

In addition, generating a target walking speed by Eq.(4.6) was also tested. The control torques under different T_{set} were analysed for generating target T^*. First of all, we plotted the analytical orbit of u_0 by the Eq. (4.6) when target $T^* = 0.4$ [s] and T_{set} was varied from 0.1 [s] to 0.3 [s] in Fig. 4.3. Then, the numerical simulations were conducted under the analytical solutions of the control input and other control parameters for three cases. The step periods converged to the steady step periods in Fig. 4.4, and recorded the steady step periods in Table 4.2. The error between steady walking period and the target one was less than 0.5%. As the result, the steady step periods were calculated and the target walking states were generated well in the two-period stepwise control system.

Table 4.1: Verification results for T^* in two-period stepwise control system

u_0 [N×m]	3.0	3.1	3.2
T^* in simulation [s]	0.356	0.341	0.327
T^*in function [s]	0.357	0.342	0.328

Table 4.2: Verification results for target T^* in two-period stepwise control system

T_{set} [s]	0.1	0.2	0.3
Analytical soultion u_0 [N×m]	7.205	3.9158	2.7679
T^* in simulation [s]	0.398	0.398	0.398

4.1.5 Critical Condition of Two-period Stepwise Control System

Considering that we have calculated the steady step period, T^*, more details of the gait property in the steady gait can be found. According to Eqs. (3.3) and (3.5), we can calculate the steady angular velocity after impact, $\dot{\theta}^+_{\text{eq}}$ as below.

$$\dot{\theta}^+_{\text{eq}} = \frac{-\lambda \sinh(T^*\omega) + 2u_0(\sinh(T^*\omega) - \sinh(T_c\omega))}{2l^2M\omega(k - \cosh(T^*\omega))} \tag{4.7}$$

Time evolution of angular velocity in steady gait can also be calculated by the Eq. (4.8) as below.

$$\dot{\theta}(t) = \begin{cases} \dot{\theta}^+_{\text{eq}} \cosh(t\omega) + A_3 \sinh(t\omega) & (0 \le t < T_{\text{set}}) \\ \dfrac{2\dot{\theta}^+_{\text{eq}} \cosh(t\omega) - \alpha\omega \sinh(t\omega)}{2} + P_{\text{int}} & (t \ge T_{\text{set}}) \end{cases} \tag{4.8}$$

Where $P_{\text{int}} = \dfrac{u_0(\sinh(t\omega) - \sinh((t - T_{\text{set}})\omega))}{l^2M\omega}$.

For example, when $T_{\text{set}} = 0.3$ [s] and $u_0 = 2.0$ [N×m], we can calculate the analytical solution of angular velocity in one steady step as Fig. 4.5 illustrates. It is almost the same as the step in the simulation.

In addition, when the T_{set} is very short, the analytical solution of angular velocity in one steady step will have the inflection in the second period. For example, when $T_{\text{set}} = 0.2$ [s] and $u_0 = 2.4$ [N×m], we can calculate the analytical solution of angular velocity in one steady step as Fig. 4.6 illustrates.

Similar with the constant control system, the boundary input torque in two-period stepwise control system to make the model generate a steady limit walking is also a topic.

For the constant control system, the gait properties can be calculated easily. We hope to use the same method to calculate the lowest angular in one step and make is as 0. For the two-period stepwise control system or some more complex control system we introduce in the following chapters, however, it is difficult to know in which period the lowest angular velocity is. Thus the calculation process will be too complex to be analysed on the computer. The case in Fig. 4.6 should be one of the boundary control systems.

4.2 $(n+1)$-period Stepwise Control System

4.2.1 Boundary Conditions of $(n+1)$-period Stepwise Control System

Based on the analysis of two-period control systems, the general equation of the $(n+1)$-period stepwise control system is considered as Eq. (4.9), where T_i is the end of (i)th period and u_i is the constant control torque in the (i)th period of the stepwise control system.

$$u(t) = \begin{cases} u_1 & (0 = T_0 \le t < T_1) \\ u_2 & (T_1 \le t < T_2) \\ \cdots & \\ u_j & (T_{j-1} \le t < T_j) \\ \cdots & \\ u_n & (T_{n-1} \le t < T_n = T_{\text{set}}) \\ 0 & (t \ge T_n) \end{cases} \tag{4.9}$$

Considering the steady state in this control system, $\boldsymbol{x}(T^*) = \boldsymbol{x}_{\text{eq}}^-$ becomes

$$\boldsymbol{x}_{\text{eq}}^- = \mathrm{e}^{\boldsymbol{A}T^*}\boldsymbol{x}_{\text{eq}}^+ + \sum_{j=0}^{n-1}\int_{T_j}^{T_{j+1}} \mathrm{e}^{\boldsymbol{A}(T^*-s)}\boldsymbol{B}u_{j+1}\,\mathrm{d}s \tag{4.10}$$

We can calculate the items in Eq. (4.10) one by one as below.

$$\mathrm{e}^{\boldsymbol{A}T^*}\boldsymbol{x}_{\text{eq}}^+ = \begin{bmatrix} -\dfrac{1}{2}\alpha\cosh(T^*\omega) + \dfrac{\dot{\theta}_{\text{eq}}^+\sinh(T^*\omega)}{\omega} \\ -\dfrac{1}{2}\alpha\omega\sinh(T^*\omega) + \dot{\theta}_{\text{eq}}^+\cosh(T^*\omega) \end{bmatrix} \tag{4.11}$$

$$\int_{T_j}^{T_{j+1}} \mathrm{e}^{\boldsymbol{A}(T^*-s)}\boldsymbol{B}u_{j+1}\,\mathrm{d}s = \frac{u_{j+1}}{Ml^2\omega^2}\begin{bmatrix}\cosh(\widehat{T}_j\omega)-\cosh(\widehat{T}_{j+1}\omega)\\ \omega(\sinh(\widehat{T}_j\omega)-\sinh(\widehat{T}_{j+1}\omega))\end{bmatrix}$$

Where $\widehat{T}_j = T^* - T_j$ and $\widehat{T}_{j+1} = T^* - T_{j+1}$.

Therefore when we add all the items in every period together, the equations of initial and terminal boundary conditions can be calculated as follows.

$$\begin{aligned}\frac{1}{2l^2M\omega^2}(-\alpha l^2M\omega^2\cosh(T^*\omega)+2H_1+2\dot{\theta}^+_{\mathrm{eq}}l^2M\omega\sinh(T^*\omega)) &= \frac{\alpha}{2}\\ \frac{1}{2l^2M\omega}(-\alpha l^2M\omega^2\sinh(T^*\omega))-2H_2+2\dot{\theta}^+_{\mathrm{eq}}l^2M\omega\cosh(T^*\omega)) &= k\dot{\theta}^+_{\mathrm{eq}}\end{aligned} \tag{4.12}$$

Where

$$\begin{aligned}H_1 &= u_1\cosh(T^*\omega)-u_n\cosh(T^*\omega-T_{\mathrm{n}}\omega)\\ &\quad+\sum_{j=1}^{n-1}(u_{j+1}-u_j)\cosh(T^*\omega-T_j\omega),\\ H_2 &= u_1\sinh(T^*\omega)-u_n\sinh(T^*\omega-T_n\omega)\\ &\quad+\sum_{j=1}^{n-1}(u_{j+1}-u_j)\sinh(T^*\omega-T_j\omega).\end{aligned} \tag{4.13}$$

In the end, we can eliminate $\dot{\theta}^+_{\mathrm{eq}}$ and derive the equation we want as follows.

$$\begin{aligned}2kH_1-2(H_1\cosh(T^*\omega)-H_2\sinh(T^*\omega)) =\\ \lambda(-1+k-\cosh(T^*\omega)+k\cosh(T^*\omega))\end{aligned} \tag{4.14}$$

In detail, $H_3 := H_1\cosh(T^*\omega)-H_2\sinh(T^*\omega)$ is the constant term as follows:

$$H_3 = u_1-u_n\cosh(T_{\mathrm{n}}\omega)+\sum_{j=1}^{n-1}(u_{j+1}-u_j)\cosh(T_j\omega) \tag{4.15}$$

4.2.2 Formula of Steady Step Period in $(n+1)$-period Stepwise Control System

Similarly, the formula of steady step period in $(n+1)$-period stepwise control systems can be derived by extraction of common factors as follows.

$$E_{1(n+1)}\cosh(T^*\omega)+E_{2(n+1)}\sinh(T^*\omega) = E_{3(n+1)} \tag{4.16}$$

Where $E_{1(n+1)}$ and $E_{2(n+1)}$ are coefficients and the $E_{3(n+1)}$ is the constant term as introduced in Section 4.1.2. The details are as follows.

$$\begin{aligned} E_{1(n+1)} &= -\lambda(1-k) - 2kH_3, \\ E_{2(n+1)} &= 2k(-u_n \sinh(T_n\omega) + \sum_{j=1}^{n-1} \widehat{u}_j \sinh(T_j\omega)), \\ E_{3(n+1)} &= \lambda(1-k) - 2H_3. \end{aligned} \tag{4.17}$$

Where $\widehat{u}_j = u_{j+1} - u_j$.

We choose the positive solution of the equation and the result is list as follows.

$$T^* = \frac{1}{\omega} \ln \left(\frac{E_{3(n+1)} - \sqrt{-E_{1(n+1)}^2 + E_{2(n+1)}^2 + E_{3(n+1)}^2}}{E_{1(n+1)} + E_{2(n+1)}} \right) \tag{4.18}$$

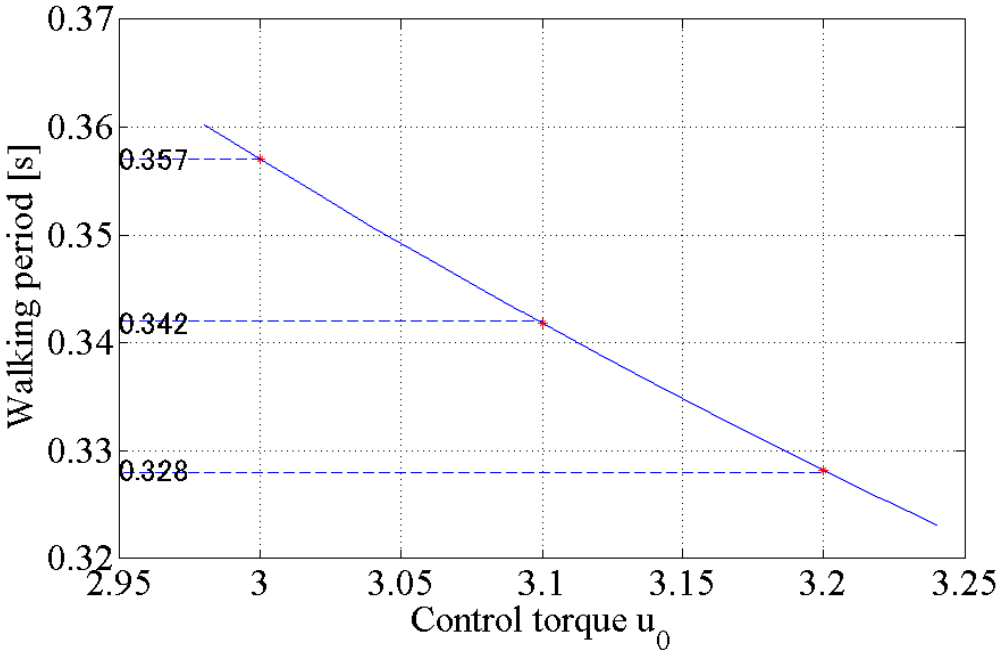

Figure 4.1: Analytical solution of T^* in two-period stepwise control systems

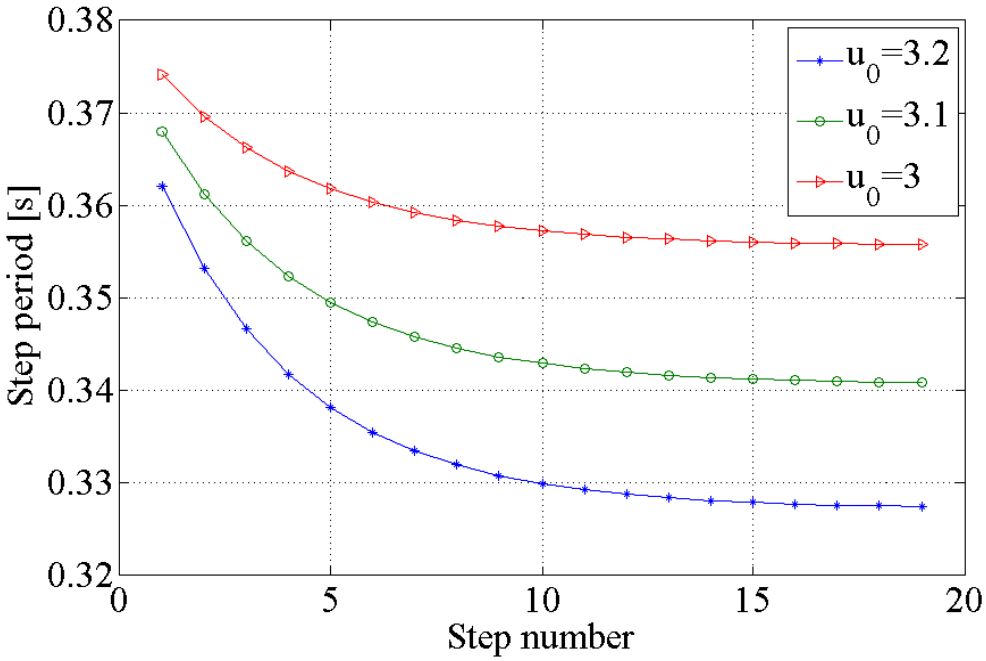

Figure 4.2: Evolutions of step periods in the simulations in two-period stepwise control systems

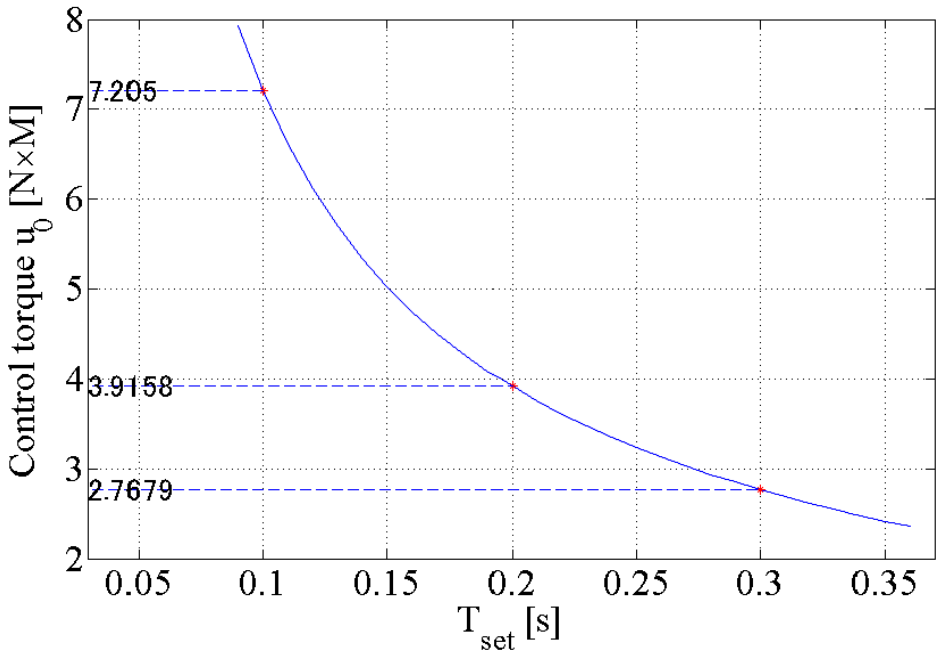

Figure 4.3: Analytical solution of u_0 for target T^* in two-period stepwise control systems

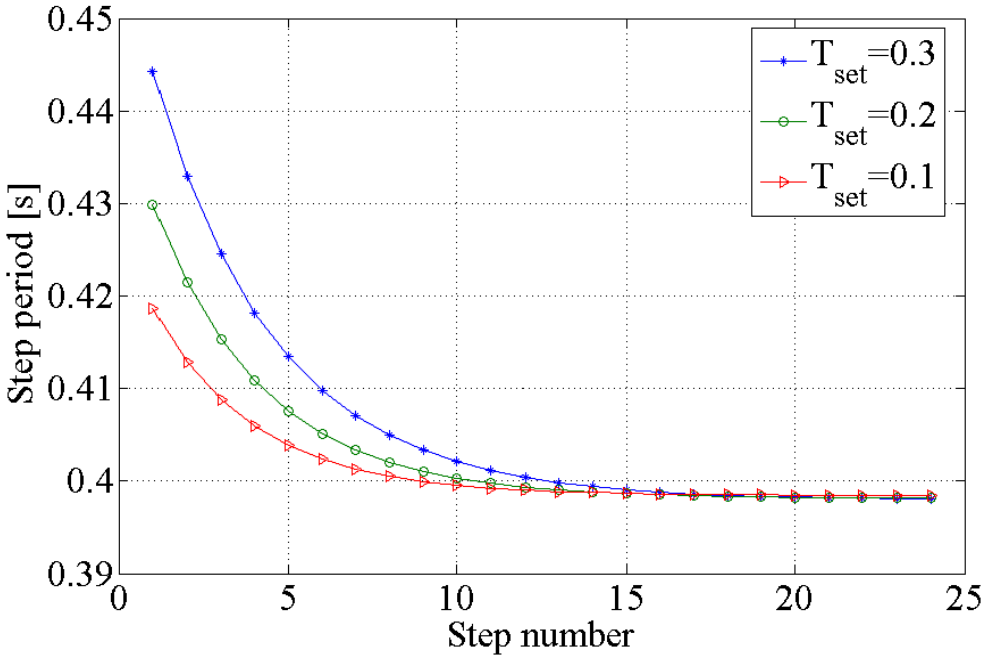

Figure 4.4: Evolutions of step periods in the simulations for target T^* in two-period stepwise control systems

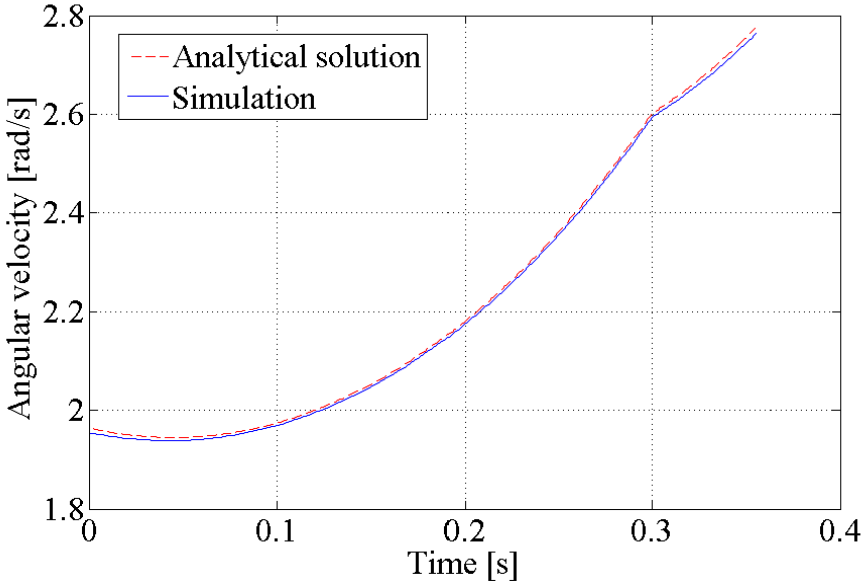

Figure 4.5: Evolution of angular velocity in the analytical solution and simulation in one steady step in two-period stepwise control system when $T_{\text{set}} = 0.3$ [s]

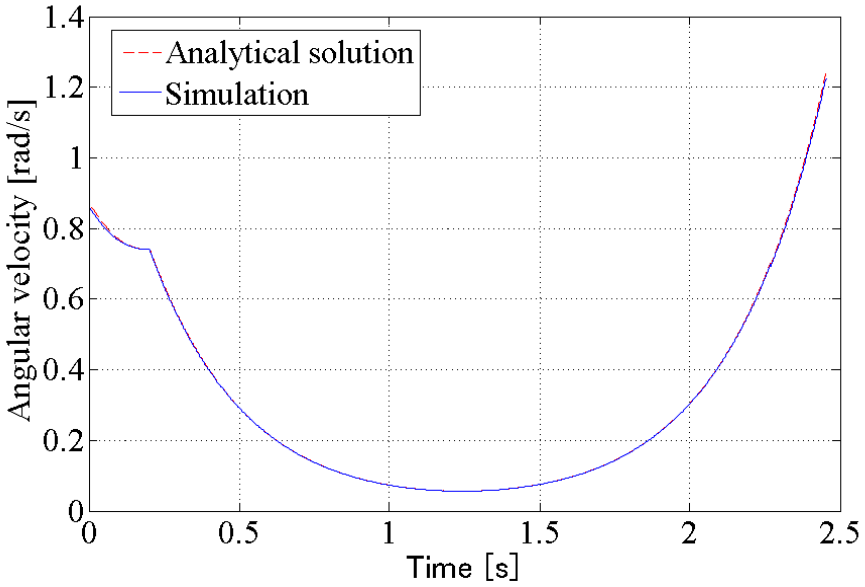

Figure 4.6: Evolution of angular velocity in analytical solution and simulation in two-period stepwise control system in one steady step when $T_{\text{set}} = 0.2$ [s]

Chapter 5

Continuous Piecewise Control System

5.1 Continuous Piecewise Control System

The $(n+1)$-period control stepwise system has been proposed and the general formula of the steady step period has been derived. Some continuous control functions, especially, the linear functions, are common in our experiments. Therefore, we hope to develop a simple and convenient method to analyse the steady step state for the linear control system, and even for all of the continuous time-settling systems.

In general, by calculating the integral of a function, we can divide the function into many small constant periods. If the division number is large enough, we can calculate the area of the discrete constant function exactly instead of the original continuous function. Similarly, when we discretize the control input of the continuous control piecewise systems and thus calculate the boundary conditions according to the general formula of the $(n+1)$-period stepwise control systems, the mathematical model of continuous piecewise control systems can be built.

5.1.1 Formula of Steady Step Period in Continuous Piecewise Control System

To explain our analysis method, we design a continuous piecewise control systems in Eq. (5.1. $f_{\mathrm{s}}(t)$ is the control system during the settling time, T_{set}.

$$u(t) = \begin{cases} f_{\mathrm{s}}(t) & (0 \leq t < T_{\mathrm{set}}) \\ 0 & (t \geq T_{\mathrm{set}}) \end{cases} \tag{5.1}$$

Then we divide T_{set} into n periods, and design an (n+1)-period stepwise function. The end time of the (j_1)th period is $T_{j_1} = \dfrac{j_1}{n} T_{\mathrm{set}}$, where $j_1 \in \{1, 2, 3, \cdots, n\}$. In each period, we set a constant value which is the middle point of the linear control function in the corresponding period as the control input. Thus the constant torque u_{j_1} in the discrete function can be calculated as :$u_{j_1} = f_{\mathrm{s}}\left(\dfrac{(2j_1 - 1)T_{\mathrm{set}}}{2n}\right)$. Fig. 5.1 illustrates a linear control function and its 10-period discrete function when $t < T_{\mathrm{set}}$.

Even though there are total (n+1) periods in the approximative discrete function (the last period, $u_{n+1} = 0$ [N×m] when $t \geq T_{\mathrm{set}}$, is included), we can still calculate the steady step period according to Eq. (4.18) in the Chapter 4. $E_{1(n+1)}$, $E_{2(n+1)}$, $E_{3(n+1)}$ and H_3 are the same as Eqs. (4.17) and (4.15).

In general, similar with the integral of a function, a large division number can reduce the error of the integral. When the division number is 1000, however, there is only an error of 0.5% between the result of numerical simulation and the analysis solution, which is caused by the state-space realization, and the calculation can be finished immediately. The error of calculation will be analysed in Section 5.2 in details.

5.1.2 Target Walking Speed in Continuous Piecewise Control System

In the section above, we have introduced the analysis of steady walking state driven by piecewise continuous control systems based on the discretizing control input. In addition, we can also design different kinds of control systems to generate target walking speed

according to the general formula of the boundary conditions. In detail, the calculation of the control coefficient in the continuous piecewise control system will be proposed for generating a target step period in this section.

First, we will design the continuous function as follows.

$$u(t) = \begin{cases} \beta f(t) & (0 \leq t < T_{\text{set}}) \\ 0 & (t \geq T_{\text{set}}) \end{cases} \tag{5.2}$$

Where $f(t)$ is the continuous function during the settling time, and β is the control coefficient to generate the target walking speed.

Then we divide T_{set} into n periods, and thus design the approximative discrete function of $f(t)$. The end time of the (j)th period is $T_j = \frac{j}{n} T_{\text{set}}$, where $j \in \{1, 2, 3, \cdots, n\}$. In each period, we set the middle point in the corresponding period as the constant control input in the period. The constant torque u_j in the discrete function can thus be calculated as follows.

$$u_j = \beta f_j = \beta f\left(\frac{(2j-1)T_{\text{set}}}{2n}\right) \tag{5.3}$$

Based on the Eqs. (4.13)and (4.15), we define $G_1 = \frac{H_1}{\beta}$ and $G_3 = \frac{H_3}{\beta}$ as follows.

$$\begin{aligned} G_1 =& f_1 \cosh(T^*\omega) - f_n \cosh(T^*\omega - T_{\text{n}}\omega) + \sum_{j=1}^{n-1} (f_{j+1} - f_j) \cosh(T^*\omega - T_j\omega), \\ G_3 =& f_1 - f_n \cosh(T_n\omega) + \sum_{j=1}^{n-1} (f_{j+1} - f_j) \cosh(T_j\omega) \end{aligned} \tag{5.4}$$

Therefore, we calculate the control coefficient, β, by Eq. (5.5) as follows.

$$\beta = \frac{\lambda(-1 + k - \cosh(T^*\omega) + k\cosh(T^*\omega))}{2kG_1 - 2G_3} \tag{5.5}$$

In addition, T_{set} in this section is defined as a known parameter. For some continuous piecewise control system, however, T_{set} is also a control coefficient we can adjust. As a future work, the equation of boundary condition thus becomes much more complex, and we need to use the Ridders' method to solve the analytical solutions of the control coefficient.

5.2 Linear Piecewise Control System and Error Analysis

First of all, the linear piecewise control system is considered as the most simplest continuous system. The general formula of the steady step period will be derived and the error of calculation will be analysed.

5.2.1 Simulate Linear Piecewise Control Systems by 11-period Stepwise Control Systems

First we design a simple linear piecewise control systems as Eq. (5.6).

$$u(t) = \begin{cases} u_0 - t & (0 \le t < T_{\text{set}}) \\ 0 & (t \ge T_{\text{set}}) \end{cases} \tag{5.6}$$

Where u_0 is the initial control torque which we can adjust. The torque decreases during the settling time, T_{set}. Then we divide T_{set} into 10 periods, and design an 11-period stepwise function. The end time of the (j_1)th period is $T_{j_1} = \frac{j_1}{10} T_{\text{set}}$, where $j_1 \in \{1, 2, 3, \cdots, 10\}$. In each period, we set a constant value which is the middle point of the linear control function in the corresponding period. Thus the constant torque u_{j_1} in the discrete function can be calculated as :$u_{j_1} = u\left(\frac{(2j_1 - 1)T_{\text{set}}}{20}\right)$. Fig. 5.1 illustrates a linear control function and its 10-period discrete function when $t < T_{\text{set}}$.

Even though there are 11 periods in the approximative discrete function totally (the last period, $u_{11} = 0$ [N·m] when $t \ge T_{\text{set}}$, is included), we can still calculate the steady step period according to Eq. (4.18) in the Chapter 4. $E_{1(11)}$, $E_{2(11)}$, $E_{3(11)}$ and H_3 are the same as Eqs. (4.17) and (4.15). Where

$$\begin{aligned} u_{j_1} &= u_0 - \frac{(2j_1 - 1)T_{\text{set}}}{20}, \\ T_{j_1} &= \frac{j_1}{10} T_{\text{set}}. \end{aligned}$$

For verifying our result, we calculated the steady step period according to the equation above and verified the data by numerical simulations of the linear piecewise control

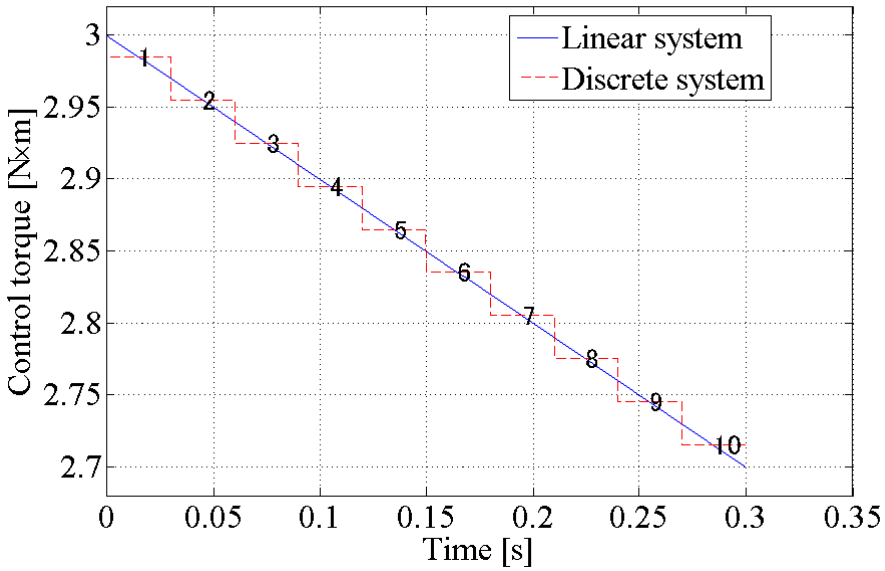

Figure 5.1: Linear control function and its approximative discrete function when $t < T_{\text{set}}$

systems. The parameters were listed in Table 3.1 and $T_{\text{set}} = 0.3$ [s]. First we set the control parameter, u_0 to 2.5, 2.9, and 3.3 [N×m] for three cases. Second, we input all the parameters in the equations and calculate the orbit of the steady step period. As the result, the red star points on the orbit of function in Fig. 5.2 were the calculation results in the three cases. Then, we conducted the simulations of the linear control system of CRW with the same parameters. Fig. 5.3 illustrated step periods of every step in three cases. When the step period did not change any more, we defined the value as the results of steady step periods in the simulation. Finally, the comparison between two sets of results of simulations and calculation were listed in Table 5.1 which illustrated that the error was less than 1%. As a result, we could analyse the steady step state based on the discretized control input when the model was driven by the linear piecewise control systems.

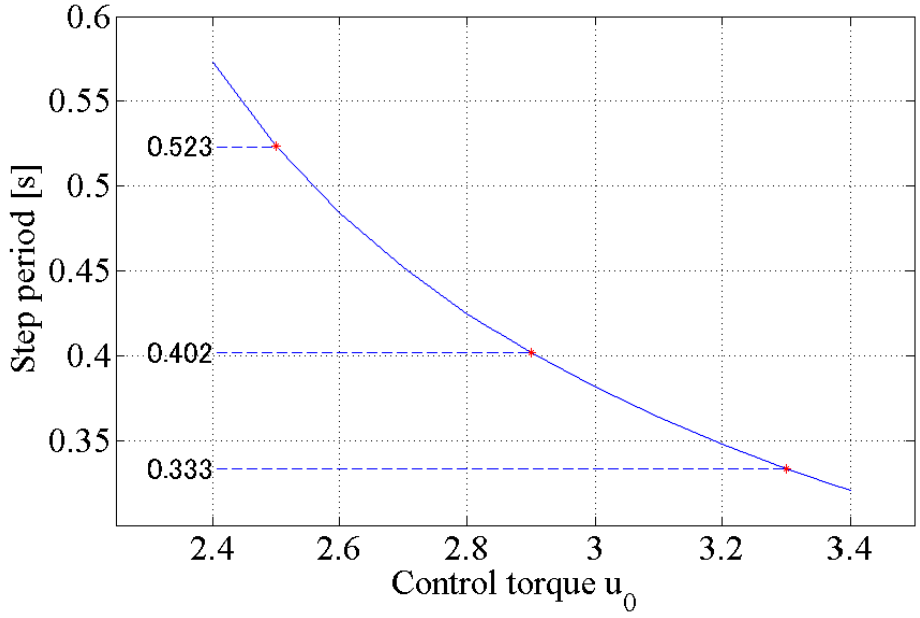

Figure 5.2: Orbit of analytical solutions T^* in the linear piecewise control systems

Table 5.1: Verification results of linear piecewise control systems

Control input u_0	2.5	2.9	3.3
T^* in simulation [s]	0.518	0.400	0.333
T^* of calculation [s]	0.523	0.402	0.333

5.2.2 Target Walking Speed in Linear Piecewise Control Systems

Furthermore, we design a linear piecewise control function as Eq. (5.7) where β is the control coefficient and b_1 are the parameters we can define in advance in the linear control system. The torque changes during the settling time, T_{set}.

$$u(t) = \begin{cases} \beta(t - b_1) & (0 \leq t < T_{\text{set}}) \\ 0 & (t \geq T_{\text{set}}) \end{cases} \tag{5.7}$$

First we divide T_{set} into 10 periods. The end time of the (j_1)th period is $T_{j_1} = \dfrac{j_1}{10} T_{\text{set}}$,

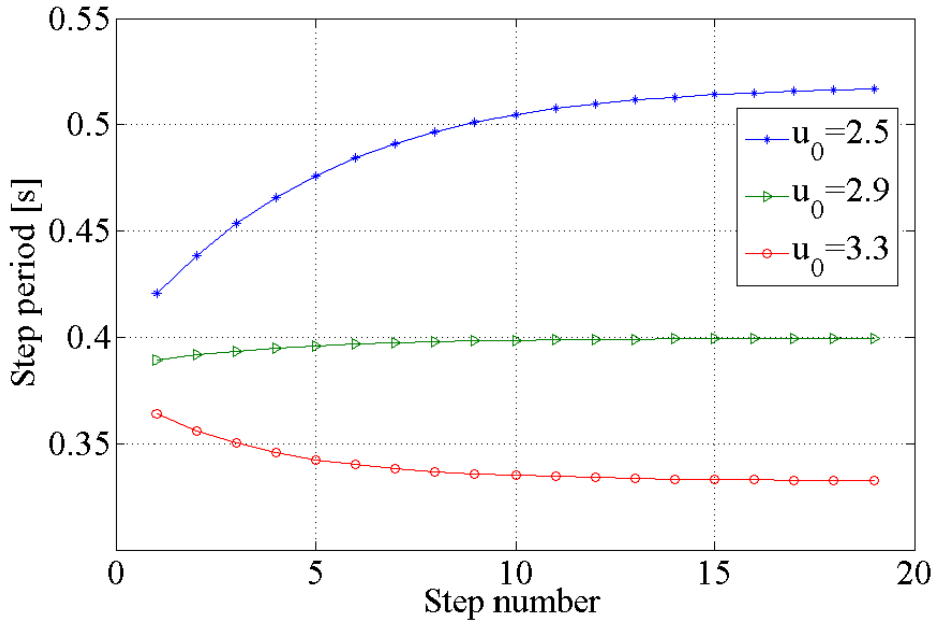

Figure 5.3: Evolutions of step periods in the simulations of linear piecewise control systems

where $j_1 \in \{1, 2, 3, \cdots, 10\}$. In each period, we set the middle point of the corresponding period as the constant control input. We can calculate the analytical solution of β by Eq. (5.5), where

$$\begin{aligned} f_{j_1} &= \frac{(2j_1 - 1)T_{\text{set}}}{20} - b_{\text{l}}, \\ T_{j_1} &= \frac{j_1}{10} T_{\text{set}}. \end{aligned}$$

For verifying our result, we calculated the control coefficient β and verified the data by numerical simulations. The parameters were listed in Table 3.1. First, we chose $T_{\text{set}} = 0.3$, target $T^* = 0.4$ [s], and set the system parameter, b_{l},, to -1, 0, and 1 for three cases. Second, we input all the parameters in the equations and calculated the orbit of the analytical solution β in Fig. 5.4. We thus chose the three red star points on the orbit to make comparison with the results of simulations. Then we conducted the simulations of CRW when it was driven by the linear control system with the analytical solutions of control coefficient and the same other conditions. Fig. 5.5 illustrated step periods of every step in three cases. Finally, we recorded simulation results in Table 5.2. The target

steady step periods were generated, and the error was less than 1.1%. As a result, we could generate the target steady walking speed when the CRW was driven by the linear piecewise control systems.

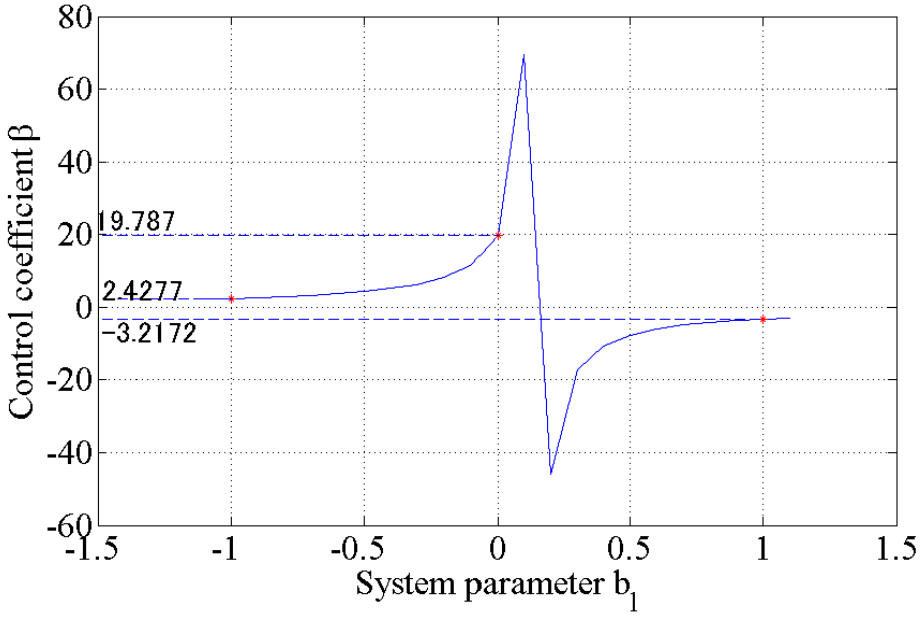

Figure 5.4: Orbit of control coefficient for a target T^* in linear piecewise control systems

Table 5.2: Verification results for a target T^* in linear piecewise control systems

System parameter b_1	-1	0	1
Control coefficient β	2.4277	19.787	-3.2172
T^* of simulations [s]	0.3981	0.3958	0.3980

5.2.3 Error Analysis

In general, when we calculate the integral of a function, if the division number is large enough, the error of the integral will be small. Therefore, a linear piecewise control system was analysed by increasing the period number and the constant torque in each

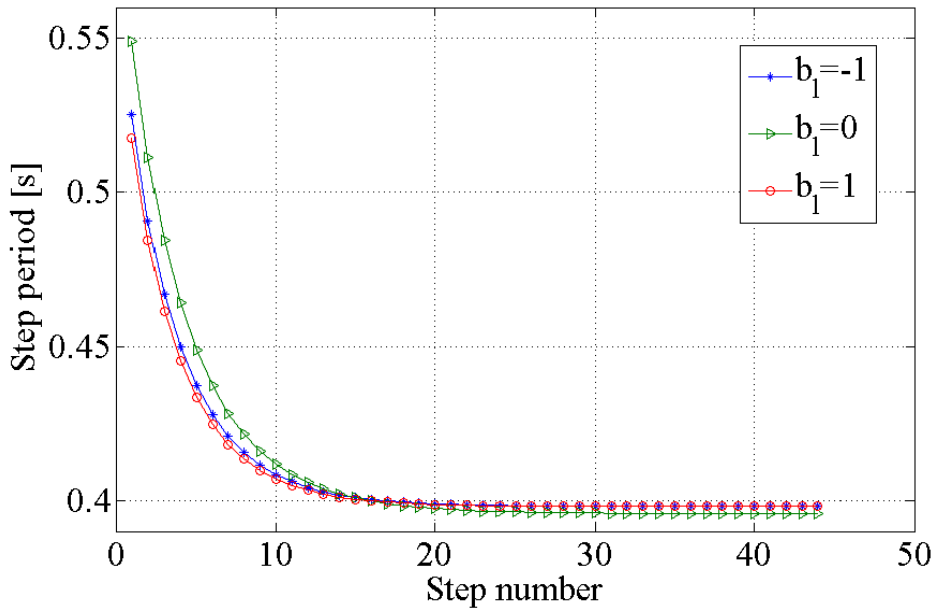

Figure 5.5: Evolutions of step period in the simulations of linear piecewise control systems for a target T^*

period in our method to decrease the error. When the system was $u(t) = 2.9 - t$ during the settling time and $T_{\text{set}} = 0.3$ [s], the CRW could thus generate a target steady step period, $T^* = 0.3996$ [s] in the simulation. The calculation could also be finished in a second even if we set the division number as 1000. Therefore we tested the error when division number is from 10 to 1000. Furthermore, we chose the first, the middle and the last point on the orbit of each period as the constant torque as Fig. 5.6 illustrated. Finally, the result was shown as Fig. 5.7. We found that the first point case, the middle point case and the last point case all converged to the same value when the division number was large enough. Therefore the different point cases could not affect the calculation result when the division number was large enough. When the division number was 1000, however, there was still a small error of 0.5% between the result of numerical simulations, because we used θ instead of $\sin\theta$ for linearization.

For the linear control system, the 11-period discrete function of the middle point case

can calculate the steady step period exactly. For most of the continuous control systems, however, we need to increase the division number in the discrete functions to reduce the error between continuous function and discrete functions. In some complex continuous control systems, we will always choose 1001-period of the middle point case stepwise control system to minimize the error.

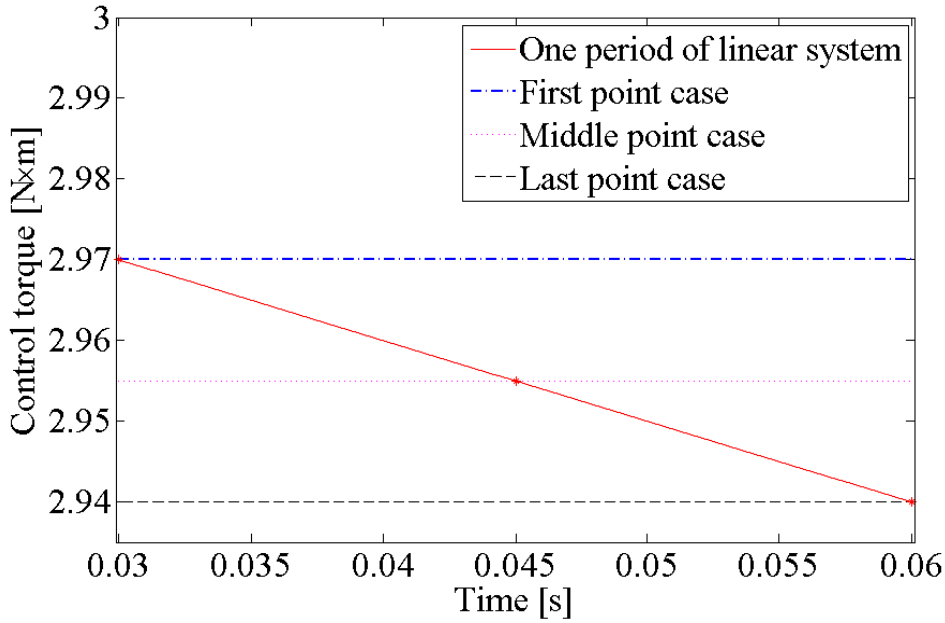

Figure 5.6: Three cases of constant torque in one period

5.3 Cosine Piecewise Control Systems

Formula of Steady Step Period in Cosine Piecewise Control Systems

A cosine piecewise control function as Eq. (5.8) is proposed. The torque changes during the settling time T_{set}. γ is the control coefficient we can adjust without any physical significance. Fig. 5.8 plots the input in one step when $\gamma = 4.0$ and $T_{\text{set}} = 0.3$ [s].

$$u(t) = \begin{cases} \gamma \cos\left(\dfrac{\pi t}{2T_{\text{set}}}\right) & (0 \le t < T_{\text{set}}) \\ 0 & (t \ge T_{\text{set}}) \end{cases} \tag{5.8}$$

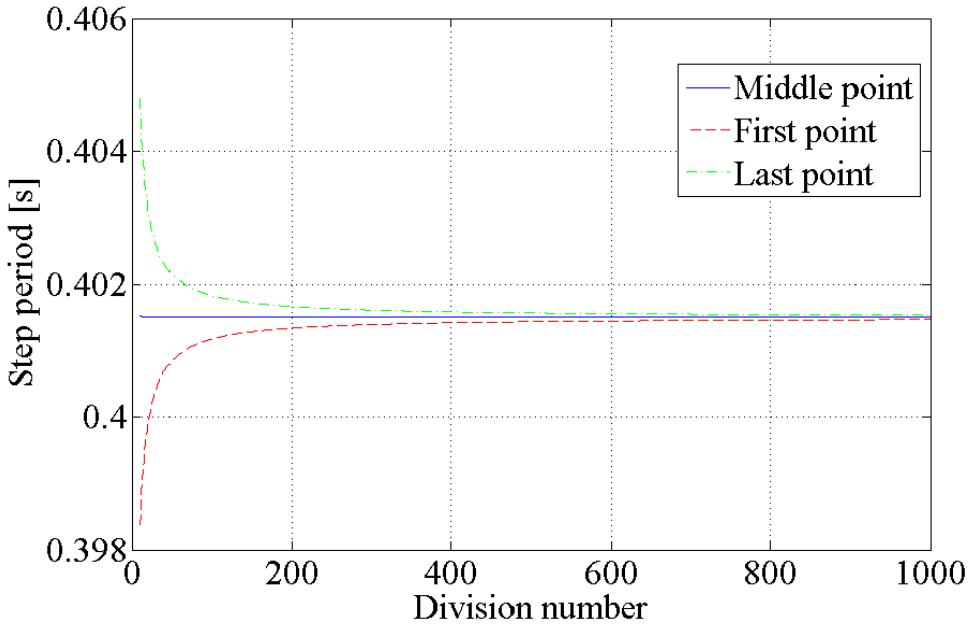

Figure 5.7: Calculation results of different division numbers and different constant torque cases

First we divided T_{set} into 1000 periods and thus designed a 1001-period stepwise control system to minimize the error. We set the middle point of the corresponding period as the constant control input in this period. The steady step period thus could be calculated by the Eq. (4.18) in Chapter 4. $E_{1(1001)}$, $E_{2(1001)}$, $E_{3(1001)}$ and H_3 were as Eqs. (4.17) and (4.15). Where

$$\begin{aligned} u_{j_2} &= \gamma \cos\left(\frac{\pi(2j_2-1)}{4000}\right), \\ T_{j_2} &= \frac{j_2}{1000} T_{\text{set}}, \\ j_2 &\in \{1, 2, 3, \cdots, 1000\}. \end{aligned}$$

Then we calculated the steady step period according to the equations above, and verified the result of calculation by numerical simulations. The value of γ was set from 4 to 5, $T_{\text{set}} = 0.3$ and the other parameters were chosen as listed in Table 3.1. We thus

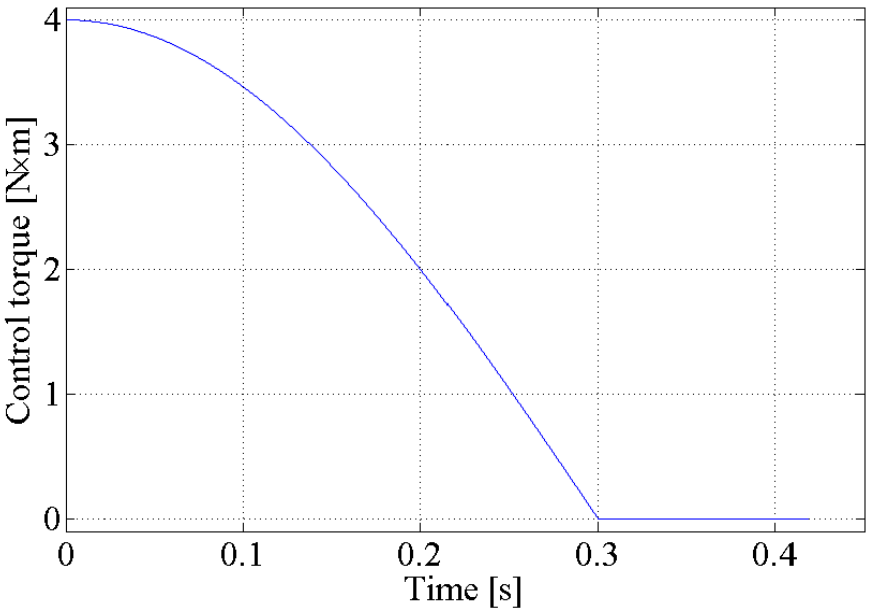

Figure 5.8: The cosine piecewise control system in one step

input all the parameters and calculated the orbit of the steady step periods in Fig. 5.9. We chose the three red star points on the orbit to make comparison with the results of simulations. Then we simulated the model of CRW driven by the cosine piecewise control systems with the three same conditions of the analytical solutions. Fig. 5.10 plotted step periods of every step in the three cases, and the convergence values were recorded as the steady step periods in the numerical simulation. Finally we made comparison between two sets of results in Table 5.3. The error between two sets of values was less than 0.4%.

Table 5.3: Verification results of T^* calculation of the cosine piecewise control systems

Control parameter γ	4	4.5	5
T^* in simulation [s]	0.417	0.355	0.311
T^* of calculation [s]	0.418	0.356	0.312

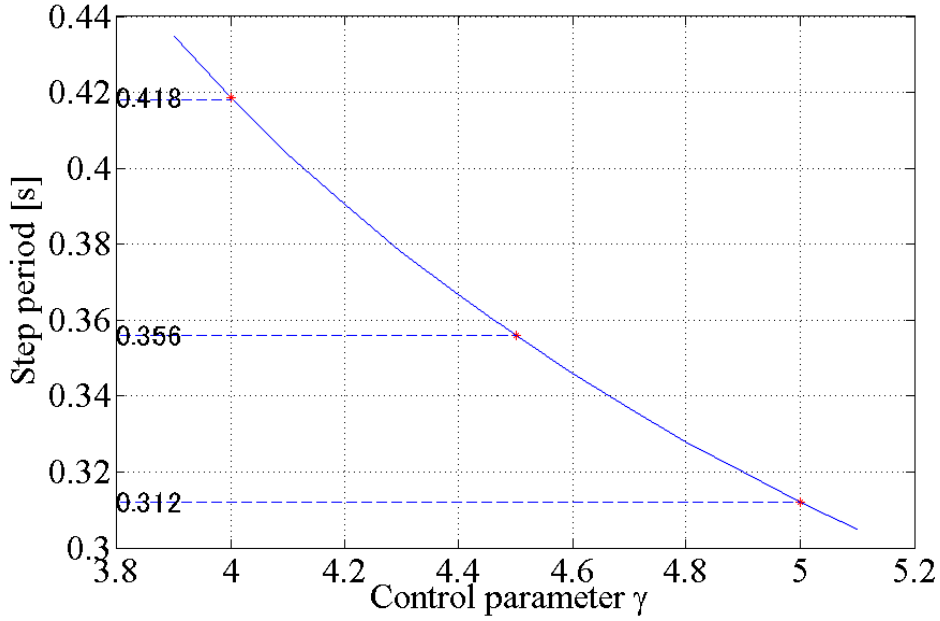

Figure 5.9: Orbit of the analytical solutions T^* in the cosine piecewise control systems

Target Walking Speed in Cosine Piecewise Control Systems

Similarly, a target walking speed can also be generated by adjusting the control coefficient of the cosine piecewise control systems. First, we design a cosine piecewise control function as Eq. (5.9). The torque changes during the settling time, T_{set}, in each step. b_{c} is the system parameter, and β is the control coefficient we can adjust to generate the target walking speeds.

$$u(t) = \begin{cases} \beta\left(\cos\left(\dfrac{\pi t}{2T_{\text{set}}}\right) + b_{\text{c}}\right) & (0 \le t < T_{\text{set}}) \\ 0 & (t \ge T_{\text{set}}) \end{cases} \tag{5.9}$$

We divided T_{set} into 1000 periods, and designed the 1001-period discrete function. The end time of the (j_2)th period is $T_{j_2} = \dfrac{j_2}{1000} T_{\text{set}}$, where $j_2 \in \{1, 2, 3, \cdots, 1000\}$. In each period, we set the middle point of the corresponding period as the constant control

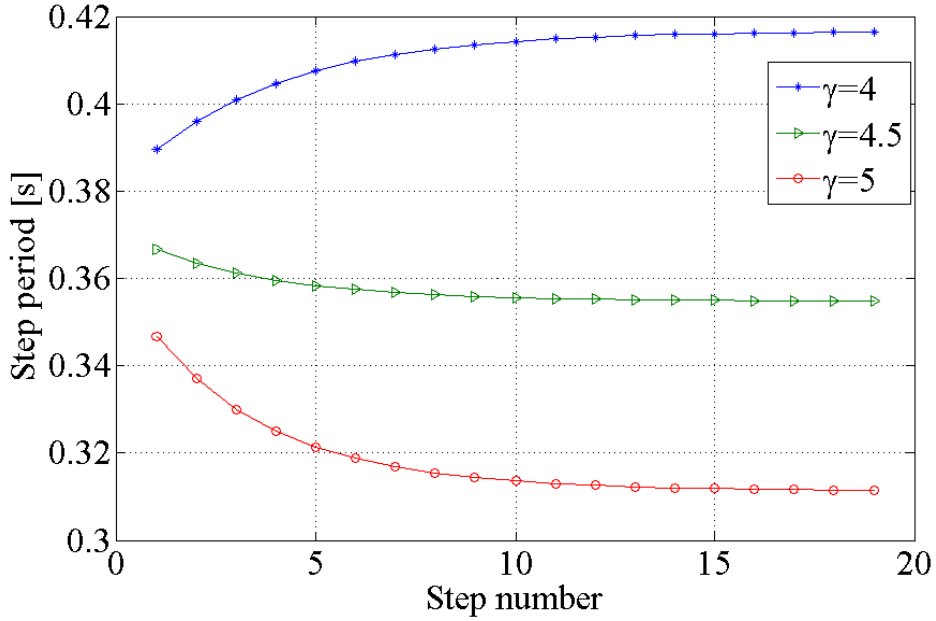

Figure 5.10: Evolutions of step periods in the simulations of the cosine piecewise control systems

input. The analytical solution of β were calculated by Eq. (5.5), where

$$f_{j_2} = \cos\left(\frac{\pi(2j_2-1)}{4000}\right) + b_{\mathrm{c}},$$
$$T_{j_2} = \frac{j_2}{1000} T_{\mathrm{set}}.$$

For verifying our result, we verified the control coefficient, β by simulations to generate the target walking speed. We chose $T_{\mathrm{set}} = 0.3$, target $T^* = 0.4$ [s], and set the system parameter b_{c} to -1, 0, and 1 for three cases. The other parameters were chosen as listed in Table 3.1. Then we input all the parameters and calculated the orbit of β in Fig. 5.11, and thus chose the three red star points on the orbit to generate simulations. Then we conducted the simulations of CRW when it was driven by the analytical solutions of control coefficient and the same other conditions with the calculation. Fig. 5.12 illustrated evolutions of step periods in the three cases. Finally we recorded simulation results in Table 5.4. The target steady step period was generated, and the error was less than 0.6%.

In general, the steady step period were calculated and the target steady walking speed were generated well when the CRW was driven by the cosine piecewise control systems.

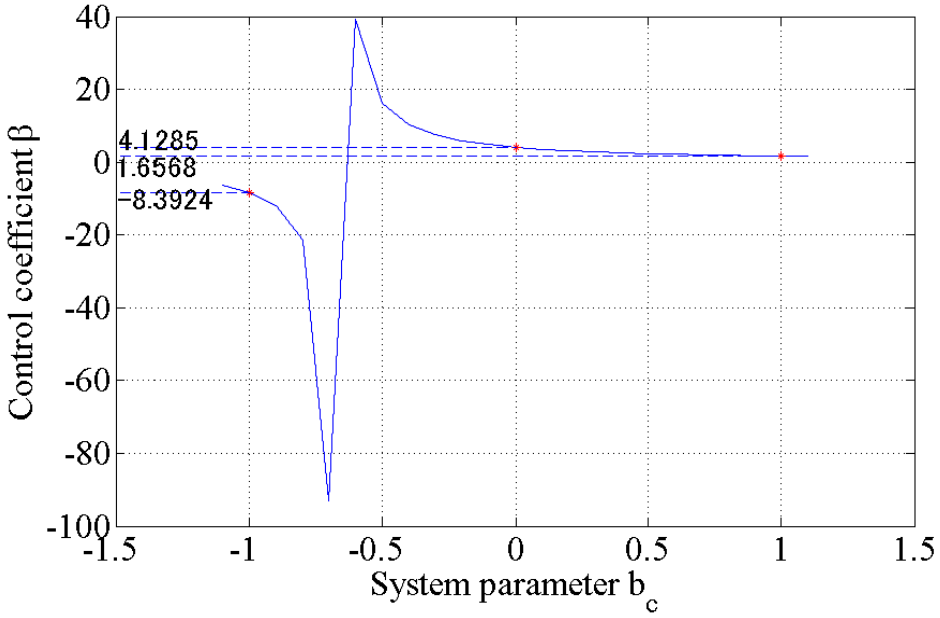

Figure 5.11: Orbit of control coefficient for a target T^* in cosine piecewise control systems

Table 5.4: Verification results of target T^* generation of the cosine piecewise control systems

System parameter b_c	-1	0	1
Control coefficient β	-8.3924	4.1285	1.6568
T^* of simulations [s]	0.3977	0.3982	0.3981

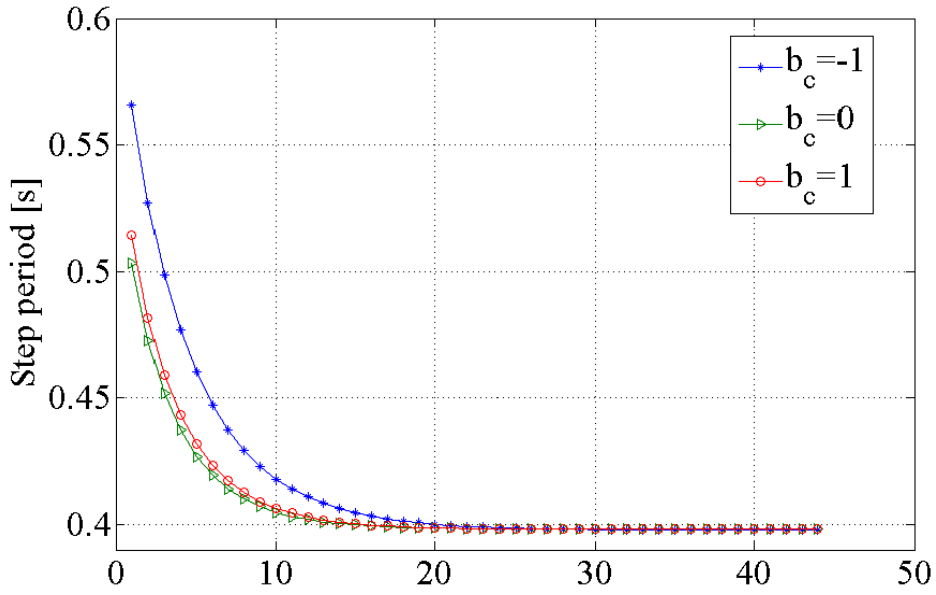

Figure 5.12: Evolutions of step period in the simulations of cosine piecewise control systems for a target T^*

Chapter 6

Feed-forward Control System

Even though the limit cycle walkers driven by open-loop control systems generated the target steady walking speed states, however, the gaits before the steady state could not be kept at a target walking speed. Different from generating a target angular position or a target angular velocity, a target walking speed for legged robot is based on an overall planning for a discrete time period and a space segment in one step. Therefore, accurately controlling the legged robot to keep a target walking speed is a complicated issue due to the irreversibility of time and space. The feed-forward control systems are thus considered as the solution because of the precise control and high energy efficiency.

6.1 Feed-forward Control System Based on Constant Control System

We begin our feed-forward control by the simplest control system, the constant control system. The torque in the (i)th step is $u = u_i \quad (0 < t \leq T_i)$, where T_i is the step period of the (i)th step and input u_i is calculated by the feed-forward control systems, for generating the target walking period state, $T_i = T_{\mathrm{s}}^*$ [35, 36]. As a result, the walker will establish a steady rolling cycle on level ground.

6.1.1 Feed-forward Solution of u_i for Target Step Period State

Considering the boundary equations in Chapter 3, the details of Eq. (3.3), the terminal boundary condition in the (i)th step, is derived as follows.

$$\frac{-2u_i + A_1 + A_2}{2l^2 M\omega^2} = \frac{\alpha}{2} \tag{6.1}$$

$$\dot{\theta}_i^+ \cosh(T_i\omega) + A_3 \sinh(T_i\omega) = \dot{\theta}_{i+1}^- \tag{6.2}$$

Where

$$\begin{aligned} A_1 &= \left(2u_i - \alpha l^2 M\omega^2\right)\cosh(T_i\omega), \\ A_2 &= 2\dot{\theta}_i^+ l^2 M\omega \sinh(T_i\omega),\ A_3 = \frac{u_i}{l^2 M\omega} - \frac{\alpha\omega}{2}. \end{aligned}$$

Based on Eq. (6.1), if $\dot{\theta}_i^+$ can be measured at the beginning of the (i)th step, we can derive u_i for generating the target step period state, $T_i = T_{\mathrm{s}}^*$, as follows.

$$u_i = \frac{l^2 M\omega(\alpha\omega(1 + \cosh(T_{\mathrm{s}}^*\omega) - 2\dot{\theta}_i^+ \sinh(T_{\mathrm{s}}^*\omega)))}{2(\cosh(T_{\mathrm{s}}^*\omega) - 1)} \tag{6.3}$$

We thus develop the feed-forward constant control system and use the function $u(\dot{\theta}_i^+, T_{\mathrm{s}}^*)$ to calculate the control torque u_i for each step. As the result, the walker can generate a limit cycle walking with the target step period T_{s}^* [41].

6.1.2 Stability Analysis of Feed-forward Constant Control System

The convergence speed in limit cycle walker is the property which can affect the stability of walking. If a limit cycle walker becomes stable in only one or two steps, then the walker has a high convergence speed and thus has a high stability. In general, we analyse the transition function of state error in one step to measure the convergence speed as follows.

First, by eliminating u_i by Eq. (6.3) in the angular velocity of the terminal boundary condition in the (i)th step in Eq. (6.2), the new equation becomes:

$$-\dot{\theta}_i^+ + \alpha\omega \coth\left(\frac{T_{\mathrm{s}}^*\omega}{2}\right) = \dot{\theta}_{i+1}^-. \tag{6.4}$$

As a result, $\dot{\theta}_i^+ + \dot{\theta}_{i+1}^-$ is constant in the limit cycle walking with the target step period T_s^*. In addition, the condition $\dot{\theta}_i^+ \leq \alpha\omega \coth\left(\frac{T_\mathrm{s}^*\omega}{2}\right)$ should be satisfied to keep $\dot{\theta}_{i+1}^- \geq 0$. Otherwise, the walker cannot finish the designed control input before the impact, and thus cannot generate the target walking speed state in this step.

When we consider the steady steps, similarly, we can also derive the same result as follows.

$$\dot{\theta}_\mathrm{eq}^- + \dot{\theta}_\mathrm{eq}^+ = \alpha\omega \coth\left(\frac{T_\mathrm{s}^*\omega}{2}\right). \tag{6.5}$$

Furthermore, we define the state error vector immediately after or before the (i)th impact as $\Delta\boldsymbol{x}_i^\pm = \boldsymbol{x}_i^\pm - \boldsymbol{x}_\mathrm{eq}^\pm$. Thus, when we subtract Eqs. (6.4) and (6.5), we can generate the transition function of state error as follows.

$$\Delta\dot{\theta}_{i+1}^- = -\Delta\dot{\theta}_i^+ \tag{6.6}$$

In addition, in the collision phase, based on the collision equation in the $(i+1)$th step and in a steady step, $\Delta\dot{\theta}_{i+1}^- = \cos\alpha\Delta\dot{\theta}_{i+1}^+$ can be derived. Therefore, the transition function of state error in the (i)th step is derived as

$$\Delta\dot{\theta}_{i+1}^+ = -\cos\alpha\Delta\dot{\theta}_i^+. \tag{6.7}$$

In general, when the initial angular velocity satisfies $0 \leq \dot{\theta}_0^+ \leq \alpha\omega \coth\left(\frac{T_\mathrm{s}^*\omega}{2}\right)$, the transition function of state error in one step is always $(-\cos\alpha)$ when the walker is driven by the feed-forward constant control systems.

6.1.3 Simulation and Verification of Feed-forward Constant Control System

Based on the function $u(\dot{\theta}_i^+, T_\mathrm{s}^*)$ in Eq. (6.3), the walker can generate a limit cycle walking at a target walking speed by the feed-forward constant control systems. To verify our results, we simulated the CRW driven by the feed-forward constant control systems and checked whether each step period was the same with our target step period or not. In the simulations, the physical parameters were chosen as listed in Table 3.1.

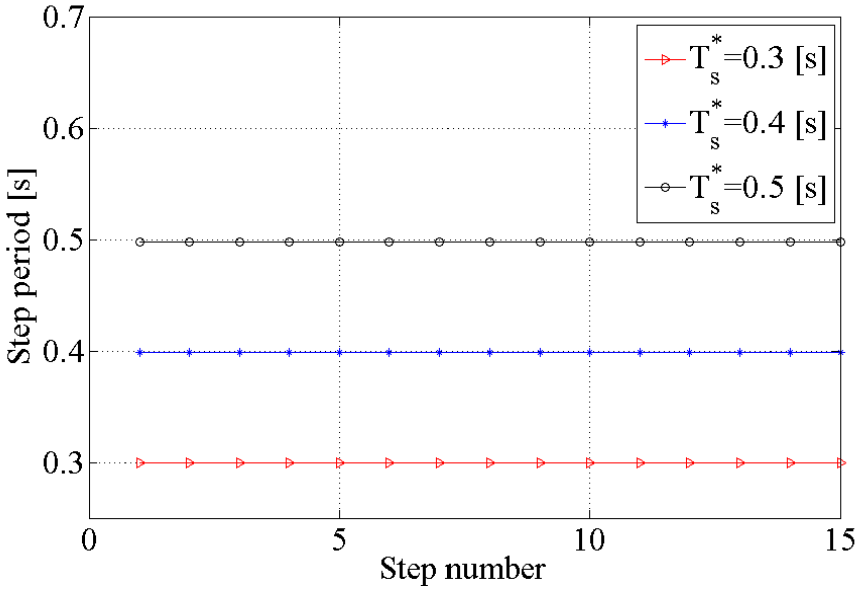

Figure 6.1: Step-evolutions of step period in the simulations driven by the feed-forward constant control systems

We chose T_s^* as 0.3, 0.4, and 0.5 [s] for the three simulations. First, we substituted T_s^* in Eq. (6.3) and designed our feed-forward constant control systems. Second, the step period of each step in the simulation were recorded in Fig. 6.1. The error between T_s^* and T^* were all less than 0.4%. As the result, the limit cycle walking at target walking speeds were generated by our feed-forward constant control systems.

In detail, the time-evolutions of control input u_i are showed in Fig. 6.2. The control inputs keep the constant torque in each step, and become asymptotically and vibrationally stable. When the control input becomes stable and constant, the walker generates the limit cycle walking. Fig. 6.3 illustrates the time-evolutions of angular velocity. We set all the initial angular velocities, $\dot{\theta}_0^+$, as 0 [rad/s].

Fig. 6.4 illustrated the step-evolutions of the angular velocity immediately before impacts. We discussed that the transition function of state error in one step was always constant when the walker was driven by the feed-forward constant control systems. As a result, all these three cases had the same convergence speed.

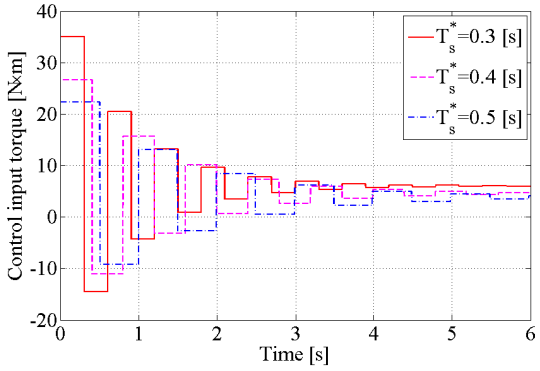

Figure 6.2: Time-evolutions of control input in the simulations driven by the feed-forward constant control systems

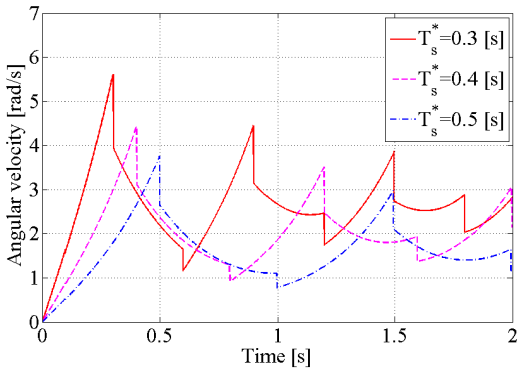

Figure 6.3: Time-evolutions of angular velocities in the simulations driven by the feed-forward constant control systems

In addition, we also tested the range of our target step period. When the initial angular velocities, $\dot{\theta}_0^+ = 0$ [rad/s], only $0 < T_s^* < 1.4$ [s] could be generated for the feed-forward constant control systems.

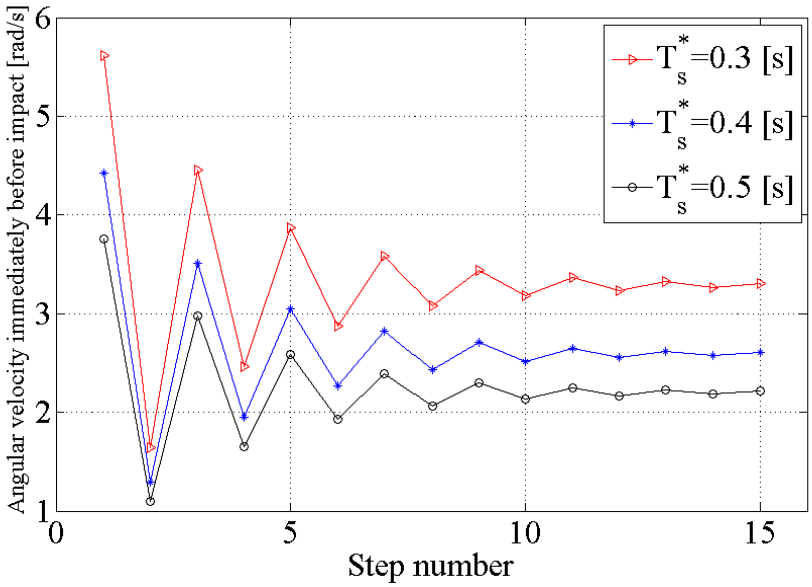

Figure 6.4: Step-evolutions of angular velocities immediately before impact in the simulations driven by the feedforward constant control systems

6.2 Feed-forward Control System based on Two-period Stepwise Control System

6.2.1 Feed-forward Two-period Stepwise Control System

We analysed the feed-forward constant control systems to calculate the control input u_i in each step for generating limit cycle walking at a target walking speed. The transition function of state error which stands for the stability of the walker, however, is uncontrollable. In the previous research [30], the two-period stepwise control system could help us to control the transfer function of state error. Therefore, we need to reconsider the two-period stepwise control system in Chapter 4 as follows to generate the limit cycle walking at a target walking speed.

$$u(t) = \begin{cases} u_i & (0 \leq t < T_{\text{set}}) \\ 0 & (t \geq T_{\text{set}}) \end{cases} \tag{6.8}$$

According to the control system in Eq. (6.8), when the time is longer than the settling time, $T_{\rm set}$, in one step, the control torque is always 0 until the next impact. Therefore, the solution of Eq. (2.2) in the (i)th step is arranged as follows.

$$\begin{aligned} \boldsymbol{x}_{i+1}^{-} &= \mathrm{e}^{\boldsymbol{A}T_i}\boldsymbol{x}_i^{+} + \int_{0^+}^{T_i} \mathrm{e}^{\boldsymbol{A}(T_i-s)}\boldsymbol{B}u(s)\ \mathrm{d}s & (6.9)\\ &= \mathrm{e}^{\boldsymbol{A}T_i}\boldsymbol{x}_i^{+} + \int_{0^+}^{T_{\rm set}} \mathrm{e}^{\boldsymbol{A}(T_i-s)}\boldsymbol{B}u_i\ \mathrm{d}s & (6.10) \end{aligned}$$

Similarly, the boundary conditions are the same as Eqs. (3.5) and (3.6). Therefore, we can derive the details of Eq. (6.10), the terminal boundary condition in the (i)th step, as follows.

$$\frac{-2u_i\cosh(T_i\omega - T_{\rm set}\omega) + A_1 + A_2}{2l^2M\omega^2} = \frac{\alpha}{2} \tag{6.11}$$

$$\dot{\theta}_i^{+}\cosh(T_i\omega) + A_3\sinh(T_i\omega) - \frac{u_i}{l^2M\omega}A_4 = \dot{\theta}_{i+1}^{-} \tag{6.12}$$

Where

$$A_4 = \sinh(T_i\omega - T_{\rm set}\omega).$$

For generating the target step period $T_i = T_{\rm s}^*$ state, $\dot{\theta}_i^{+}$ is measured at the beginning of the (i)th step, and thus u_i is derived as follows.

$$u_i = \frac{l^2M\omega(\alpha\omega(1+\cosh(T_{\rm s}^*\omega) - 2\dot{\theta}_i^{+}\sinh(T_{\rm s}^*\omega)))}{2(\cosh(T_{\rm s}^*\omega) - \cosh(T_{\rm s}^*\omega - T_{\rm set}\omega))} \tag{6.13}$$

As the result, we develop the feed-forward two-period stepwise control systems which measure $\dot{\theta}_i^{+}$ at the beginning of the (i)th step and then decide the control input torque for each step. By this control system, the walker can generate the limit cycle walking with the target step period $T_{\rm s}^*$.

6.2.2 Stability Analysis of Feed-forward Two-period Stepwise Control System

We analyse the transition function of state error for controlling the convergence speed in the feed-forward two-period stepwise control systems as follows. In order to ensure

all the control must be finished in one step, T_{set} must be satisfied $0 < T_{\text{set}} \leq T_{\text{s}}^*$, and thus $\sinh\left(T_{\text{s}}^*\omega - \dfrac{T_{\text{set}}\omega}{2}\right) \neq 0$. Therefore, when we eliminate u_i by in Eq. (6.13) in the angular velocity of the terminal boundary condition in the (i)th step in Eq. (6.12), the new equation becomes:

$$-k_1\dot{\theta}_i^+ + C_2 = \dot{\theta}_{i+1}^-. \tag{6.14}$$

Where

$$k_1 = \frac{\sinh\left(\dfrac{T_{\text{set}}\omega}{2}\right)}{\sinh\left(T_{\text{s}}^*\omega - \dfrac{T_{\text{set}}\omega}{2}\right)} \tag{6.15}$$

and C_2 is the constant item as follows.

$$C_2 = \frac{\alpha\omega\left(\cosh\left(\dfrac{T_{\text{set}}\omega}{2}\right) + \cosh\left(T_{\text{s}}^*\omega - \dfrac{T_{\text{set}}\omega}{2}\right)\right)}{2\sinh\left(T_{\text{s}}^*\omega - \dfrac{T_{\text{set}}\omega}{2}\right)} \tag{6.16}$$

As a result, $k_1\dot{\theta}_i^+ + \dot{\theta}_{i+1}^-$ is constant in our limit cycle walking with the target step period T_{s}^*. In general, the condition $\dot{\theta}_i^+ < C_2/k_1$ should be satisfied to keep $\dot{\theta}_{i+1}^- \geq 0$. Similarly, for the steady steps, we can also generate the same result as follows.

$$\dot{\theta}_{\text{eq}}^- + k_1\dot{\theta}_{\text{eq}}^+ = C_2. \tag{6.17}$$

Thus, when we subtract Eqs. (6.14) and (6.17), we can derive the transition function of state error as follows.

$$\Delta\dot{\theta}_{i+1}^- = -k_1\Delta\dot{\theta}_i^+ \tag{6.18}$$

As a result, when $T_{\text{set}} = T_{\text{s}}^*$, $k_1 = 1$. The system just becomes the same case with the feed-forward constant control system. Conversely, when T_{set} is close to 0, for example, 0.003 [s], $k_1 \approx 0$. The stability of the limit cycle walking is so high that the model can become stable in one step.

In addition, in the collision phase, based on the collision equation in the $(i+1)$th step and in a steady step, $\Delta\dot{\theta}_{i+1}^- = \cos\alpha\Delta\dot{\theta}_{i+1}^+$ can be derived. Therefore, the transition function of state error in the (i)th step is derived as

$$\Delta\dot{\theta}_{i+1}^+ = -k_1\cos\alpha\Delta\dot{\theta}_i^+. \tag{6.19}$$

As a conclusion, when the walker is driven by the feed-forward two-period stepwise control systems, the transition function of state error can be controlled by the settling time, $T_{\rm set}$.

6.2.3 Simulation and Verification of Feed-forward Two-period Stepwise Control System

We chose $T_{\rm set}$ as 0.1, 0.2, and 0.3 [s] for three simulations for generating the limit cycle walking with $T_{\rm s}^* = 0.4$ [s]. First, we substituted $T_{\rm s}^*$ and $T_{\rm set}$ into Eq. (6.13) and designed our control systems in the simulations. Second, we generated the simulations and recorded the step period of each step in the simulations in Fig. 6.5. The error between $T_{\rm s}^*$ and T^* in the simulation were all less than 0.4%. Thus, we designed the feed-forward two-period stepwise control systems for generating the limit cycle walking at a target walking speed.

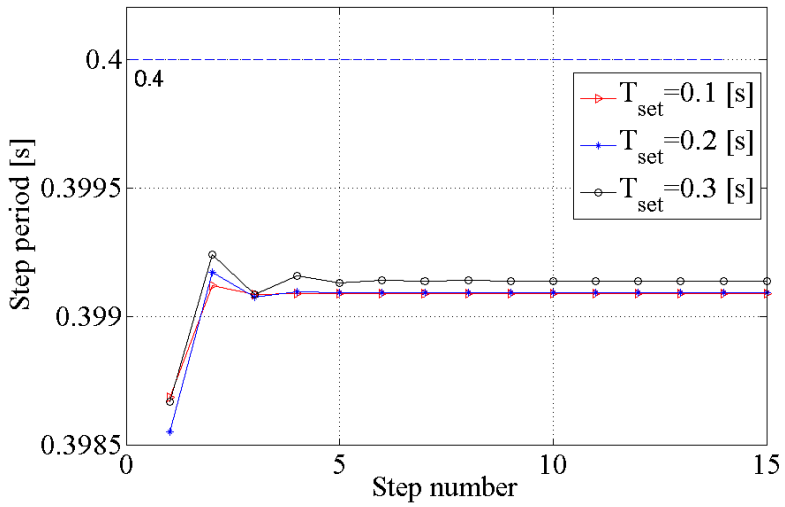

Figure 6.5: Step-evolutions of step period in the simulations driven by the feed-forward two-period stepwise control systems

In addition, the time-evolutions of control input u_i were showed in Fig. 6.6. The control inputs kept the constant torque during $T_{\rm set}$ in each step, and asymptotically and vibrationally become stable. When the control input became stable and constant,

the walker generated its limit cycle walking. Fig. 6.7 illustrated the time-evolutions of angular velocity for 4 steps. We set all the initial angular velocities, $\dot{\theta}_0^+$, as 0 [rad/s].

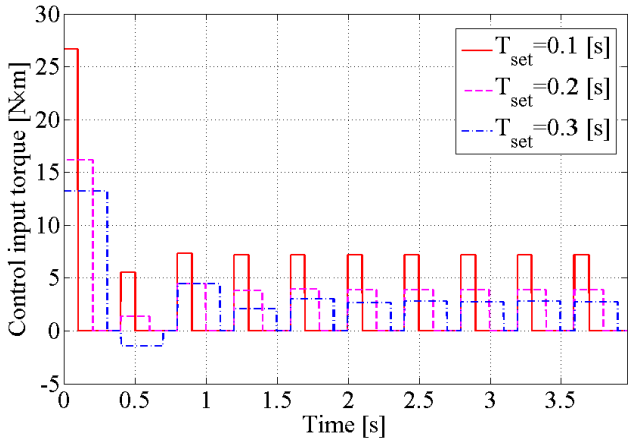

Figure 6.6: Time-evolutions of control input in the simulations driven by the feed-forward two-period stepwise control systems

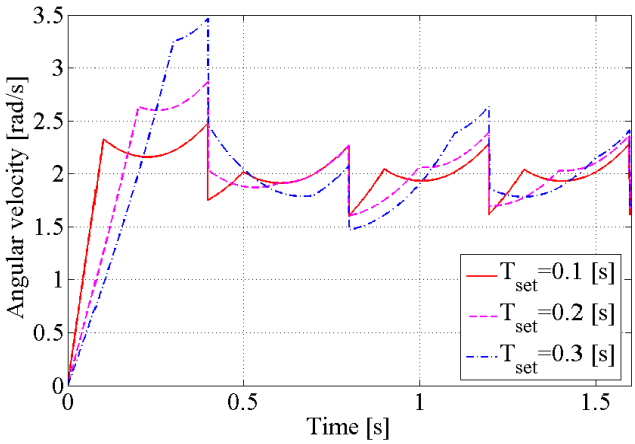

Figure 6.7: Time-evolutions of angular velocities in the simulations driven by the feed-forward two-period stepwise control systems

Fig. 6.8 illustrated the step-evolutions of the angular velocity immediately before impacts. We discussed that the transition function of state error in one step could be controlled by $T_{\rm set}$ when the walker was driven by the feed-forward two-period stepwise control systems. As a result, the case when $T_{\rm set} = 0.1$ [s] had the best convergence speed.

Furthermore, when T_{set} was very closed to 0, for example, 0.003 [s] as Fig. 6.9 illustrated, the model in this case became stable in only one step. Therefore, the transition function of state error in this case would be closed to 0. In addition, considering the condition $\dot{\theta}_0^+ \leq C_2/k_1$, the case that T_{set} was closed to 0 could deal with a fast initial angular velocity, $\dot{\theta}_0^+$, however, the input torque became large.

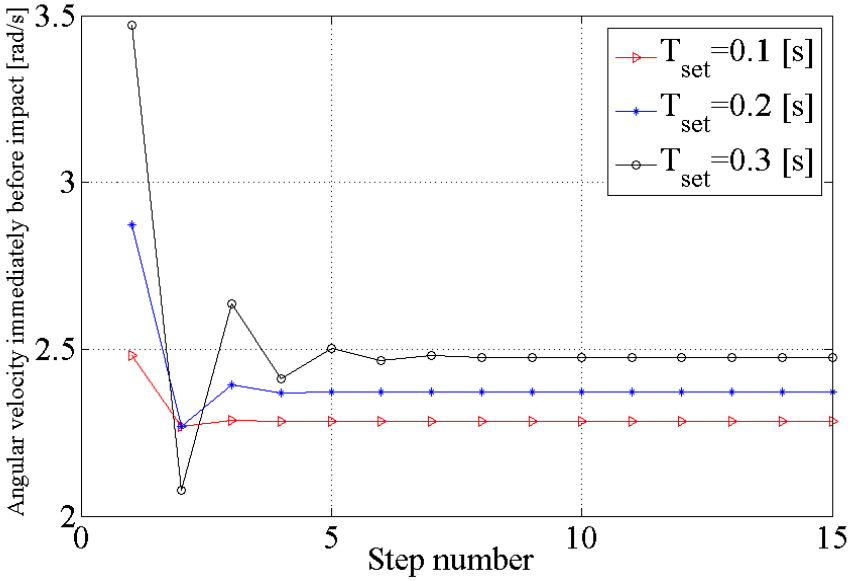

Figure 6.8: Step-evolutions of angular velocities immediately before impact in the simulations driven by the feed-forward two-period stepwise control systems whenT_{set} = 0.1, 0.2 and 0.3 [s]

6.3 Feed-forward and Feedback Control System

In the sections above the information is fed at the beginning of each step, only for one loop. The CRW thus designed the control parameters for generating a target state gait. When a disturbance happens after the feed gain, the feed-forward control cannot deal with it, and thus the target walking state cannot be generated in this step. In addition, the persistent disturbance, especially, the friction, affects the walker all the time. Therefore,

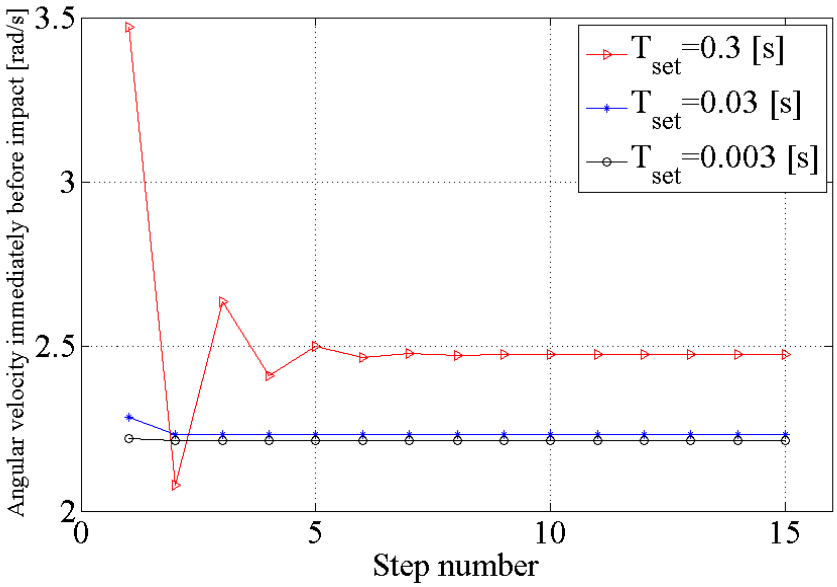

Figure 6.9: Step-evolutions of angular velocities immediately before impact in the simulations driven by the feed-forward two-period stepwise control systems when$T_{\rm set}$ =0.3, 0.03 and 0.003 [s]

as an extension, if the CRW can feed the walking state in every short moment for more loops, and thus update the control parameters by real-time, a target walking state can be generated even if there are disturbances during each step [39, 40]. In this section, we designed a feed-forward and feedback control system and tested its robustness.

Based on Eq. (6.1), if the time t and the state at t [s], $\dot{\theta}_i(t)$, can be measured every moment, and are fed to the model, the $u_i(t)$ can be derived for generating the target step period state, $T_i = T_{\rm s}^*$, as follows.

$$u_i(t) = \frac{l^2 M\omega(\alpha\omega - 2\omega\theta_i(t)\cosh((T_{\rm s}^* - t)\omega) - 2\dot{\theta}_i(t)\sinh((T_{\rm s}^* - t)\omega)))}{2(\cosh((T_{\rm s}^* - t)\omega) - 1)} \tag{6.20}$$

When t is closed to $T_{\rm s}^*$, however, $\cosh(T_{\rm r}\omega) - 1 \approx 0$ and it will cause a system error. Therefore, two solutions are proposed to solve this problem. Solution 1 (S1) which is more energy efficiency is designed for the no-disturbance case, and Solution 2 (S2) is designed for the case with large disturbance.

S1. When t is closed to T_{s}^{*} ($T_{\mathrm{r}} < 0.001$ [s]), we define $u_i(t) = 0$.

S2. A upper bound of $u_i(t)$ as $u_{\max}$ is defined. When the calculation of $u_i(t)$ is larger than $u_{\max}$, we just define $u_i(t) = u_{\max}$.

6.3.1 Simulation of Feed-forward and Feedback Control System

We chose T_{s}^{*} as 0.4 [s], and conducted the three simulations with other parameters in Table 3.1. First, we substitute T_{s}^{*} in Eq. (6.20) and design our feed-forward and feedback control systems. Then, the step period of each step in these simulations is recorded in Fig. 6.10. The error between T_{s}^{*} and T^{*} are all close 0 ($2.5\times10^{-7}\%$), which was even less than the feed-forward constant control system. Therefore the feed-forward and feedback control system could even revise the error caused by the linearized equation of motion. As the result, the limit cycle walking at target walking speeds are generated by our feed-forward and feedback control systems. In detail, the evolution of control torque and angular velocity are illustrated in Fig. 6.11 and Fig. 6.12.

6.3.2 Simulation with Disturbance

Unexpected sudden change in angular velocity

To verify the ability of handle disturbance, a simulation was conducted to test if the feed-forward constant control system could deal with an unexpected sudden change in angular velocity. The CRW was kept walking at the constant speed when $T_{\mathrm{s}}^{*} = 0.4$ [s]. Then we pushed the CRW at $t = 2.1$ [s] and made the angular velocity increase 0.5 [rad/s] suddenly without any other effect on CRW. As a result, the torque in Fig. 6.15 was changed at 2.1 [s] compared with Fig. 6.11 by feed-forward and feedback control system and thus the CRW still could keep a perfectly constant speed in each step in Fig. 6.13. In detail, the evolution of angular velocity and control torque were illustrated in Fig. 6.14 and Fig. 6.15.

Joint viscosity

In the section above we have discussed the ability of handle an unexpected sudden disturbance. In addition, a persistent disturbance is also common and has a serious impact on the precise control. In general, for the CRW, a viscous friction at the connection between the rear RW and the body frame is inevitable and thus affects the walker all the time as a persistent disturbance. Therefore, for generating the target walking speed, we need to handle the viscous friction by the feed-forward and feedback control system. In detail, the torque of the joint viscosity is defined as $f_{\mathrm{v}} = -k_{\mathrm{v}}\dot{\theta}$, and the equation of motion is arranged as follows.

$$\ddot{\theta} = \omega^2 \sin\theta + \frac{u}{Ml^2} - \frac{k_{\mathrm{v}}\dot{\theta}}{Ml^2} \tag{6.21}$$

Thus the state-space equation is revised as follows.

$$\frac{\mathrm{d}}{\mathrm{d}t}\begin{bmatrix} \theta \\ \dot{\theta} \end{bmatrix} = \begin{bmatrix} 0 & 1 \\ \omega^2 & -k_{\mathrm{v}}/Ml^2 \end{bmatrix}\begin{bmatrix} \theta \\ \dot{\theta} \end{bmatrix} + \begin{bmatrix} 0 \\ 1/Ml^2 \end{bmatrix} u. \tag{6.22}$$

Even though the equation of motion is changed, the formula of the feed-forward and feedback control system is still the same as Eq. (6.20). Then the simulations were conducted when $k_{\mathrm{v}} = 5$, $T_{\mathrm{s}}^* = 0.4$ [s] and $u_{\max}$ of Solution 2 is set as 40 and 100 [N×m] for two conditions. As a result, the step period of each step in these simulations is recorded in Fig. 6.16. When $u_{\max} = 40$, the error between T_{s}^* and T^* are around 1%, and when $u_{\max} = 100$, the error is very closed to 0. Therefore, a higher torque boundary could help the feed-forward control to perform better. In detail, the evaluation of control input, $u_i(t)$, were illustrated in Fig. 6.17 and Fig. 6.18.

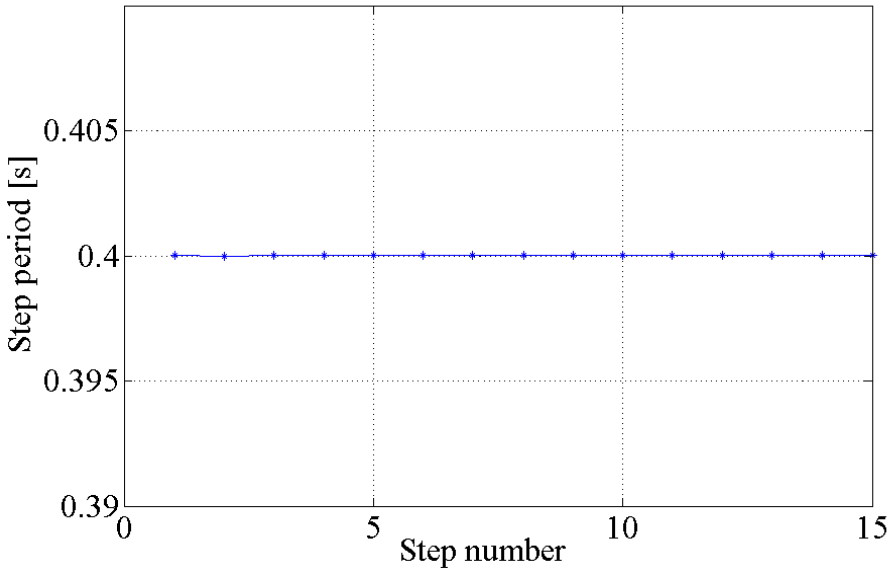

Figure 6.10: Step-evolution of step period driven by the feed-forward and feedback control systems

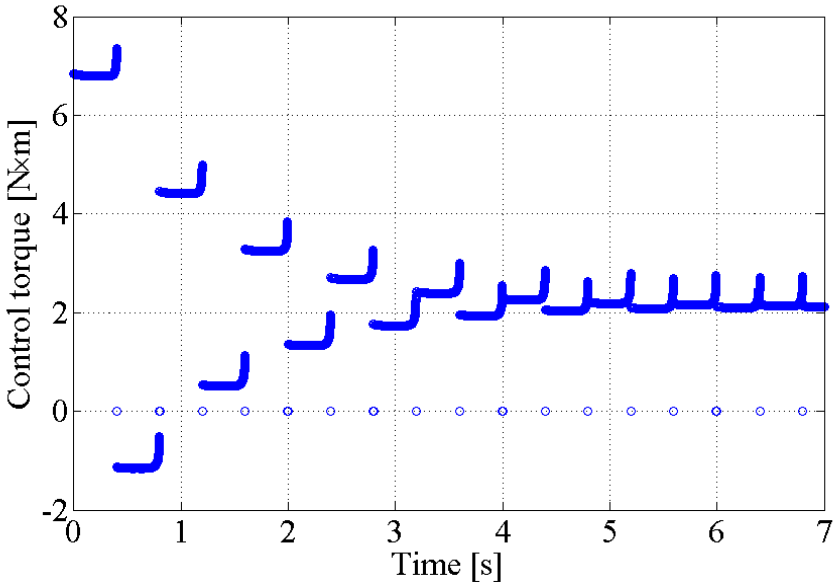

Figure 6.11: Evolution of control input driven by the feed-forward and feedback control systems

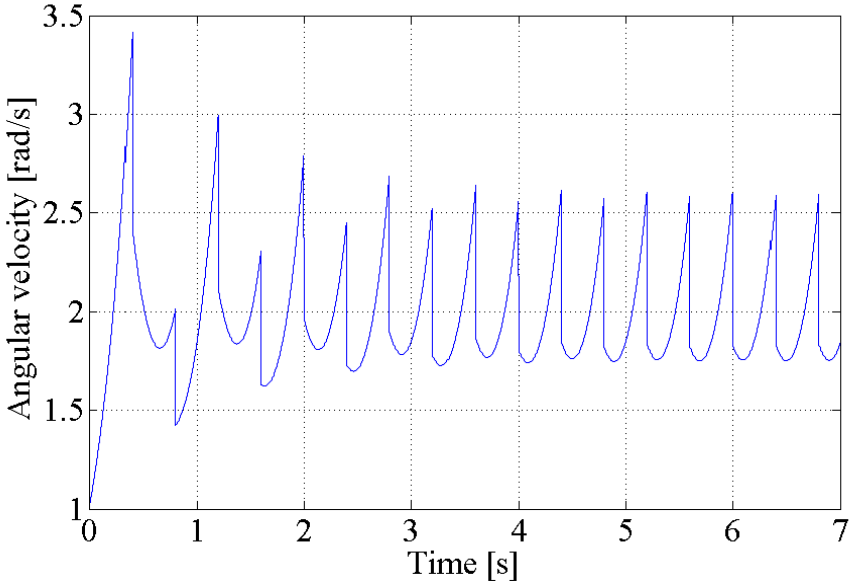

Figure 6.12: Evolution of of angular velocities driven the feed-forward and feedback control systems

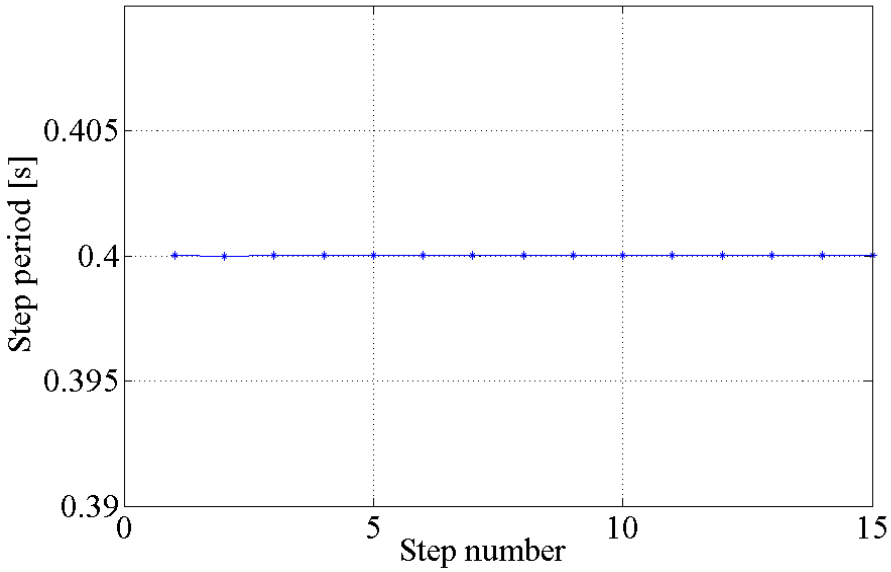

Figure 6.13: Step-evolution of step periods driven by the feed-forward and feedback control system and an unexpected disturbance

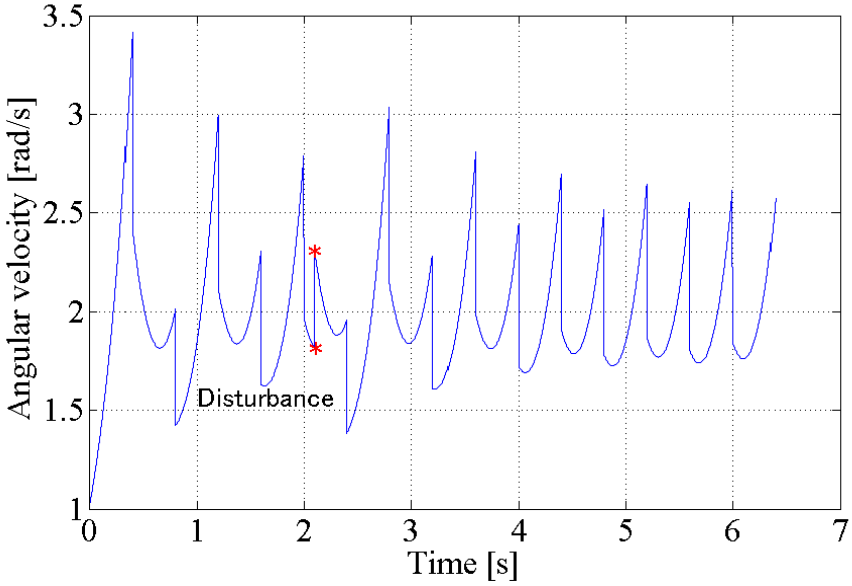

Figure 6.14: Evolution of angular velocities driven by the feed-forward and feedback control system and an unexpected disturbance

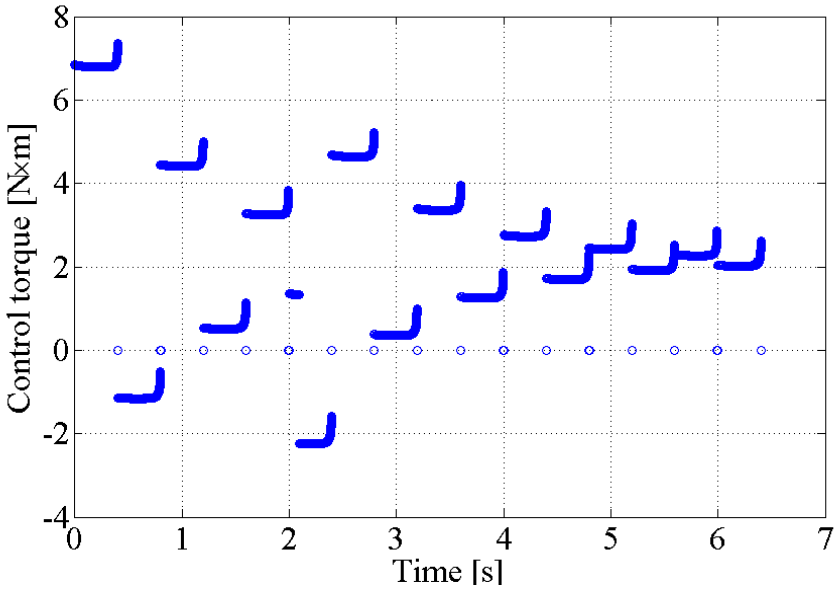

Figure 6.15: Evolution of control input driven by the feed-forward and feedback control system and an unexpected disturbance

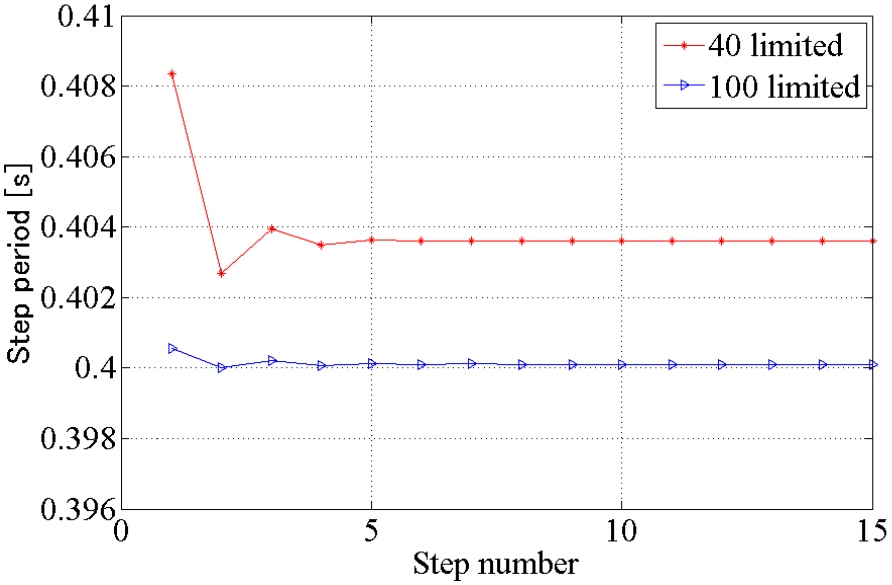

Figure 6.16: Step-evolutions of step periods driven by the feed-forward and feedback control system and joint viscosity

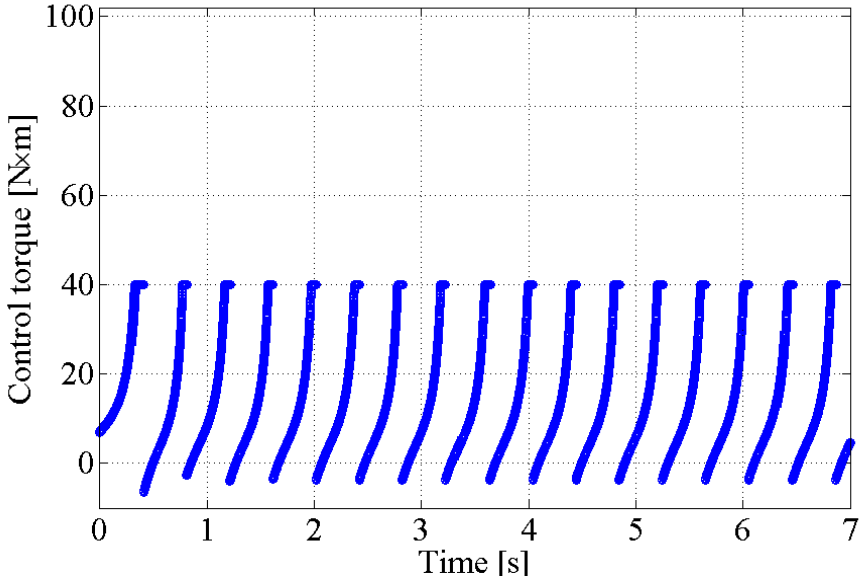

Figure 6.17: Evolutions of control input driven by the feed-forward and feedback control system and joint viscosity when $u_{\max} = 40$

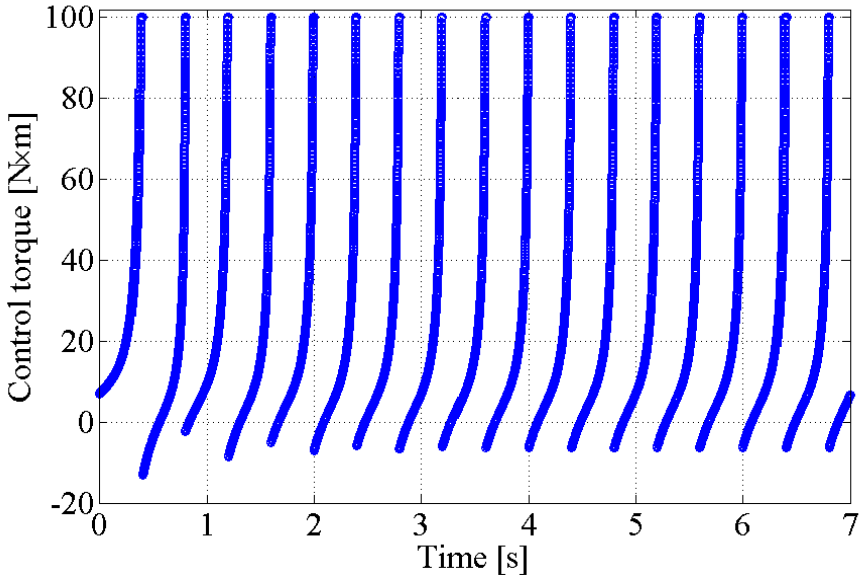

Figure 6.18: Evolutions of control input driven by the feed-forward and feedback control system and joint viscosity when $u_{\max} = 100$

Chapter 7

Extension to the Complex Model

In previous chapters, mathematical analysis of the actuated CRW driven by time-settling control systems was proposed. Gait properties were analysed mathematically and the optimal walking states were generated. In addition, the feed-forward control systems were thus proposed based the mathematical model of actuated CRW. Optimal walking states were analysed and generated by the feed-forward control systems. If the mathematical method can be extended to some more complex model, more gait properties and optimal walking states can be discovered. In previous research, underactuated rimless wheel (URW) generated deadbeat mode and could walk on the uneven ground better than the CRW. Therefore, URW is considered as an extension of our mathematical analysis model.

7.1 Underactuated Rimless Wheel

7.1.1 URW Model

Fig. 7.1 illustrates the model of an URW with a torso. This walker consists of an eight-legged rimless wheel and a torso link. The radius of the RW which is equivalent to the leg-frame length is l [m]. The relative angle between two adjacent leg frames, α, is $\pi/4$ [rad]. The mass of the RW is m_1 [kg], and that of the torso is m_2 [kg]. The total mass is

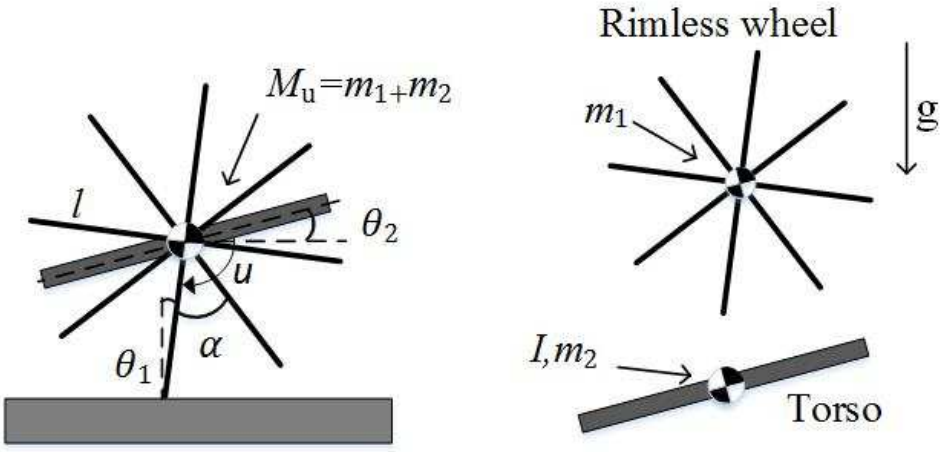

Figure 7.1: An underactuated rimless wheel (URW) model

$M_u := m_1 + m_2$ [kg]. The torso link is connected to the RW at the central position, and the moment of inertia about the joint is I [kg·m^2]. The URW can exert a joint torque between the torso and RW. We assume that the contact point of the stance leg with the ground does not slide or jump during motion. The URW model then becomes a 2-DOF system. We then define θ_1 as the angular position of the stance leg with respect to vertical, and θ_2 as the angular position of the torso link with respect to horizontal, respectively.

7.1.2 Equations of Motion and Linearization of URW

Let $\boldsymbol{\theta} = [\theta_1 \quad \theta_2]^{\mathrm{T}}$ be the generalized coordinate vector. The equation of motion then becomes

$$\begin{bmatrix} M_u l^2 & 0 \\ 0 & I \end{bmatrix} \begin{bmatrix} \ddot{\theta}_1 \\ \ddot{\theta}_2 \end{bmatrix} + \begin{bmatrix} -M_u g l \sin\theta_1 \\ 0 \end{bmatrix} = \begin{bmatrix} 1 \\ -1 \end{bmatrix} u. \tag{7.1}$$

By linearizing Eq. (7.1) around $\boldsymbol{\theta} = \dot{\boldsymbol{\theta}} = \mathbf{0}_{2\times 1}$, we derive the equation as following Eq. (7.2).

$$\begin{bmatrix} M_u l^2 & 0 \\ 0 & I \end{bmatrix} \begin{bmatrix} \ddot{\theta}_1 \\ \ddot{\theta}_2 \end{bmatrix} + \begin{bmatrix} -M_u g l & 0 \\ 0 & 0 \end{bmatrix} \begin{bmatrix} \theta_1 \\ \theta_2 \end{bmatrix} = \begin{bmatrix} 1 \\ -1 \end{bmatrix} u \tag{7.2}$$

We denote Eq. (7.2) as

$$\boldsymbol{M}_0\ddot{\boldsymbol{\theta}} + \boldsymbol{G}_0\boldsymbol{\theta} = \boldsymbol{S}u.$$

To verify our linearization calculation, we make comparisons with the results of non-linearization simulation in the following sections. There is an error due to the linearization.

7.1.3 Collision Equation of URW

We define the state vector immediately before the (i)th impact as $\boldsymbol{\theta}^{-}_{(i)} = [\theta^{-}_{1(i)} \quad \theta^{-}_{2(i)}]^{\mathrm{T}}$ and the state vector immediately after the (i)th impact as $\boldsymbol{\theta}^{+}_{(i)} = [\theta^{+}_{1(i)} \quad \theta^{+}_{2(i)}]^{\mathrm{T}}$. The subscript "$i$" in the standard brackets denotes the step number. In the collision phase, we assume that the rear leg frame at impacts (the previous stance leg) begins to leave the ground immediately after the landing of the fore leg frame (the next stance leg) according to the law of inelastic collision. We assume the following.

- The walker falls down as a 1-DOF rigid body or achieves the condition of $\dot{\theta}^{-}_{1(i)} = \dot{\theta}^{-}_{2(i)}$ immediately before the next impact.
- The torso is mechanically locked to the RW during the collision. This condition is mathematically represented by $\dot{\theta}^{+}_{1(i)} = \dot{\theta}^{+}_{2(i)}$.

Based on the above assumptions, we outline the collision dynamics. The transition equation for the angular velocity becomes

$$\dot{\theta}^{+}_{1(i)} = \dot{\theta}^{+}_{2(i)} = k_{\mathrm{u}}\dot{\theta}^{-}_{1(i)}, \quad k_{\mathrm{u}} = \frac{M_{\mathrm{u}}l^2\cos\alpha + I}{M_{\mathrm{u}}l^2 + I}. \tag{7.3}$$

Here, the transition equation for the angular positions is also determined as

$$\theta^{\pm}_{1(i)} = \mp\frac{\alpha}{2}, \quad \theta^{+}_{2(i)} = \theta^{-}_{2(i)} = 0. \tag{7.4}$$

7.1.4 Control System of URW

Let

$$y := \boldsymbol{S}^{\mathrm{T}}\boldsymbol{\theta} = \theta_1 - \theta_2$$

be the control output. The second-order derivative of y with respect to time becomes

$$\ddot{y} = \boldsymbol{S}^{\mathrm{T}}\ddot{\boldsymbol{\theta}} = \boldsymbol{S}^{\mathrm{T}}\boldsymbol{M}_0^{-1}\left(\boldsymbol{S}u - \boldsymbol{G}_0\boldsymbol{\theta}\right) \tag{7.5}$$

We then control y from $y^+ = \theta_1^+ - \theta_2^+ = -\alpha/2$ to $y^- = \theta_1^- - \theta_2^- = \alpha/2$ during every stance phase by strictly tracking to the following Eq. (7.6).

$$\ddot{y}_{\mathrm{d}}(t) = \begin{cases} \dfrac{4\alpha}{T_{\mathrm{set}}^2} & (0 \le t < \dfrac{T_{\mathrm{set}}}{2}) \\ -\dfrac{4\alpha}{T_{\mathrm{set}}^2} & (\dfrac{T_{\mathrm{set}}}{2} \le t < T_{\mathrm{set}}) \\ 0 & (t \ge T_{\mathrm{set}}) \end{cases} \tag{7.6}$$

The control input, u, for achieving $\ddot{y} = \ddot{y}_{\mathrm{d}}(t)$ can be determined as

$$\begin{aligned} u &= \frac{\ddot{y}_{\mathrm{d}}(t) + \boldsymbol{S}^{\mathrm{T}}\boldsymbol{M}_0^{-1}\boldsymbol{G}_0\boldsymbol{\theta}}{\boldsymbol{S}^{\mathrm{T}}\boldsymbol{M}_0^{-1}\boldsymbol{S}} \\ &= \frac{M_{\mathrm{u}}l^2 I}{M_{\mathrm{u}}l^2 + I}\left(\ddot{y}_{\mathrm{d}}(t) - \frac{g}{l}\theta_1\right). \end{aligned} \tag{7.7}$$

7.2 Analysis of Boundary Conditions of URW

When we substitute the u in Eq. (7.2) by Eq. (7.7), we derive a new equation as follows.

$$\ddot{\theta_1} = \hat{\omega}^2\theta_1 + I_0\ddot{y_{\mathrm{d}}}(t),\ \hat{\omega} := \sqrt{\frac{M_{\mathrm{u}}gl}{M_{\mathrm{u}}l^2 + I}},\ I_0 := \frac{I}{M_{\mathrm{u}}l^2 + I}. \tag{7.8}$$

The state-space realization of Eq. (7.8) then becomes

$$\frac{\mathrm{d}}{\mathrm{d}t}\begin{bmatrix} \theta_1 \\ \dot{\theta}_1 \end{bmatrix} = \begin{bmatrix} 0 & 1 \\ \hat{\omega}^2 & 0 \end{bmatrix}\begin{bmatrix} \theta_1 \\ \dot{\theta}_1 \end{bmatrix} + \begin{bmatrix} 0 \\ I_0 \end{bmatrix}\ddot{y}_{\mathrm{d}}(t). \tag{7.9}$$

In the following sections, we denote Eq. (7.9) as

$$\dot{\boldsymbol{x}} = \hat{\boldsymbol{A}}\boldsymbol{x} + \hat{\boldsymbol{B}}\ddot{y}_{\mathrm{d}}(t).$$

As the solution of Eq. (5.1) [29], when we define the (i)th step period as T_i, the state vector immediately before the $(i+1)$th impact, $\boldsymbol{x}_{i+1}^-$, is written by the state vector immediately after the ith impact, $\boldsymbol{x}_i^+$, as

$$\boldsymbol{x}_{i+1}^- = \mathrm{e}^{\hat{\boldsymbol{A}}T_i}\boldsymbol{x}_i^+ + \int_{0^+}^{T_i^-} \mathrm{e}^{\hat{\boldsymbol{A}}(T_i - s)}\hat{\boldsymbol{B}}\ddot{y}_{\mathrm{d}}(s)\ \mathrm{d}s. \tag{7.10}$$

The state vector at t [s], $\boldsymbol{x}(t)$, can be written by the time t and the initial state vector $\boldsymbol{x}(0)$ as

$$\boldsymbol{x}(t) = \begin{bmatrix} \theta_1(t) \\ \dot{\theta}_1(t) \end{bmatrix} = \mathrm{e}^{\hat{\boldsymbol{A}}t}\boldsymbol{x}(0) + \int_{0^+}^{t} \mathrm{e}^{\hat{\boldsymbol{A}}(t-s)}\hat{\boldsymbol{B}}\ddot{y}_{\mathrm{d}}(s)\ \mathrm{d}s. \tag{7.11}$$

The equation in the steady state also becomes

$$\begin{aligned} \boldsymbol{x}_{\mathrm{eq}}^{-} &= \mathrm{e}^{\hat{\boldsymbol{A}}T^*}\boldsymbol{x}_{\mathrm{eq}}^{+} + \int_{0^+}^{T^*} \mathrm{e}^{\hat{\boldsymbol{A}}(T^*-s)}\hat{\boldsymbol{B}}\ddot{y}_{\mathrm{d}}(s)\ \mathrm{d}s \\ &= \mathrm{e}^{\hat{\boldsymbol{A}}T^*}\boldsymbol{x}_{\mathrm{eq}}^{+} + \int_{0^+}^{\frac{T_{\mathrm{set}}}{2}} \mathrm{e}^{\hat{\boldsymbol{A}}(T^*-s)}\hat{\boldsymbol{B}}\frac{4\alpha}{T_{\mathrm{set}}^2}\ \mathrm{d}s \\ &\quad - \int_{\frac{T_{\mathrm{set}}}{2}}^{T_{\mathrm{set}}} \mathrm{e}^{\hat{\boldsymbol{A}}(T^*-s)}\hat{\boldsymbol{B}}\frac{4\alpha}{T_{\mathrm{set}}^2}\ \mathrm{d}s, \end{aligned}$$

where the subscript "eq" means the steady state and T^* means the steady step period. The initial and terminal boundary conditions in a steady step are as follows.

$$\boldsymbol{x}_{\mathrm{eq}}^{+} = \boldsymbol{x}^*(0^+) = \begin{bmatrix} \theta_1^*(0^+) \\ \dot{\theta}_1^*(0^+) \end{bmatrix} = \begin{bmatrix} -\dfrac{\alpha}{2} \\ \dot{\theta}_{1\mathrm{eq}}^{+} \end{bmatrix} \tag{7.12}$$

$$\boldsymbol{x}_{\mathrm{eq}}^{-} = \boldsymbol{x}^*((T^*)^-) = \begin{bmatrix} \theta_1^*((T^*)^-) \\ \dot{\theta}_1^*((T^*)^-) \end{bmatrix} = \begin{bmatrix} \dfrac{\alpha}{2} \\ \dot{\theta}_{1\mathrm{eq}}^{-} \end{bmatrix} \tag{7.13}$$

Thus we eliminate the $\dot{\theta}_{1\mathrm{eq}}^{-}$ and $\dot{\theta}_{1\mathrm{eq}}^{+}$ in Eqs. (7.12) and (7.13) according to the transition equation of impact. After the simplification of the initial and terminal boundary conditions based on the properties of hyperbolic functions [31], we derive the single boundary equation as follows.

$$\begin{aligned} &T_{\mathrm{set}}^2\hat{\omega}^2\left(\frac{1}{k_{\mathrm{u}}} - 1\right)(1 + \cosh(T^*\hat{\omega})) - 16I_0\cosh(\frac{T_{\mathrm{set}}}{2}\hat{\omega}) \\ &+8I_0\left(1 - \frac{\cosh(T_{\mathrm{set}}\hat{\omega})}{k_{\mathrm{u}}} + \cosh(T_{\mathrm{set}}\hat{\omega})\right) - \frac{8I_0}{k_{\mathrm{u}}}F_1 = 0 \end{aligned} \tag{7.14}$$

Where F_1 is defined to simplify the formula as following equation.

$$F_1 = \cosh(T^*\hat{\omega} - T_{\mathrm{set}}\hat{\omega}) - 2\cosh(T^*\hat{\omega} - \frac{T_{\mathrm{set}}}{2}\hat{\omega}) \tag{7.15}$$

7.3 Steady Gait Property Analysis of URW

7.3.1 Steady Step Period, T^*

To calculate T^*, we need to extract the common factors in Eq. (7.14) and the result thus becomes

$$E_{\cosh}\cosh(T^*\omega) + E_{\sinh}\sinh(T^*\omega) = E_{\mathrm{c}}. \tag{7.16}$$

Where $E_{\cosh}$ and $E_{\sinh}$ are coefficients of the hyperbolic cosine function and the hyperbolic sine function, and E_{c} (< 0) is the constant term. The details of $E_{\cosh}$, $E_{\sinh}$ and E_{c} are as follows.

$$\begin{aligned}
E_{\cosh} &= \frac{8I_0}{k_{\mathrm{u}}}\left(1 - 2\cosh\left(\frac{T_{\mathrm{set}}\hat{\omega}}{2}\right) + \cosh(T_{\mathrm{set}}\hat{\omega})\right) - \left(\frac{1}{k_{\mathrm{u}}} - 1\right)T_{\mathrm{set}}^2\hat{\omega}^2 \\
E_{\sinh} &= \frac{8I_0}{k_{\mathrm{u}}}\left(2\sinh\left(\frac{T_{\mathrm{set}}\hat{\omega}}{2}\right) - \sinh(T_{\mathrm{set}}\hat{\omega})\right) \\
E_{\mathrm{c}} &= 8I_0\left(1 - 2\cosh\left(\frac{T_{\mathrm{set}}\hat{\omega}}{2}\right) + \cosh(T_{\mathrm{set}}\hat{\omega})\right) + \left(\frac{1}{k_{\mathrm{u}}} - 1\right)T_{\mathrm{set}}^2\hat{\omega}^2
\end{aligned}$$

Finally we simplify the equation and solve the solution by computer. The positive solution is chosen and the result is as follows [31].

$$T^* = \frac{1}{\hat{\omega}}\ln\left(\frac{E_{\mathrm{c}} - \sqrt{-E_{\cosh}^2 + E_{\sinh}^2 + E_{\mathrm{c}}^2}}{E_{\cosh} + E_{\sinh}}\right) \tag{7.17}$$

In addition, if $-E_{\cosh}^2 + E_{\sinh}^2 + E_{\mathrm{c}}^2 < 0$, then the equation cannot be solved. There are two possible causes for this. The first one is that the motor cannot supply enough kinetic energy to make the URW overcome the potential barrier. The second one is the model cannot generate a one-step-cycle limit cycle walking [32]. Multi-step-cycle limit cycle walking is an important topic which is left as a future work.

7.3.2 Steady Angular Velocity Immediately after Impact, $\dot{\theta}_{\mathrm{eq}}^+$

Since we have calculated the steady step period, T^*, we can also find more details of the gait property in the steady gait. According to Eq. (7.12), we can calculate the steady

angular velocity immediately after impact, $\dot{\theta}^{+}_{1\mathrm{eq}}$ as follows.

$$\dot{\theta}^{+}_{1\mathrm{eq}} = \frac{\alpha\left(T^2_{\mathrm{set}}\hat{\omega}^2 - (8I_0 - T^2_{\mathrm{set}}\hat{\omega}^2)\cosh(T^*\hat{\omega}) - 8I_0F_1\right)}{2T^2_{\mathrm{set}}\hat{\omega}\sinh(T^*\omega)} \tag{7.18}$$

Where T^* are derived as Eq. (7.17) and F_1 is defined as Eq. (7.15).

In addition, the steady angular velocity immediately before impact, $\dot{\theta}^{-}_{1\mathrm{eq}}$ can also be calculated by $\dot{\theta}^{-}_{1(i)} = \dot{\theta}^{+}_{1(i)}/k_{\mathrm{u}}$ based on the transition equation Eq. (7.3).

7.3.3 Verification Based on Numerical Simulations

To verify our results, we made the simulation of URW and checked whether the URW generated the same steady step period with the result of the analytical solution of T^*. The physical parameters were chosen as listed in Table 7.1. With Eq. (7.17), we calculated T^* where T_{set} is the input parameter.

We chose T_{set} as 0.5, 0.65, 0.8 [s] for the three cases. First we calculated the value of T^* for these three cases. The red star points on the orbit of function in Fig. 7.2 were the calculation results.

Table 7.1: Physical parameters of URW

Parameters	Value	Unit
l	1.0	[m]
g	9.81	[m/s^2]
M_{u}	2.0	[kg]
α	$\frac{\pi}{4}$	[rad]
I	1.0	[kg·m^2]

Next, we made the simulations for these three cases. The step period converged to a constant value as illustrated in Fig. 7.3. When the step period did not change any more, it was the steady step period T^* in the simulation. Finally the comparison between two sets of values in Table 7.2 illustrated that the error was about 1%. Our equation could calculate the steady step period exactly.

Table 7.2: Verification results for analytical solution of T^* on the URW model

T_{set} [s]	0.5	0.65	0.8
T^* in function [s]	0.8845	1.097	1.366
T^* in simulation [s]	0.8836	1.094	1.357

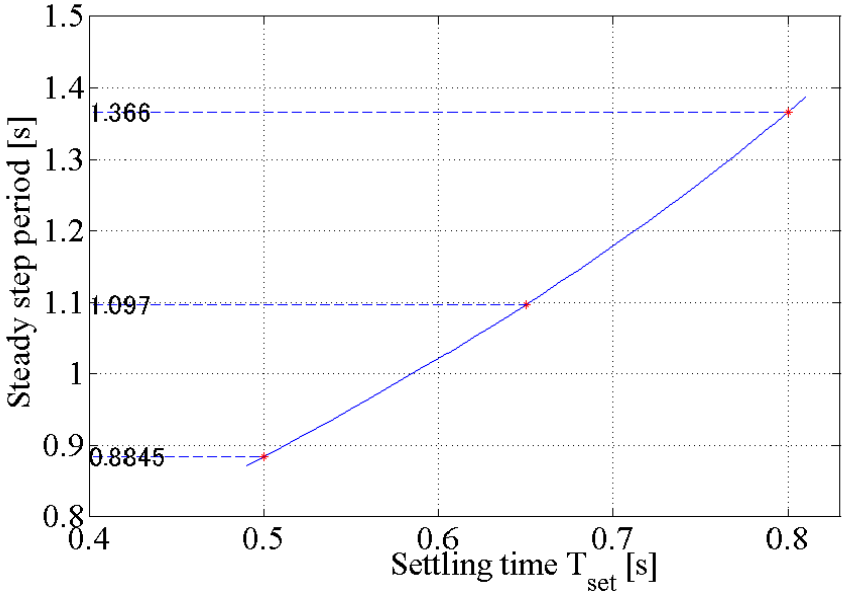

Figure 7.2: Analytical solution of T^* as a function of T_{set} on URW model

7.4 Analysis of Deadbeat Gait Generation

7.4.1 Transition Function of State Error

To drive the transition function of state error which can help us to generate a deadbeat mode, first, we need to reconsider Eq. (7.9) which was denoted as $\dot{\boldsymbol{x}} = \hat{\boldsymbol{A}}\boldsymbol{x} + \hat{\boldsymbol{B}}\ddot{y}_{\text{d}}(t)$.

As we define, $\ddot{y}_{\text{d}}(t) = 0$ when $t > T_{\text{set}}$. Thus the solution of Eq. (5.1) [29] is solved as follows.

$$\boldsymbol{x}_{i+1}^{-} = \mathrm{e}^{\hat{\boldsymbol{A}}T_i}\boldsymbol{x}_i^{+} + \int_{0^+}^{T_{\text{set}}} \mathrm{e}^{\hat{\boldsymbol{A}}(T_i - s)}\hat{\boldsymbol{B}}\ddot{y}_{\text{d}}(s)\ \mathrm{d}s. \tag{7.19}$$

Here, we define

$$\boldsymbol{\eta} = \int_{0^+}^{T_{\text{set}}} \mathrm{e}^{-\hat{\boldsymbol{A}}s}\hat{\boldsymbol{B}}\ddot{y}_{\text{d}}(s)\ \mathrm{d}s \tag{7.20}$$

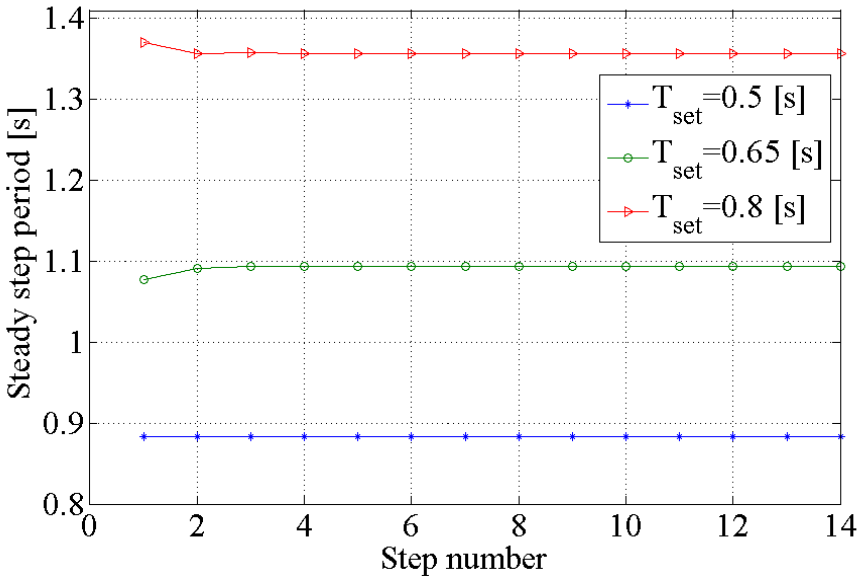

Figure 7.3: Evolutions of step periods in the simulations of URW model

. In this case, the Eq. (7.19) becomes

$$\boldsymbol{x}_{i+1}^{-} = \mathrm{e}^{\hat{\boldsymbol{A}}T_i}\left(\boldsymbol{x}_i^{+} + \boldsymbol{\eta}\right). \tag{7.21}$$

Furthermore, we define the state error vector immediately after or before the (i)th impact as $\Delta\boldsymbol{x}_i^{\pm} = \boldsymbol{x}_i^{\pm} - \boldsymbol{x}_{\mathrm{eq}}^{\pm}$ and the error of step period as $\Delta T_i = T_i - T^*$. Thus when we substitute $\boldsymbol{x}_i^{+}$ and T_i into the Eq. (7.21), the new equation after the simplification becomes

$$\begin{aligned}
\boldsymbol{x}_{i+1}^{-} &= \mathrm{e}^{\hat{\boldsymbol{A}}(T^*+\Delta T_i)}\left(\boldsymbol{x}_{\mathrm{eq}}^{+} + \eta + \Delta\boldsymbol{x}_i^{+}\right) \\
&= \mathrm{e}^{\hat{\boldsymbol{A}}\Delta T_i}\left(\mathrm{e}^{\hat{\boldsymbol{A}}T^*}\left(\boldsymbol{x}_{\mathrm{eq}}^{+} + \eta\right) + \mathrm{e}^{\hat{\boldsymbol{A}}T^*}\Delta\boldsymbol{x}_i^{+}\right) \\
&= \mathrm{e}^{\hat{\boldsymbol{A}}\Delta T_i}\left(\boldsymbol{x}_{\mathrm{eq}}^{-} + \mathrm{e}^{\hat{\boldsymbol{A}}T^*}\Delta\boldsymbol{x}_i^{+}\right).
\end{aligned}$$

Based on the approximation of $\mathrm{e}^{\hat{\boldsymbol{A}}\Delta T_i}$ as following Eq. (7.22)

$$\mathrm{e}^{\hat{\boldsymbol{A}}\Delta T_i} \approx \boldsymbol{I}_2 + \hat{\boldsymbol{A}}\Delta T_i, \tag{7.22}$$

we ignore the error term higher than second order and rearrange the equation as follows.

$$\boldsymbol{x}_{i+1}^{-} \approx \boldsymbol{x}_{\mathrm{eq}}^{-} + \hat{\boldsymbol{A}}\boldsymbol{x}_{\mathrm{eq}}^{-}\Delta T_i + \mathrm{e}^{\hat{\boldsymbol{A}}T^*}\Delta\boldsymbol{x}_i^{+} \tag{7.23}$$

According to the boundary conditions, we can know

$$\boldsymbol{x}_{i+1}^{-} = \begin{bmatrix} \dfrac{\alpha}{2} \\ \dot{\theta}_{1(i+1)}^{-} \end{bmatrix}, \quad \boldsymbol{x}_{\mathrm{eq}}^{-} = \begin{bmatrix} \dfrac{\alpha}{2} \\ \dot{\theta}_{1\mathrm{eq}}^{-} \end{bmatrix}. \tag{7.24}$$

Therefore, we define $\boldsymbol{p} = [1 \quad 0]$ and thus $\boldsymbol{p}\boldsymbol{x}_{i+1}^{-} = \boldsymbol{p}\boldsymbol{x}_{\mathrm{eq}}^{-} = \alpha/2$. When we multiply Eq. (7.23) by $\boldsymbol{p}$, the result becomes

$$\frac{\alpha}{2} = \frac{\alpha}{2} + \boldsymbol{p}\hat{\boldsymbol{A}}\boldsymbol{x}_{\mathrm{eq}}^{-}\Delta T_i + \boldsymbol{p}\mathrm{e}^{\hat{\boldsymbol{A}}T^*}\Delta\boldsymbol{x}_i^{+}. \tag{7.25}$$

Since $\boldsymbol{p}\hat{\boldsymbol{A}}\boldsymbol{x}_{\mathrm{eq}}^{-} = \dot{\theta}_{1\mathrm{eq}}^{-} \neq 0$ holds, finally we can solve ΔT_i as follows.

$$\Delta T_i = -\frac{\boldsymbol{p}\mathrm{e}^{\hat{\boldsymbol{A}}T^*}\Delta\boldsymbol{x}_i^{+}}{\boldsymbol{p}\hat{\boldsymbol{A}}\boldsymbol{x}_{\mathrm{eq}}^{-}} \tag{7.26}$$

In addition, $\Delta\boldsymbol{x}_{i+1}^{-} = \boldsymbol{x}_{i+1}^{-} - \boldsymbol{x}_{\mathrm{eq}}^{-}$. Based on Eqs. (7.23) and (7.26), we can calculate the transition function of state error as

$$\Delta\boldsymbol{x}_{i+1}^{-} = \boldsymbol{Q}\Delta\boldsymbol{x}_i^{+}, \tag{7.27}$$

where

$$\boldsymbol{Q} = \left(\boldsymbol{I}_2 - \frac{\hat{\boldsymbol{A}}\boldsymbol{x}_{\mathrm{eq}}^{-}\boldsymbol{p}}{\boldsymbol{p}\hat{\boldsymbol{A}}\boldsymbol{x}_{\mathrm{eq}}^{-}}\right)\mathrm{e}^{\hat{\boldsymbol{A}}T^*}. \tag{7.28}$$

Since we only need to consider about the angular velocity, we define $\boldsymbol{v} = [0 \quad 1]^{\mathrm{T}}$ and finally we can derive the transition function of angular velocity error as

$$\Delta\dot{\theta}_{i+1}^{-} = \bar{Q}\Delta\dot{\theta}_i^{+}, \quad \bar{Q} := \boldsymbol{v}^{\mathrm{T}}\boldsymbol{Q}\boldsymbol{v}. \tag{7.29}$$

7.4.2 Deadbeat Gait Generation

According to the previous research of McGeer, when $0 < \bar{Q} < 1$, the walker is in the speed mode, and when $-1 < \bar{Q} < 0$, the walker is in the totter mode. Asano and Xiao proposed a new mode, deadbeat mode, when $\bar{Q} = 0$. In this mode, the walker can keep the stable gait perfectly and recover from the disturbance only in one step. Obviously, a deadbeat mode is a kind of optimal state.

When we substitute the parameters into Eq (7.29), the equation of $\bar{Q}$ becomes

$$\bar{Q} = \cosh(\hat{\omega}T^*) - \frac{\hat{\omega}\theta_{1\mathrm{eq}}^-}{\dot{\theta}_{1\mathrm{eq}}^-}\sinh(\hat{\omega}T^*). \tag{7.30}$$

In the section above, we derived the formulas of T^* and $\dot{\theta}_{1\mathrm{eq}}^-$ as Eqs. (7.17) and (7.18) in the stable step state. Therefore, we can calculate $\bar{Q}$ mathematically. When $\bar{Q} = 0$, the value of T_{set} is solved as 0.751 [s] by Ridders' Method.

We then tried to verify the result using simulations. We set all the parameters as shown in Table 3.1 and plotted the figure of T_{set}-evolution of $\bar{Q}$ in Fig. 7.4. $\bar{Q} = 0$ when T_{set} was around 0.751 [s]. Thus we set $T_{\mathrm{set}} = 0.751$ [s] and run the simulation. The model generated a fast convergent gait; however, it did not generate a strict deadbeat mode since there was an error due to the linearization. We also tested other value around 0.751, and found the deadbeat mode when $T_{\mathrm{set}} = 0.753$ [s]. In this case the walker reached stability in only one step. Both the step-evolutions of $\dot{\theta}_1^-$ in the simulations were shown in Fig. 7.5.

7.5 Target Steady Walking Speed

For a URW model, the steady walking speed can also be calculated by the ratio of the step length to the step period of the URW. Therefore, generating a target steady step period is the equivalent of generating a target walking speed. We can calculate the steady step period, T^*, when we know the value of T_{set}. On the contrary, setting the value of T_{set} to generate a target steady step period is still an unclear issue. We will solve this issue in this section.

7.5.1 Target Steady Step Period

The mathematical analysis illustrates that there is a one-to-one relationship between T_{set} and T^*. Based on the expression on the left side of Eq. (7.14), we develop a function of

the boundary condition, $F_{\mathrm{c}}(T_{\mathrm{set}}, T^*)$ as follows.

$$\begin{aligned} F_{\mathrm{c}}(T_{\mathrm{set}}, T^*) &= 8I_0\left(1 - \frac{\cosh(T_{\mathrm{set}}\hat{\omega})}{k - \mathrm{u}} + \cosh(T_{\mathrm{set}}\hat{\omega})\right) \\ &\quad + T_{\mathrm{set}}^2\hat{\omega}^2\left(\frac{1}{k_{\mathrm{u}}} - 1\right)(1 + \cosh(T^*\hat{\omega})) \\ &\quad - 16I_0\cosh(\frac{T_{\mathrm{set}}}{2}\hat{\omega}) - \frac{8I_0}{k_{\mathrm{u}}}F_1 \end{aligned}$$

Where F_1 is defined in Eq. (7.15). For each pair of T_{set} and T^*, $F_{\mathrm{c}}(T_{\mathrm{set}}, T^*) = 0$.

7.5.2 Verification for Target Steady Step Period

To verify our results, we generated a target steady step period $T^* = 1.6$ [s]. The other parameters were listed in the Table 7.1. Thus, the value of T_{set} was solved as $T_{\mathrm{set}} = 0.8976$ by Ridders' Method.

For the verification, Fig. 7.6 plotted the step-evolution of the step periods in the numerical simulation when $T_{\mathrm{set}} = 0.8976$ [s]. Through the root of Ridders' Method, we generated the target steady step period $T^* = 1.584$ [s] in the simulation. The error of 1% was caused by the linearization of the equation.

7.6 Feed-forward Control on URW

Similar with the CRW, the T_{set} in the (i)th step can also be calculated by the feed-forward control systems at the beginning of one step, for generating the target walking period state, $T_i = T_{\mathrm{s}}^*$ [39, 40].

7.6.1 URW Walks on Level Ground

Based on the boundary conditions introduced in Eqs. (7.12) and (7.13), the general function is designed as follows.

$$\begin{aligned} F_{\mathrm{URW}}(T_{\mathrm{set}}) &= \frac{1}{T_{\mathrm{set}}^2\hat{\omega}^2}\left(4\alpha I_0 + \theta^+_{\mathrm{URW(i)}}T_{\mathrm{set}}^2\hat{\omega}^2\right)\cosh(T_{\mathrm{s}}^*\hat{\omega}) \\ &+ 4\alpha F_1 + \dot{\theta}^+_{\mathrm{URW}}T_{\mathrm{set}}^2\hat{\omega}\sinh(T_{\mathrm{s}}^*\hat{\omega}) - \theta^-_{\mathrm{URW(i+1)}} \end{aligned}$$

Where $\theta^{+}_{\mathrm{URW(i)}} = -\dfrac{alpha}{2}$ and $\theta^{-}_{\mathrm{URW(i+1)}} = \dfrac{alpha}{2}$ are the angular positions immediately after and before impacts in the (i)th step on level ground. Therefore, $F_{\mathrm{URW}}(T_{\mathrm{set}}) = 0$ means the URW arrivals to the angular position immediately before impacts in the $(i+1)$th at T^{*}_{s}, and the settling-time T_{set} can thus generate a target step period, T^{*}_{s} in the (i)th step. As a continuous function, $F_{\mathrm{URW}}(T_{\mathrm{set}}) = 0$, the root of T_{set} in each step can be calculated by Ridders' method.

The simulation was conducted to verify the result. We set all the initial angular velocities, $\dot{\theta}^{+}_{0}$, as 0 [rad/s], and chose T^{*}_{s} as 1.0 [s] for generating the target limit cycle walking speed. First, we substituted T^{*}_{s} into $F_{\mathrm{URW}}(T_{\mathrm{set}}) = 0$ and generated the simulations by solving the value of T_{set} by Ridders' method at the beginning of each steps. Second, we recorded the step period of each step in the simulations in Fig. 7.7. The error between T^{*}_{s} and T_i in the simulation were all less than 2%. Thus, we designed the feed-forward control systems on the URW for generating the limit cycle walking at target walking speeds. In addition, the time-evolutions of control input u_i were showed in Fig. 7.8.

7.6.2 URW Walks on Uneven Ground

When the initial and terminal angular positions,$\theta^{+}_{\mathrm{URW(i)}}$ and $\theta^{-}_{\mathrm{URW(i+1)}}$ can also be known and fed, we can even generate a target walking speed on uneven ground. In that case, the general function is designed as follows.

$$\begin{aligned} F_{\mathrm{URW}}(T_{\mathrm{set}}, \theta^{+}_{\mathrm{URW}(i)}, \theta^{-}_{\mathrm{URW}(i+1)}) = \frac{1}{T^{2}_{\mathrm{set}}\hat{\omega}^{2}} \left(4\alpha I_0 + \theta^{+}_{\mathrm{URW}(i)} T^{2}_{\mathrm{set}}\hat{\omega}^{2}\right) \cosh(T^{*}_{\mathrm{s}}\hat{\omega}) \\ +4\alpha F_1 + \dot{\theta}^{+}_{\mathrm{URW}(i)} T^{2}_{\mathrm{set}}\hat{\omega} \sinh(T^{*}_{\mathrm{s}}\hat{\omega}) - \theta^{-}_{\mathrm{URW}(i+1)} \end{aligned} \tag{7.31}$$

Then, $F_{\mathrm{URW}}(T_{\mathrm{set}}, \theta^{+}_{\mathrm{URW}(i)}, \theta^{-}_{\mathrm{URW}(i+1)}) = 0$ is analysed and the solution of T_{set} is solved by Ridder's method at the beginning of each step. Thus, based on the condition of the uneven ground, the URW derives the settling-time in each step and generates the target walking speed on the uneven ground [38, 42].

The simulations were conducted for verifying the results. First, we designed a random uneven ground. The slope in each step was a random value between -0.05 and 0,05 [rad] in

each step. The initial condition of the URW was standing on level ground and the initial angular velocity was 0.85 [rad/s]. The target step period, T_{s}^{*} was set as 1.0 [s]. The other parameters were the same with the Table 7.1. Then, we generated the simulations. To make the comparison, a simulation of the URW driven by a no-feed control system which generated a target constant step period 1.0 [s] (Section 7.5) was also conducted walking on the same uneven ground. The evaluations of step period in both cases were recorded in Fig. 7.9. As a result, the error between T_i and T_{s}^{*} of the feed-forward case was only around 3%, which was caused by the linearized equation of motion. Conversely, the URW driven by no-feed control systems could not generate a steady gait.

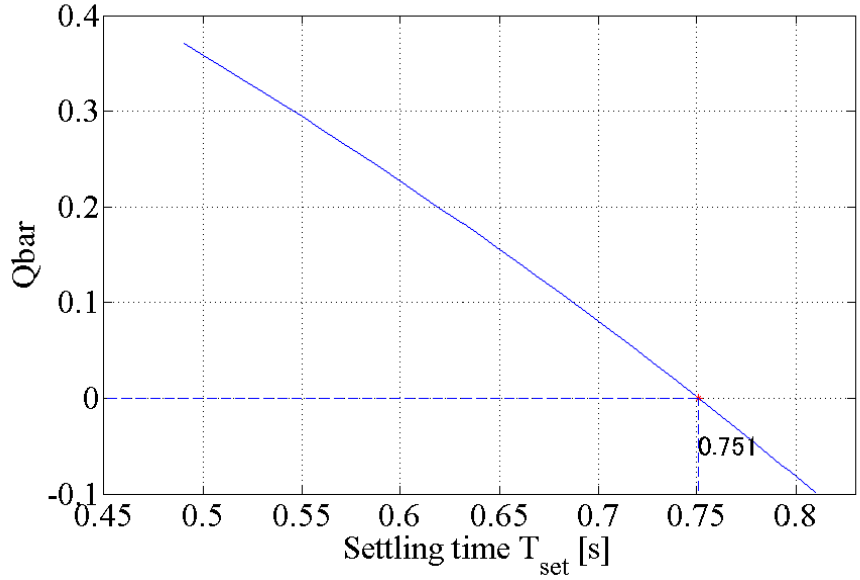

Figure 7.4: Analytical solution of $\bar{Q}$ as a function of T_{set} on URW model

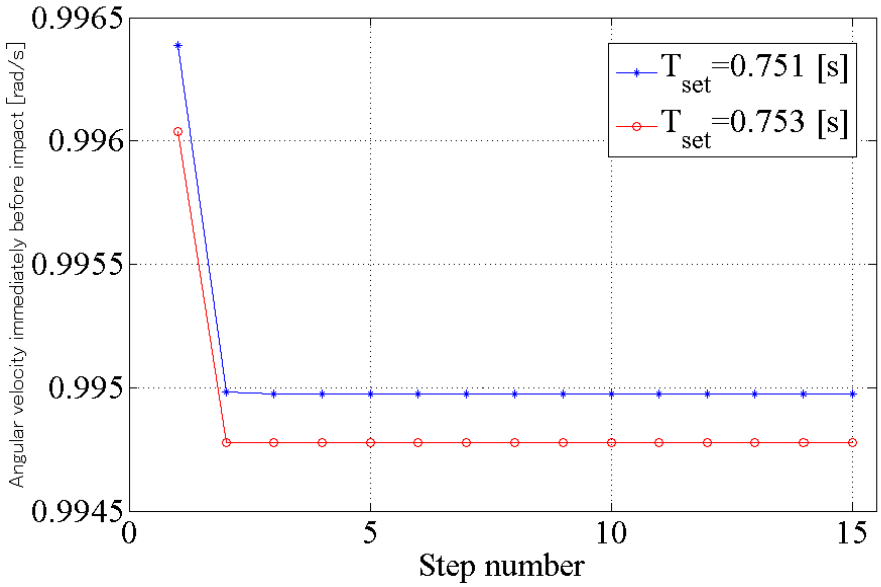

Figure 7.5: Step-evolutions of $\dot{\theta}_1^-$ for deadbeat mode generation in the simulations of URW model

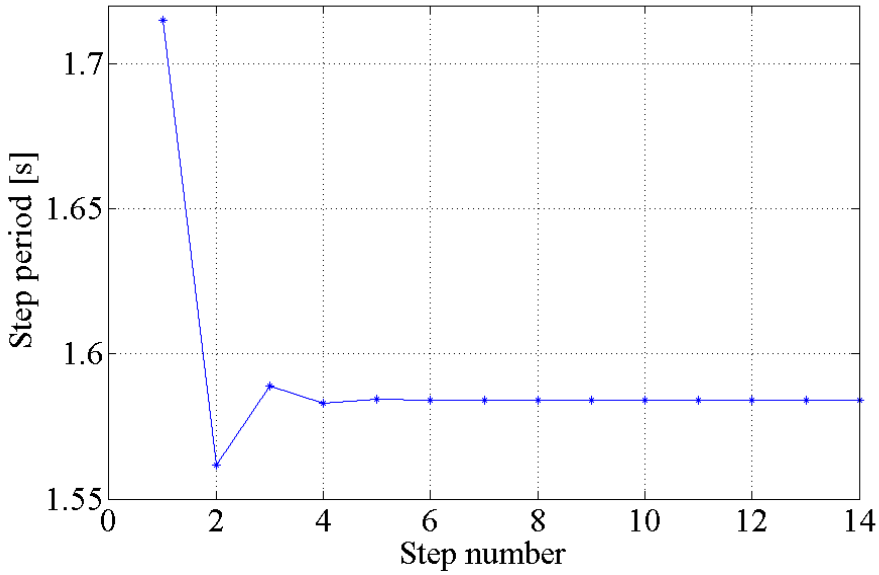

Figure 7.6: Step-evolutions of step periods for target walking speed in the simulations of URW model

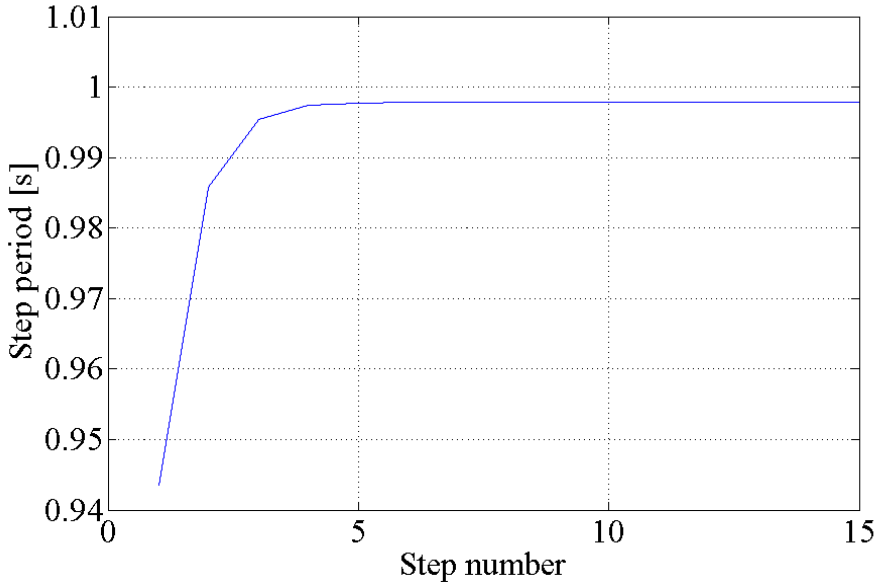

Figure 7.7: Step-evolution of step period in the simulations driven by the feed-forward control system on URW

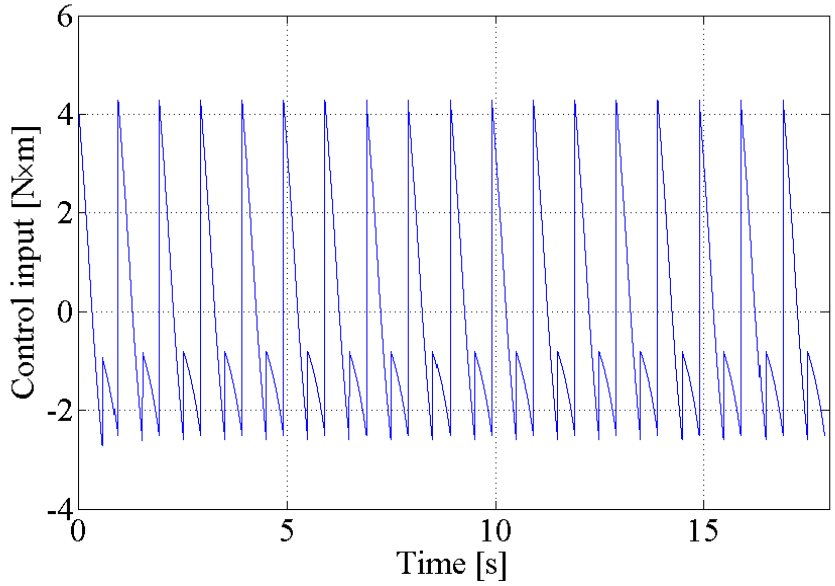

Figure 7.8: Evolution of control input in the simulations driven by the feed-forward control system on URW

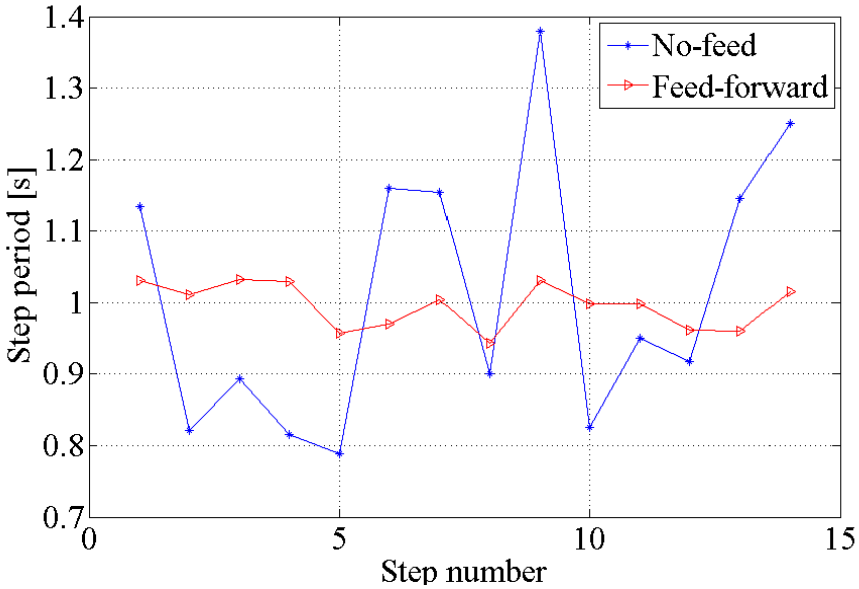

Figure 7.9: Step-evolutions of step periods driven by the feed-forward control system and no-feed control system on URW

Chapter 8

Conclusion and Future Work

8.1 Conclusion

In this thesis, first, mathematical analysis of the actuated CRW driven by time-settling control systems was proposed. Gait properties were analysed mathematically and the optimal walking states were generated. Second, the feed-forward control systems were thus proposed based the mathematical model of actuated CRW. Optimal walking states were analysed and generated by the feed-forward control systems. Finally, the mathematical analysis was extended to an URW successfully by analysing and generating optimal walking states and proposing the limit-cycle-walking-based feed-forward control systems.

The originality in this thesis are listed as follows.

- The thesis proposed a general method of analysing the mathematical model of actuated limit cycle walking. Through the analysis of discrete control systems, the general formula was proposed for all discrete control systems. Thus when the control input of the continuous control systems was discretized, the mathematical model of the continuous control systems could be built by the general formula of the discrete control systems.

- Feed-forward control which was based on the mathematical model of walkers could inherit the high energy efficiency of limit cycle walking and improved the ability of

handle disturbance of walkers by feed gains. In addition, the mathematical analysis of limit cycle walking could help to discover and generate more optimal walking states. The extension of the mathematical analysis to the complex model was successful.

In general, the approximate mathematical model has a significant contribution to dynamics walking. Instead of the analysis of numerical simulations, the mathematical model can provide us a better understanding of dynamics walking. Thus the correlation between control system and gait properties can be discovered and the trend of the gait properties can be analysed to discover the optimal walking states. Target walking states can be generated precisely based on the mathematical analysis. In addition, the approximate mathematical model also contributes to the non-linear dynamics on the research of bifurcation and chaos. Even though bifurcation and chaos have been discovered in dynamics walking in many researches based on the analysis of numerical simulations, the physical meaning and physical condition are still unclear. The approximate mathematical model can help us to understand the physical meaning of bifurcation and chaos, thus we can predict, avoid or recover from the chaos.

8.2 Future Work

As the most important future work, if the approximated mathematical models of bipedal walkers or even 3-D walkers can be derived, the motion can be controlled precisely and efficiently by the feedback control systems. As the limitations of the approximated mathematical models, however, the control systems and the computational complexity are the most challenging topics. In my thesis, the method is mainly based on settling-time control system, which means we know the control input can be finished by one step. Extending the settling-time control system to a general control system will be a very important future work. In addition, when we make the extension to the bipedal walkers or even 3-D walkers, the boundary conditions will be much more complex. Therefore, reducing the computational complexity will be the key of the precise control system. As the solution,

we can only derive some main parts of the walkers or make the walkers derive their own mathematical model by machine learning. In general, the extension of the mathematical model to the complicated walker is challenging and promising.

In addition, the understanding of the physical meaning of dynamic walking and the analysis of the non-linear dynamics are also promising future works. The physical meaning of the items in boundary condition of dynamic walking are also important and interesting topics, which can help us to understand the physical analysis of the dynamic walking. Thus the physical meaning of bifurcation and chaos can be discovered and analysed mathematically.

Publications

Journal

[1] Xuan Xiao and Fumihiko Asano, "Analysis of steady and target walking speeds in limit cycle walking," International Journal of Dynamics and Control, published as an online first view article. doi: 10.1007/s40435-015-0212-z

International conference

[2] Fumihiko Asano and Xuan Xiao, "Output deadbeat control approaches to fast convergent gait generation of underactuated spoked walker," Proceedings of the 2012 IEEE/SICE International Symposium on System Integration (SII), pp. 265-270, Dec. 16, 2012.

[3] Fumihiko Asano and Xuan Xiao, "Role of deceleration effect in efficient and fast convergent gait generation," Proceedings of the 2013 IEEE International Conference on Robotics and Automation, pp. 5649-5654, May 9, 2013.

[4] Xuan Xiao and Fumihiko Asano, "Limit cycle walker that forms various impact postures using mid-body," Proceedings of the 2013 10th International Conference on Ubiquitous Robots and Ambient Intelligence (URAI), pp. 571-576, Nov. 1, 2013.

[5] Xuan Xiao and Fumihiko Asano, "Analytical solution of steady step period in 1-dof limit cycle walking driven by stepwise control inputs," Proceedings of the 2014 IEEE

International Conference on Mechatronics and Automation, pp. 245-250, Aug. 4, 2014.

[6] Xuan Xiao and Fumihiko Asano, "Approximate solution of steady step period in one-period limit cycle walking based on discretization of control input," Proceedings of the 11th International Conference on Ubiquitous Robots and Ambient Intelligence (URAI), pp. 585-590, Nov. 14, 2014.

[7] Xuan Xiao, Yasunori Kikuchi, Fumihiko Asano and Tetsuro Fujimoto, "Limit cycle walking of underactuated bipedal humanoid on slippery road surface," Proceedings of the 14th IEEE-RAS International Conference on Humanoid Robots, pp. 622-627, Nov. 20, 2014.

[8] Xuan Xiao and Fumihiko Asano, "Analytical solution of target steady walking speed in 1-DOF limit cycle walking," Proceedings of the 2015 IEEE International Conference on Robotics and Automation, pp. 4525-4531, May 29, 2015.

[9] Xuan Xiao and Fumihiko Asano, "Generating 1-DOF Limit Cycle Walking at Target Walking Speed by Feedforward Limit Cycle Control," Proceedings of the 2015 IEEE Conference on Decision and Control, pp. 1316-1321, Dec. 2015.

[10] Xuan Xiao, Fukuda Go and Fumihiko Asano, "Mathematical Analysis of Steady Walking States in Underactuated Limit Cycle Walking," Proceedings of the IEEE ROBIO2015, to be present, Dec. 2015.

References

[1] Waterland. Joan C., "STANCE CHARACTERISTICS OF A QUADRILATERAL-AMPUTEE," Bulletin of Prosthetics Research, 1970.

[2] M. Vukobratovic, A. Frank, and D. Juricic, "On the Stability of Biped Locomotion," *IEEE Transactions on Biomedical Engineering*, Vol. 17, Iss. 1, pp. 25-36, 1970.

[3] S. Kajita, M. Morisawa, K. Harada, K. Kaneko, F. Kanehiro, K. Fujiwara, and H. Hirukawa, "Biped walking pattern generator allowing auxiliary zmp control," *Intelligent Robots and Systems, 2006 IEEE/RSJ International Conference on. IEEE*, pp. 2993-2999, 2006.

[4] S. Kajita, F. Kanehiro, K. Kaneko, K. Fujiwara, K. Harada, K. Yokoi and H. Hirukawa, "Biped walking pattern generation by using preview control of zero-moment point," *Proc. of the IEEE Int. Conf. on Robotics and Automation*, pp. 1620-1626, 2003.

[5] S. H. Collins and A. Ruina, "A Bipedal Walking Robot with Efficient and Human-Like Gait," *In Proceedings of International Conference on Robotics and Automation*, pp. 1983 - 1988, 2005.

[6] L. Roussel, C. Canudas-de-Wit and A. Goswami, "Generation of energy optimal complete gait cycles for biped robots," *Proc. of the IEEE Int. Conf. on Robotics and Automation*, pp. 2036-2041, 1998.

[7] Y. Okumura, T. Tawara, K. Endo and M. Shimizu, "Realtime zmp compensation for biped walking robot using adaptive inertia force control," *Proceedings. 2003 IEEE/RSJ International Conference*, pp. 335-339, 2003.

[8] M. Yamakita, F. Asano and K. Furuta. "Passive velocity field control of biped walking robot," *Proc. of the IEEE Int. Conf. on Robotics and Automation*, pp. 3057-3062, 2000.

[9] M. Garcia, A. Chatterjee and A. Ruina, "Efficiency, speed, and scaling of two-dimensional passive-dynamic walking," *Dynamics and Stability of Systems*, Vol. 15 Iss. 2, pp. 75-99, 2000.

[10] D. G. E. Hobbelen, "Controlling the Walking Speed in Limit Cycle Walking," *Int. J. of Robotics Research*, Vol. 27, No. 9, pp. 989-1005, 2008

[11] D. G. E. Hobbelen and M. Wisse, "A disturbance rejection measure for limit cycle walkers: The gait sensitivity norm," *IEEE Trans. on Robotics*, Vol. 23, Iss. 6, pp. 1213–1224, 2007.

[12] Zhou, Kemin, J. C. Doyle, and K. Glover. "Robust and optimal control," *New Jersey*, Prentice Hall, Vol. 40, 1996.

[13] D. G. E. Hobbelen. "Limit cycle walking," TU Delft, Delft University of Technology, 2008.

[14] T. McGeer, "Passive dynamic walking," *Int. J. of Robotics Research*, Vol. 9, No. 2, pp. 62–82, 1990.

[15] J. W. Grizzle, G. Abba and F. Plestan, "Asymptotically stable walking for biped robots: Analysis via systems with impulse effects," *IEEE Trans. on Automatic Control*, Vol. 46, No. 1, pp. 51–64, 2001.

[16] F. Asano, "Stability analysis of underactuated compass gait based on linearization of motion," *Multibody System Dynamics*, Vol. 33, Iss. 1, pp. 93-111, 2015.

[17] F. Asano, "Fully analytical solution to discrete behavior of hybrid zero dynamics in limit cycle walking with constraint on impact posture," *Multibody System Dynamics*, Vol. 35, Iss. 2, pp. 191-213, 2015.

[18] T. Nanayakkara, K. Byl, H. Liu and X. Song, "Dominant sources of variability in passive walking," *Proc. of the IEEE Int. Conf. on Robotics and Automation*, pp. 1003-1010, 2012.

[19] M. J. Coleman, A. Chatterjee and A. Ruina, "Motions of a rimless spoked wheel: a simple three-dimensional system with impacts," *Dynamics and Stability of Systems*, Vol. 12, Iss. 3, pp. 139-159, 1997

[20] M. J. Coleman, "Dynamics and stability of a rimless spoked wheel: a simple 2D system with impacts," *Dynamical Systems*, Vol. 25 No. 2 pp. 215-238, 2010.

[21] D. E. Rivera, M. Morari and S. Skogestad, "Internal model control: PID controller design," *Industrial and engineering chemistry process design and development*, Vol. 25, Iss. 1, pp. 252-265, 1986.

[22] J. H. Kim and J. H. Oh, "Walking control of the humanoid platform KHR-1 based on torque feedback control," *Proc. of the IEEE Int. Conf. on Robotics and Automation*, pp. 623-628, 2004.

[23] B. A. Francis and W. M. Wonham, "The internal model principle of control theory," *Automatica*, Vol. 12, Iss. 5, pp. 457-465, 1976.

[24] K. Zhou, J. C. Doyle and K. Glover, Robust and optimal control, New Jersey: Prentice hall, 1996.

[25] S. Kajita, F. Kanehiro, K. Kaneko and K. Yokoi, "The 3D Linear Inverted Pendulum Mode: A simple modeling for a biped walking pattern generation," *Intelligent Robots and Systems, 2001. Proceedings. 2001 IEEE/RSJ International Conference on. IEEE*, pp.: 239-246, 2001.

[26] J G. Juang, "Fuzzy neural network approaches for robotic gait synthesis," *Systems, Man, and Cybernetics, Part B: Cybernetics, IEEE Transactions on*, Vol. 30, No. 4, pp. 594-601, 2000.

[27] E. C. Whitman and C. G. Atkeson, "Control of a walking biped using a combination of simple policies," *9th IEEE-RAS International Conference*, pp. 520-527, 2009.

[28] C. Ridders, "A new algorithm for computing a single root of a real continuous function," *IEEE Transactions on circuits and systems*, pp. 979-980, 1979.

[29] F. Asano, "Stability analysis of passive compass gait using linearized model," *Proc. of the IEEE Int. Conf. on Robotics and Automation*, pp. 557–562, 2011.

[30] F. Asano and X. Xiao, "Role of deceleration effect in efficient and fast convergent gait generation," *Proc. of the IEEE Int. Conf. on Robotics and Automation*, pp. 5649–5654, 2013.

[31] X. Xiao and F. Asano, "Analytical solution of steady step period in 1-DOF limit cycle walking driven by stepwise control inputs," *Proc. of the IEEE Int. Conf. on Mechatronics and Automation (ICMA)*, pp. 245-250, 2014. J. S. Camp, A. Chatterjee

[32] M. J. Coleman, M. Garcia, A. L. Ruina, J. S. Camp and A. Chatterjee. "Stability and chaos in passive-dynamic locomotion," *IUTAM Symposium on New Applications of Nonlinear and Chaotic Dynamics in Mechanics.* Springer Netherlands, pp. 407-416, 1999.

[33] M. Wisse, A. L. Schwab, R. Q. van der Linde and and F. C. T. van der Helm "How to keep from falling forward: elementary swing leg action for passive dynamic walkers," *IEEE Trans. on robotics* Vol. 21 Iss. 3, pp. 393-401, 2005.

[34] X. Xiao and F. Asano, "Analytical solution of target steady walking speed in 1-DOF limit cycle walking," *Proc. of the 2015 IEEE International Conference on Robotics and Automation*, pp. 4525-4531, 2015.

Shuuji Kajita, Fumio Kanehiro, Kenji Kaneko, Kiyoshi Fujiwara, Kazuhito Yokoi and Hirohisa Hirukawa

[35] S. Kajita, F. Kanehiro, K. Kaneko, K. Fujiwara, K. Yokoi and H. Hirukawa, "A realtime pattern generator for biped walking," *Proc. of the IEEE Int. Conf. on Robotics and Automation*, pp. 31-37, 2002.

[36] K. Lffler, M. Gienger, F Pfeiffer and H. Ulbrich, "Sensors and control concept of a biped robot," *Industrial Electronics, IEEE Transactions* , Vol. 51 Iss. 5, pp. 972-980, 2004.

[37] D. J. Braun and M. Goldfarb, "A control approach for actuated dynamic walking in biped robots," *Robotics, IEEE Transactions*, Vol. 25 Iss. 6, pp. 1292-1303, 2009.

[38] T. Buschmann, S. Lohmeier and H. Ulbrich, "Biped walking control based on hybrid position/force control," *IEEE/RSJ International Conference*, pp. 3019-3024, 2009.

[39] Q. Huang, Y. Nakamura and T. Inamura, "Humanoids walk with feedforward dynamic pattern and feedback sensory reflection," *Proc. of the IEEE Int. Conf. on Robotics and Automation*, pp. 4220-4225, 2001.

[40] A. De Luca, "Feedforward/feedback laws for the control of flexible robots," *Proc. of the IEEE Int. Conf. on Robotics and Automation*, pp. 233-240, 2000.

[41] D. Nguyen-Tuong, M Seeger and J. Peters, "Computed torque control with nonparametric regression models," *American Control Conference*, pp. 212-217, 2008.

[42] K. Byl and R. Tedrake, "Approximate optimal control of the compass gait on rough terrain," *Proc. of the IEEE Int. Conf. on Robotics and Automation*, pp. 1258-1263, 2008.

Acknowledgments

First my deepest gratitude would go to my beloved parents for their support and great confidence in me all through these years. I could never make it without their help and encouragement.

Second I would like to express my heartfelt gratitude to Professor Fumihiko Asano, who spread the dream of robotics in my heart when I was confused and self-doubt. I was also very grateful to the patience help from Professor Jianwu Dang and Professor Isao Tokuda.

Last my thanks would go to my friends Yang Liu and Millie Ma for their understanding and support. I also owed my sincere gratitude to all the members of Asano Lab and my friends in Jaist from China, Japan and Korea. I would miss them forever.